Nanocrystal Assemblies: Current Advances and Open Problems

Carlos L. Bassani, Greg van Anders, Uri Banin, Dmitry Baranov, Qian Chen, Marjolein Dijkstra, Michael S. Dimitriyev, Efi Efrati, Jordi Faraudo, Oleg Gang, Nicola Gaston, Ramin Golestanian, G. Ivan Guerrero-Garcia, Michael Gruenwald, Amir Haji-Akbari, Maria Ibáñez, Matthias Karg, Tobias Kraus, Byeongdu Lee, Reid C. Van Lehn, Robert J. Macfarlane, Bortolo M. Mognetti, Arash Nikoubashman, Saeed Osat, Oleg V. Prezhdo, Grant M. Rotskoff, Leonor Saiz, An-Chang Shi, Sara Skrabalak, Ivan I. Smalyukh, Mario Tagliazucchi, Dmitri V. Talapin, Alexei V. Tkachenko, Sergei Tretiak, David Vaknin, Asaph Widmer-Cooper, Gerard C. L. Wong, Xingchen Ye, Shan Zhou, Eran Rabani, Michael Engel, and Alex Travesset*

Cite This: https://doi.org/10.1021/acsnano.3c10201
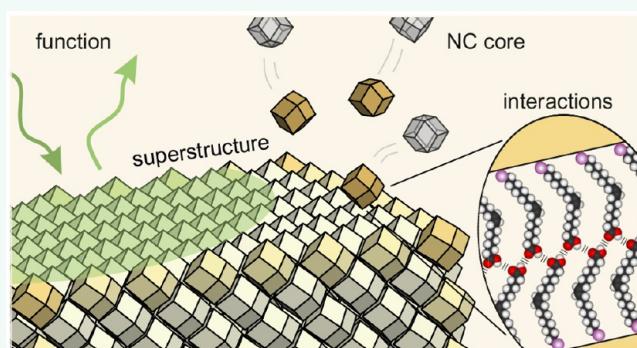
Read Online

ACCESS | Metrics & More | Article Recommendations

ABSTRACT: We explore the potential of nanocrystals (a term used equivalently to nanoparticles) as building blocks for nanomaterials, and the current advances and open challenges for fundamental science developments and applications. Nanocrystal assemblies are inherently multiscale, and the generation of revolutionary material properties requires a precise understanding of the relationship between structure and function, the former being determined by classical effects and the latter often by quantum effects. With an emphasis on theory and computation, we discuss challenges that hamper current assembly strategies and to what extent nanocrystal assemblies represent thermodynamic equilibrium or kinetically trapped metastable states. We also examine dynamic effects and optimization of assembly protocols. Finally, we discuss promising material functions and examples of their realization with nanocrystal assemblies.
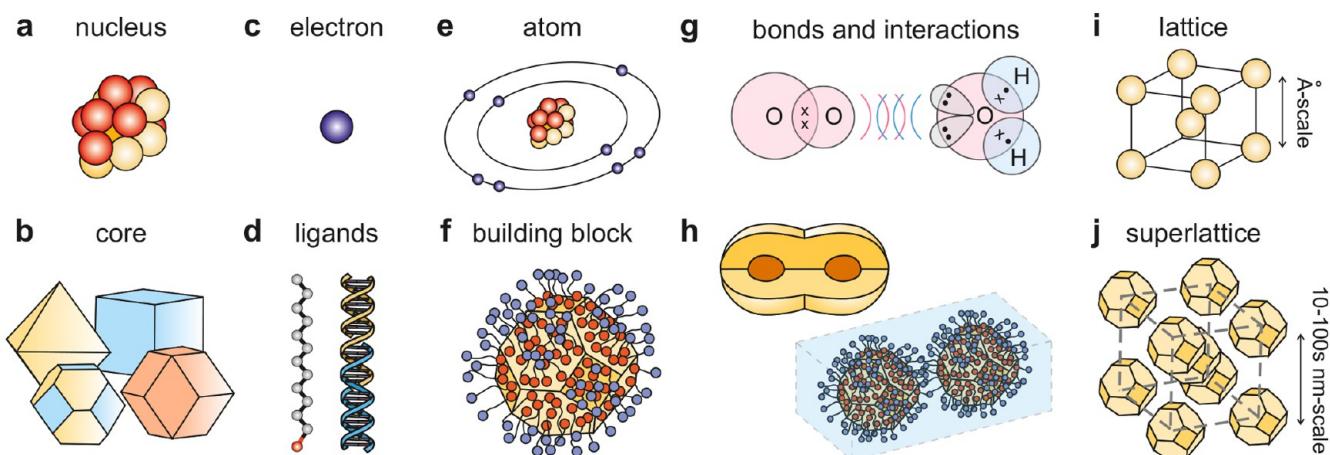
KEYWORDS: *nanocrystal, nanoparticle, quantum dots, nanocrystal assembly, colloidal crystal, superlattice, self-assembly, assembly protocols, structure prediction, material properties*

1. INTRODUCTION

Nanocrystals (NCs), a term used herein interchangeably with nanoparticles, provide building blocks for nanomaterials.[1−4] NC superstructures are a form of matter possible by the progress in synthesizing NCs with different shapes, sizes, and chemical compositions with monodispersed distributions,[5,6] allowing tuning superlattice parameters from tens to hundreds of nanometers. This permits creating materials with properties and functionalities believed unattainable on the basis of the crystallization of atoms into lattices at the Å-scale. An important challenge is to assemble materials that perform many functions simultaneously and undergo structural transformations on demand. *Robust assembly* that is precise and configurable or programmable is particularly desirable.

The assembly of NCs can be rationalized by drawing an analogy to atoms, their constituents, interactions, and the emergence of structures, as depicted in Figure 1. That is, NCs can be regarded as big atoms,[7] or *programmable atom equivalents*[8] (PAEs), defining a virtually infinite-dimensional periodic table of NCs with degrees of freedom including shape, size, chemical composition, the capping ligand, and others. The shape of NC cores (Figure 1b) is partially responsible for

Figure 1. Analogy between NCs and atoms. (a, b) NC cores play the role of atomic nuclei. (c, d) Ligands such as polymers and DNA are equifunctional to the electron shell. (e, f) Their combination gives rise to NC building blocks analogous to atoms. (g, h) Similarly to atoms, NCs can interact and bond. NCs interact via ligands through steric forces, van der Waals forces, or specific sites for hydrogen bonding. Solvent conditions modulate NC interactions. NCs can also bond by hybridization of quantum states, forming NC molecules. (i) Quantum chemistry explains the formation of crystalline lattices at the Å-scale. (j) NCs self-assemble into superlattices. The degrees of freedom of NC core habits and ligand chemistry, length, and coverage, tune superlattice parameters in the range of tens to hundreds of nanometers.

anisotropy in NC interactions[9] and is, in its centrality, analogous to the atomic nucleus (Figure 1a).

Interactions between NCs are controlled by functionalizing NC surfaces using ligands (Figure 1d). Similar to the electronic states dictating the type of interactions between atoms (Figure 1c), ligand chemistry, chain length, and coverage can modulate interactions between NCs. Besides conventional ligands already present during NC synthesis,[10] highly adjustable designer ligands comprise (i) polymers with nonspecific interactions that incur in steric stabilization, such as polymer brushes[11,12] and nano- and microgels,[13] and (ii) ligands with specific hydrogen bonds that can further induce anisotropy (patchiness[14,15]), as (ii.a) partially hybridized DNA strands that complete hybridization when finding their complements,[16,17] and (ii.b) polymers with certain end groups, such as *nanocomposite tectons* (NCTs)[18,19] and *interpolymer complexation* (IC).[20] Interactions between NCs can be further modulated by solvent conditions, such as ionic strength[21] and solvent quality,[22] or by use of liquid crystal hosts[23] (i.e., nematic molecules). The ligand-functionalized NC core—called *building block* (Figure 1f)—is the analog of an atom (Figure 1e). Just like atoms bonding to form molecules (Figure 1g), NCs can have their quantum states hybridized and extended, forming NC molecules (Figure 1h), dubbed *coupled colloidal quantum dot molecules*[24] (CQDMs). Whereas atoms crystallize into lattices (Figure 1i), building blocks self-assemble into superlattices (Figure 1j). The size of the NC core together with the ligands and length scale of NCs interactions determines the superlattice parameter.

An important aim of the field comprises the ability to design tunable building blocks able to realize (if not all of it, at least to large extent) the virtually infinite periodic table for NCs. There are several assembly protocols, including solvent evaporation,[6] variation of solvent quality,[22] solvent annealing,[25] and assembly assisted by an interface.[26] Assembly of NCs undergoes the basic crystallization steps comprised of super-lattice nucleation[21,27] and growth.[28,29] Just like at the atomic scale, crystalline defects may form,[30] and geometric frustration can influence the crystallization pathway.[31−33] Despite these similarities, atom crystallization and NC self-assembly differ

with respect to the role of fluctuations (discrete) and the influence of the environment (continuum). This is when the analogy between atoms and NCs falters, thus motivating efforts to adapt or re-evaluate predictive models when upscaling from atoms to NCs.

Finally, (i) if a desired superstructure could be assembled in a robust manner, and (ii) if NC interactions could assume arbitrary functions[34,35] and ensure electronic coupling, then (iii) materials functions (properties) such as superradiance,[36] superfluorescence,[37,38] surface lattice resonance,[39] and negative refractive indexes,[40] could be produced for society use, leading to (iv) potential advances in catalysis,[41−44] electronics,[45,46] thermoelectrics,[47] photonics,[48,49] plasmonics,[50,51] clean energy,[52−55] and biomedicine,[56−58] among others. A universal strategy for designing NC cores, ligands, solvent conditions, and assembly protocol to produce superstructures with desired properties at scale for commercial applications by *inverse methods*[59] could lead to technological advances changing the world as we know it.[46,60]

The field however still faces several challenges in implementing NC assemblies into practical societal use. It is imperative to investigate and/or reexamine fundamental questions, particularly at the nanoscale. This includes but is not limited to (i) the characterization of equilibrium and metastability, (ii) the role of fluctuations, (iii) aspects relating to vitrification vs. crystallization, and (iv) the relationship between structure and material properties. This study identifies current advances and challenges in the field along the directions discussed above, also summarized in Figure 2. This paper grew from discussions on these topics among the participants of the workshop "Nanoparticle Assemblies: A New Form of Matter with Classical Structure and Quantum Function", held at the Kavli Institute for Theoretical Physics (KITP), Santa Barbara/CA, USA, from March 27 to May 19, 2023. This study is not intended to be an in-depth literature review of a specific topic but rather a broader-view study linking different scales, fundamentals, and methods, emphasizing open problems to inspire and push forward research in the field. Suggestions for specific literature review studies are given to the reader when necessary.
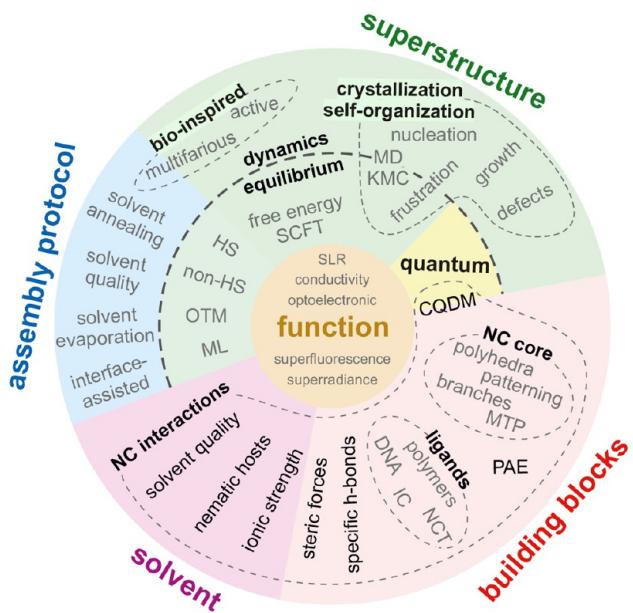
2. DESIGN OF NC CORES

Critical for successful material assembly is the ability to design NC cores precisely. NCs made of noble metals (Au, Ag, Pd) via redox reaction,[61] and of semiconductors (CdS, PbS, PbSe) via hot-injection methods,[62] have been grown with amazing precision and monodispersity in the past decade. The size of NC cores determines the characteristic length scale of the superlattice constant. The shape of NC cores—that is, the NC habit—is partially responsible for the anisotropy of NC interactions (anisotropy by NC shape). Further anisotropy comes from interactions via, e.g., ligands with specific hydrogen bonds, to be discussed in a later section on interactions between NCs.

2.1. Diversity of NC Shapes. NCs have been tailored to achieve numerous crystal habits, and some shape examples are presented in Figure 3. These shapes include (i) NCs that comply with the symmetry of the underlying crystalline structure, also known as *symmetry-preserving shapes*, comprising octahedra, cubes, and the family of cuboctahedra,[63] and rhombic dodecahedra[64] (Figure 3a); and (ii) NCs with reduced symmetry compared to the bulk crystal structure, also called *lower-symmetry habits*, including tetrahedra[65,66] (Figure 3a), nanorods,[67,68] nanoplates[69,70] (Figure 3b), and the family of *multiply-twinned particles* (MTP)—that is, bitetrahedra, decahedra, and icosahedra[66,71] (Figure 3e). The solution conditions are central to the formation of the NC core habit, such as the use of ligands (e.g., CTAB - cetyltrimethylammonium bromide, PVP - polyvinylpyrrolidone) that serve to cap[72] or direct diffusion of precursors.[73] Ions (e.g., Br^-, I^-, Cl^-) also can cap given crystallographic directions.[72] The insertion of seeds of defined shapes overcomes nucleation barriers, and depending on the chosen shape of the seed, growth follows a different kinetic pathway.[74] NC habits can be trapped in metastable configurations during the kinetic pathway of growth by changing the environment to a stabler one by, e.g., reducing temperature or changing the solution composition.

Further complexities can be inserted into NC habits by (i) growth of a given number of branches/pods with controlled size[5,75−78] (Figure 3f), (ii) patterning the surface by depositing a different metal over the NC, thus creating valence[79,80] and Janus particles[81] (Figure 3g), (iii) etching core@shell NCs formed of two distinct components, enabling convex pod-like shapes[82,83] (Figure 3h), and (iv) chiral NC habits formed by the adsorption of chiral molecules that biases NC growth in a chiral way[84−86] (Figure 3i). Selective-etching[87,88] of some of the crystallographic directions of the NC cores permits generating nanoframes (Figure 3c) and nanocages (Figure 3d) that assemble into open-channel superlattices,[40] thus forming a tunable porous material with applications in, e.g., catalysis and as a potential split-ring resonator for negative refractive index metamaterials, although the latter was realized only theoretically.

2.2. Prediction of NC Habits. Great advances have occurred in understanding when each NC habit forms and the conceptual mechanisms to explain why they form.[74] Symmetry-preserving habits are well-described by geometric construction models (Figure 4c). The classic geometric constructions are called (equilibrium) Wulff shapes,[89,90] which search for the solution of the surface area A_j of each facet j that minimizes the total surface energy $E_s = \sum_j \sigma_j A_j$, where σ_j is the surface tension of each facet. Several packages
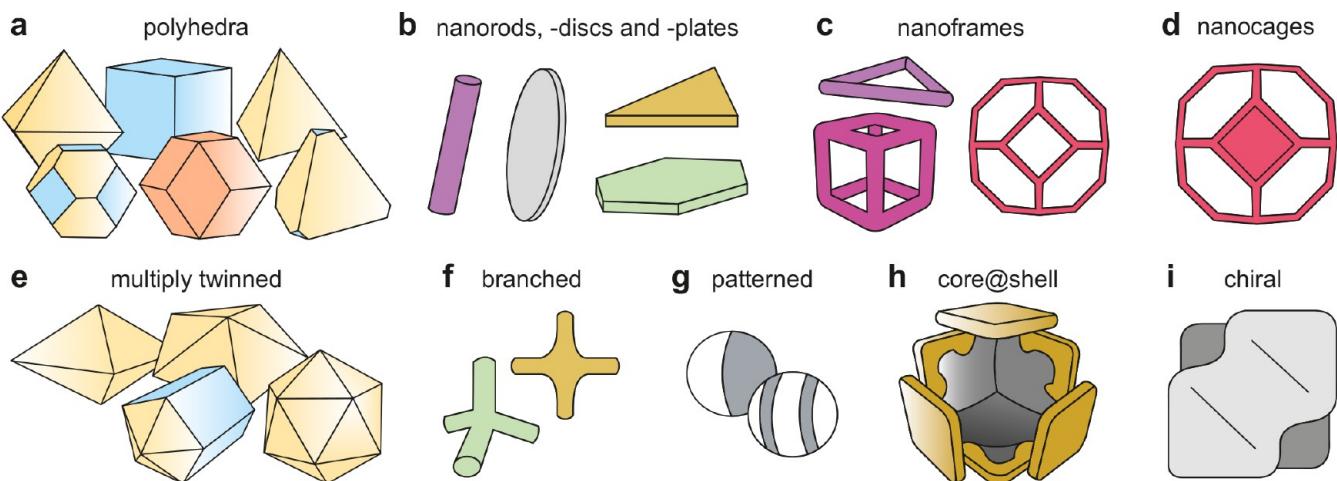
Figure 2. Summary of the topics covered in this study to assemble NCs into superstructures to a given desired function. The keyword map relates (i) acronyms coming from simulation methods and field-specific techniques, and (ii) technical jargon coming from the name of assembly protocols, to (iii) the fundamentals of different length scales covering quantum to hundreds of nanometers. Acronyms: CQDM (colloidal quantum dot molecules), HS (hard shape) and non-HS (non-hard shape), IC (interpolymer complexation), KMC (kinetic Monte Carlo), MTP (multiply-twinned particles), MD (molecular dynamics), ML (machine learning), NCT (nanocomposite tectons), PAE (programmable atom equivalent), OTM (orbifold topological model), SCFT (self-consistent field theory), SLR (surface lattice resonances).
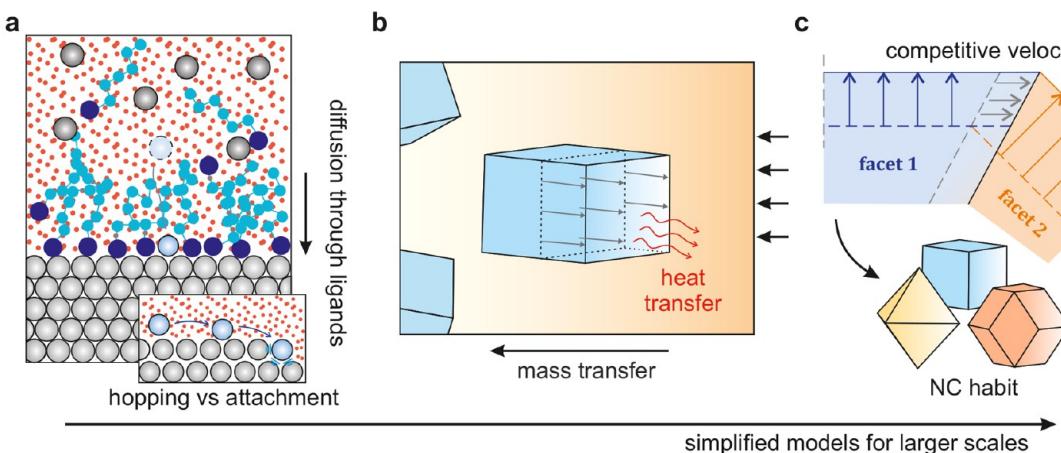
that generate Wulff shapes are available.[91,92] The Wulff shape construction presents several derived models, including[90] (i) Winterbottom shapes,[93] which consider the growth from a substrate described by the surface tension between the crystal and substrate in the energy minimization problem, (ii) Summertop shapes,[94] built from two substrates, (iii) alloy Wulff constructions,[95] for binary component systems, and (iv) kinetic Wulff shapes,[96] to predict kinetically trapped crystal habits during NC synthesis. Although crystalline growth velocities lead to a broader picture than surface tension, its estimation is substantially more challenging and requires the use of advanced methods[97,98] commonly not implemented in standard particle-based simulation packages.

The prediction of symmetry-broken NC habits is one of the top challenges currently faced by simulations. Geometric constructions cannot predict them as they jump scales from atomic (Å) to NC (50 to 100 nm) scales. Synthesis of multiply-twinned particles has received high attention in the past decade,[66,71,99,100] and its mechanism of formation relates to strain accumulation that often spreads heterogeneously along the NC habit.[90] Direct measurement of time-dependent strain accumulation requires 3D atomic resolution in timescales compatible with the crystallization of atoms, beyond the limits of current measurement techniques. Detailed atomistic simulations (aka computer experiments) seem therefore the path to proving and better understanding such mechanisms.

Molecular dynamics (MD) (Figure 4a) was extensively used to quantify and verify the different conceptual mechanisms

Figure 3. Habits of NC cores. (a) The simplest NC habits comprise spheres and polyhedra that comply with the underlying symmetry of the crystalline structure, also known as Wulff shapes, such as octahedra, cubes, rhombic dodecahedra, and their truncations. More complex habits that break symmetry from the underlying structure comprise (a) tetrahedra, (b) 1D and 2D shapes as nanorods, nanodiscs, and nanoplates, (c, d) nanoframes and nanocages, (e) multiply-twinned NCs such as bitetrahedra, decahedra, decahedral nanorods, and icosahedra, (f) branched NCs, (g) NCs with a patterned surface by the deposition of another material, and (h, i) complex-shaped habits coming from the etching of core@shell NCs, and grown in the presence of adsorption of chiral molecules forming chiral-shaped NCs.
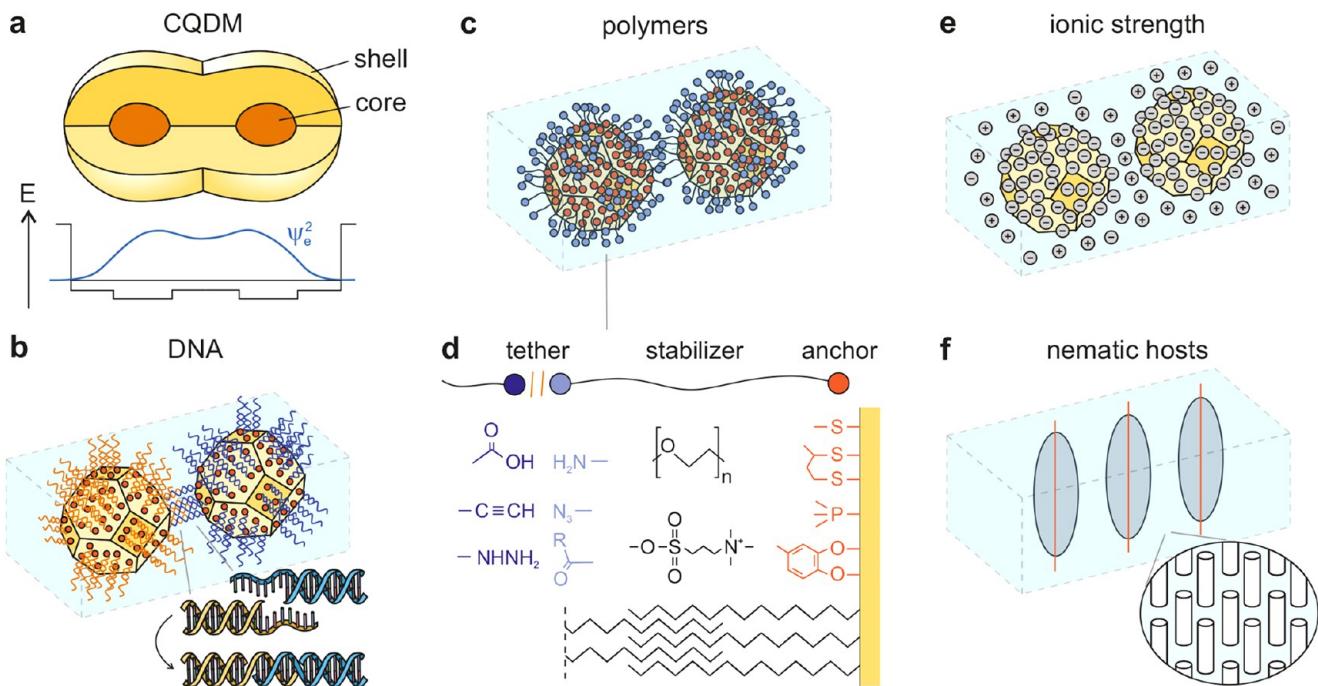
Figure 4. Challenges in multiscale simulation of the synthesis of NC cores with defined habits. (a) Diffusion of precursors over ligand layers, with subsequent surface hopping and attachment to the surface, requires MD to fully predict trajectories. The use of KMC allows scaling to larger systems at the cost of the trajectory description. **(b)** Heat and mass transfer limitations because of the exothermic nature of crystallization, precursor depletion, and interaction between NCs in dense populations require the solution of concentration and temperature fields via, e.g., finite volume method. **(c)** Competitive growth velocities of different facets lead to the formation of different crystal habits and are typically captured by geometric construction models.

proposed for NC synthesis.[73,96,100−105] There are, however, some important bottlenecks in MD simulations for crystal growth of atoms into NCs, (i) the inability to simulate realistic-sized NCs, keeping in mind that NCs on a length scale of 50 to 100s of nanometers contain tens of millions of atoms, and the inclusion of a ligand layer adsorbed in their facets adds simulation of many long-chained hydrocarbons (Figure 4a); (ii) the complexity when inserting/removing particles from the system to simulate growth/dissolution of NCs by the use of grand-canonical (Gibbs) or semi-Gibbs ensembles,[106] and (iii) the inaccuracy of the modern force fields underpinning MD simulations to describe weak long-range electrostatic and dispersive interactions critical for NC formation.

The sampling of surface energetics via kinetic Monte Carlo (KMC) to grow and dissolve atoms in the crystal lattice circumvents the first two issues mentioned.[70,82,83,107−110] The trade-offs of KMC are (i) not predicting full trajectories but

only the most probable intermediate states of the kinetic pathway of growth, therefore lacking in a complete description of diffusion, which is key for crystallization; (ii) considering a perfect lattice, thus lacking information on strain accumulation due to the formation of defects and their displacement,[90] or lattice mismatch when growing over a seed composed of a different metal,[66] both related to symmetry-breaking of NC;[74] and (iii) the consideration of a homogeneous and constant chemical potential of the solution over the entire NC surface, thus not capturing (iii.a) ligand adsorption depending on the crystalline direction of each facet, which relates to transformation between different Wulff shapes,[63,96] nor (iii.b) heat and mass transfer-limited crystallization[111−113] that relates to symmetry breaking by a inhomogeneous precursor supply to the facets of the growing NC.[114,115] Inserting such effects into the prediction of growth and dissolution rates of KMC models while keeping the low computational cost nature of the

Figure 5. Interactions between NCs. (a) Quantum dots forming dimers, also known as coupled colloidal quantum dot molecules[24] (CQDMs). Top is a schematic illustration of the CQDM composed of two fused CdSe/CdS core/shell QDs (orange and yellow shadings indicate the CdSe core and CdS shell regions, respectively). Bottom presents the CQDM conduction band (CB) potential energy landscape (black) and the density of the envelope function of the first CB bonding electron state ψ_e^2 (blue) manifesting quantum coupling. (b) Partially hybridized DNA strands with complementary chains bond NCs via further hybridization. (c) Polymers act in binding NC cores via hydrophobic interactions, or (d) present anchors that bind the polymer to the NC surface (e.g., thiolate, phosphine, catechol), stabilizers that relate to the interaction length scale between NCs (e.g., polyethylene glycol, zwitterion), and tethers that bind two polymers (e.g. amine-carboxylic acid, azide-alkyne, carbonyl-hydrazine). (e) The ionic strength of the solution modulates interaction forces between NCs. (f) Solutions composed of nematic hosts (e.g., nematic molecules) play a role in the alignment and structure formation of nonspherical NCs.

method is an important challenge to enhance the physical chemistry prediction capabilities of a framework able to handle the growth of realistic-sized NCs.

In this sense, multiscale approaches are key. They can be either coarse-grained or machine-learned models to feed simulations of larger scales, or chained-multiscale simulations where outputs of smaller scales serve as inputs for larger scales. Important advances have been made by using density functional theory (DFT) to fit a coarse-grained energetic model that predicts the metal-organic bonding between the ligands and the NC core, and then used in a complete atomistic MD simulation of the diffusion of precursors over the ligand layer in facets of different crystallographic directions.[73,96,116] This approach estimates the growth velocity of different crystallographic directions linking the crystalline structure and energetics of NC core, ligands and solution from particle-based methods, to feed geometric construction models that predict kinetic Wulff shapes. Nevertheless, such an approach can only predict symmetry-preserving habits, because it still depends on geometric construction models. If the same multiscale information could be introduced into the larger scales using, e.g., low computational-cost KMC methods, then the growth of realistic-sized symmetry-broken NC habits could potentially be simulated.

The community would also benefit from multiscale coupling with the larger scales, especially when aiming at upscaling NC production for society use. Mass transfer-limited crystallization coming from both the environment (the crystallization reactor) and the competition into depleting solute in a dense population of NCs, plays an important role in the formation of symmetry-broken NCs via a limited-precursor supply.[114,115] This could potentially be predicted via the coupling of concentration field models (Figure 4b) with particle-based models, similar to what was recently achieved for heat transfer-limited crystallization.[98] Effects of ions often present in the solution could be predicted by reaction-diffusion models[117] to estimate the local chemical potential of the solution at the NC surface via, e.g., Pitzer equations[118] or the electrolyte non-random two-liquid (eNRTL) model.[119] The latter can then feed semi-Gibbs ensembles[106] in KMC models.[82,108,110] The realization of such a multiscale framework for better predicting the kinetic pathways of growth of NCs in feasible simulation times is nontrivial. However, this approach will help our understanding of why different NC habits form, as well as potentially discovering NC habits by the use of inverse methods, e.g., where the user gives a desired NC shape, and the model gives the necessary conditions for growing such NC.

3. INTERACTIONS BETWEEN NCs

NC assembly is driven by both enthalpic and entropic effects. There are different strategies to promote interactions and/or bonding between NCs, (i) the hybridization of their quantum states (Figure 5a), (ii) by ligands with nonspecific interactions (steric forces), (iii) by ligands with specific hydrogen-bonding sites that induce valence in NC interactions (Figure 5b−d), and (iv) by modulating solvent conditions such as electrostatic forces and ionic strength (Figure 5e), by the use of nematic

hosts (Figure 5f), and via complex, nonadditive (many-body) interactions of ligands in the solvent medium.

In the analogy between NCs and atoms of Figure 1, ligands play a similar role to electrons. Superlattices can be held together by delocalized mobile NCs.[120] Similar metallization-like behaviors have been observed in models of hard-shape alloys, where size-asymmetric mixtures exhibit mobile small particles interspersed in a stable lattice of larger particles[121] and is reminiscent of depletion interactions in colloids.[122] This illustrates the relevance and promise of hard shape and other simple models to provide qualitative descriptions of many phases found in NC assemblies, further discussed in the section on structure prediction.

The superatomic concept, based on the recognition of electronic atom shells in atomically precise metal clusters, provides a direct mapping of interatomic bonding to interparticle bonding.[123] Entropy also suggests analogs for other forms of bonding. Entropic patches give rise to *entropic bonds*[124] that have a quantitative behavior similar to traditional electron-mediated bonds, where the Smoluchowski equation takes the role of the Schrödinger equation in describing the bond.[125] In all cases, the design dimensions of anisotropy/valence and interactions available to NCs resemble those that quantum mechanics ascribes to atoms, allowing the use of NCs as the basis of metachemical structures not seen in conventional systems.[126] Understanding how metachemical structures are rationally perceived in the design of materials on demand is a grand challenge for nanoassembly engineering in the coming years.

3.1. Hybridization of NC Quantum States.
Wavefunction coupling between semiconductor NCs leads to the hybridization of their electronic states. The analogy between NCs and atoms (Figure 1) becomes even more tantalizing as such wavefunction coupling leads to artificial molecules of importance to creating a library of hybrid nanostructures with different optoelectronic properties, with relevance to applications that include quantum technologies.[24]

The realization of artificial quantum molecules with sufficient coupling energy detectable at room temperature is a promising use of QDs. This can be achieved by conducting ligands or by the fusion of adjacent NCs to form a continuous inorganic bridge linking the neighbors (Figure 5a). The controlled bridge and the barrier height between two adjacent quantum dots are key variables for dictating the magnitude of the coupling energy of the confined wavefunctions.

The proof of concept is the formation of the simplest NC molecule, a homodimer formed from two core/shell NCs in analogy to a homonuclear diatomic molecule.[127] The shell material of the two NCs is structurally fused resulting in a continuous crystal. The direct manifestation of the hybridization reflects on the band edge transition shifting towards lower energy (Figure 5a) and is resolved at room temperature. The hybridization energy within the single homodimer molecule is strongly correlated with the degree of structural continuity. The barrier is affected by (i) the original shell thickness, (ii) the original core/shell building blocks, (iii) the relative orientation of the two core/shell building blocks, and (iv) the extent of neck filling.[128]

The challenges ahead lie in gaining higher degrees of control over the architecture of *colloidal quantum dot molecules* (CQDMs). Firstly, the ability to fabricate robust heterodimers at a high chemical yield. This calls for the development of selective methods to form preferentially or even exclusively A-
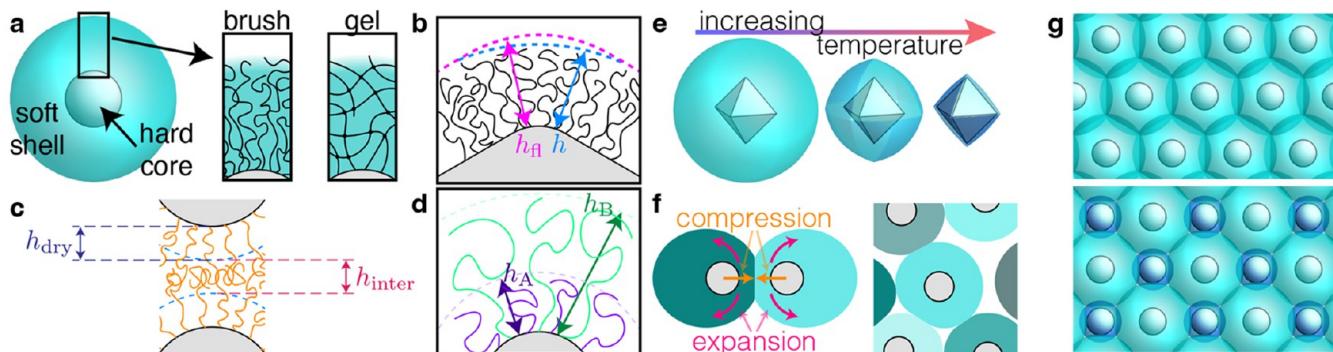
B type heterodimers, without the undesired formation of A-A and B-B homodimers. The use of selective click-chemistries provides a promising path forward. An additional challenge is having a method to make dimers on demand with the desired alignment between adjacent NC facets in the assembly. Such control needs to ensure domination of attachment during the fusion step, typically performed at moderate to high temperature, thus leading to well-defined crystalline connections between the adjacent NCs.

Fabrication of linked and fused NCs is of direct relevance to achieving hybridization of quantum states of superstructures.[129,130] Controlled fusion of such extended artificial solids was demonstrated for Pb-chalcogenides NCs,[129,131] and extension to less soft and hard QD, in particular those of technological relevance for II-VI and III-V semiconductors, will enable facile conductivity pathways.

3.2. Soft Shells of Long Polymers.
3.2.1. Polymer Brushes. Polymer brushes have long been used for steric stabilization of colloidal particles and, like other types of ligands, have been used to tune interactions in NC assemblies.[11,12,132−134] Established theories of polymer brushes[135−137] do not account for (i) reduction of brush height to $h/R = (1 - 3h_{fl}/R)^{1/3} - 1$, leading to variations with curvature (Figure 6b), where h_{fl} is the brush height for a flat monolayer, (ii) the existence of an end-exclusion zone devoid of polymer ends next to the NC core, and (iii) the increase in chain tension near the grafting surface.[138−140] These effects are important in NC assemblies, and experiments aimed at quantitative testing for them are, to a large extent, still absent. Furthermore, the effective hard shape of a polymer-functionalized NC, including its effective diameter, that determines important properties such as the lattice constant in NC assemblies, critically depends on accounting for these effects.

Solvent-free melts of polymer-grafted NCs have to compromise the requirement that grafted chains fill space vs. the reduced ability of adjacent brushes to interpenetrate[141] (Figure 6c). Sparsely-grafted NCs exhibit highly directional interactions leading to anisotropic superstructures,[142] while densely-grafted NCs can form simple or glassy liquids depending on the density of the graft and the length of the chain.[143] These jammed states can be relieved by adding free polymers, which populate the interstitial pockets between particles, resulting in materials with highly selective transport channels, with applications in gas-separation membranes for mixtures of, e.g., CO_2/CH_4 and He/H_2.[144,145] However, it remains quite challenging to construct simple but sufficiently accurate models to predict the material properties of these inhomogeneous systems, as simple analytical free energy models often fail.[145,146] More advanced mean-field theoretical frameworks may be able to address this challenge, to be discussed in a later section.

Variation of chain statistics with distance creates a depth gradient in the ligand density. When combined with curvature-induced variations and tension, careful design of depth gradients in polymer brush properties provides a versatile way of controlling NC interactions. Moreover, nonspherical cores give rise to brush environments that depend on both the mean and Gaussian curvatures of the particle.[147] The dependence of brush properties on surface gradients in grafting density and curvature remains an open problem in polymer physics. Moreover, the polydispersity of chain lengths can give

Figure 6. Depiction of soft shells over NC hard cores. (a) Schematic of a hard core particle with a soft polymer brush or polymer gel shell that is thick relative to the core diameter. (b) Gradients in core curvature result in local variations in brush thickness h (blue dashed line) when compared to a flat brush of thickness h_{fl} (magenta dashed line). (c) Interactions between brushes give rise to an interpenetration zone of thickness h_{inter} and a dry zone of thickness h_{dry}. (d) Brushes composed of different polymer lengths lead to layers of thickness h_A and $h_B - h_A$ with different compositions. (e) A shell composed of a temperature-responsive polymer can change in thickness, e.g., conforming to a potentially anisotropic core above a lower critical solution temperature. (f) Two-body interactions of an elastic shell involve a combination of compressive and expansive deformations (left). Many-body interactions involve more complex deformations and changes in contact surfaces (right). (g) Equilibration involving mass (solvent) exchange can lead to coexistence between particles of different volumes, resulting in different crystal phases, e.g., transitioning from a hexagonal lattice (top) to a square lattice (bottom).

rise to additional structures in brushes, namely the segregation of long and short polymers into different layers[148−151] (Figure 6d). This can also be used in favor of tuning NC interactions.

Many open questions regarding the effect of polydispersity in curved brushes remain. There are examples[152] where the assembly is not affected by polydispersities leading to up to 25% variations in the effective diameter of the NC. The ability of these highly dispersed systems to produce uniform superlattices was attributed to the greater polymer configurational freedom enabled by their curvature. The universality of this effect however needs to be assessed by further work.

The NC core shape has a nonlocal effect on brush properties, chain statistics, and brush interactions, which is of importance to tune properties. To what extent this is possible is an open issue and highlights fundamental questions in the basic statistical physics of how polymers and polymer brushes fill space. The interpenetration of two polymer brushes alters the local density of the monomers within a brush, modifying packing conditions elsewhere. Consequently, the nonlocal character of this alteration in chain-packing conditions changes the degree to which additional brushes can interpenetrate the shell. This leads to effective many-body interactions that have been modeled for shorter ligands,[153] but it remains unclear how to extrapolate these models to long brushes.

Changes in brush solubility permit large, in situ changes in NC interactions. For example, a swollen polymer brush shell increases the distance between cores. Since swollen polymer brushes allow for greater interpenetration from surrounding brushes, the resulting interaction is softer. Thus, a swollen polymer brush screens neighboring NC cores more effectively. Conversely, when a polymer brush collapses (Figure 6e), it forms a dense, thin, and stiff shell around the core, reducing screening. Altering the brush configuration can stabilize superstructures during drying, allowing the formation of free-standing assemblies.[154] This can even drive martensitic phase transitions, where structural defects arise to compensate for the compaction observed in polymer contraction.[155]

3.2.2. Core-Shell Nanogels and Microgels. Nano- and microgels are soft, deformable objects with an internal gel-like structure that consists of chemically and/or physically cross-

linked polymer chains[13] (Figure 6a). The total dimensions of such gels reach hundreds of nanometers for nanogels, and up to tens of micrometers for microgels. When using an appropriate solvent, microgels are swollen by large amounts of solvent molecules, making their physical classification nontrivial. The properties of microgels range somewhere between those of classical macromolecules, surfactants, and colloids.[156] Whereas the decoration of NCs with linear polymer chains (e.g., polymer brushes) is limited to rather small shell thicknesses, the encapsulation of NCs by microgel shells extends to larger length scales because of its cross-linked nature.[157] This is relevant for designing close-packed NC assemblies where the thickness of the shell and its compression state determine the distance between NCs.[158]

There are many open questions regarding the interactions between gel-grafted NCs. As microgels are cross-linked polymer networks, their response to deformation is characterized by a shear rigidity that polymer brushes and other grafted ligands lack. Consequently, contact interactions between gel-grafted particles involve nonlocal deformations of the shell as a whole, oppositely to the localized interpenetration layers as in brush-grafted NCs. This is a result of the long-range character of elasticity in rigid materials and is particularly important for situations where the internal stresses in the assembly are comparable to the stiffness scale set by the elastic moduli of the gel, which altogether can lead to large deformations. Large-deformation contact mechanics involve nonlinear elastic effects beyond those captured by typical Hertzian contact mechanics, requiring advanced computational methods. Beyond the complexities of pairwise interactions, the nonlocal character of shell deformations leads to multi-body interactions (Figure 6f). These depend on a rich interplay between the nonlinear elasticity of individual shells and changes in contact surface geometry and topology between multiple NCs.[159,160] In the many-body limit, particularly in the case of close-packed assemblies, long-range elasticity leads to a situation in which gel shells form an essentially continuous soft gel matrix with NC cores as inclusions, resulting in a composite material with distinct mechanical and rheological properties.[161]

A further challenge is the cross-link density gradients of nano- and microgels leading to a distinct swelling response.[162] The ability to design and prescribe spatial distributions of cross-links may nevertheless be useful in crafting targeted contact interactions between NCs. Moreover, patterned cross-link gradients have proven to be a useful tool for the design of macroscale, soft, shape-morphing materials,[163] prompting the question of whether such patterning may be useful for the design of shape-morphing NCs. However, patterning nanoscale variations in cross-link distributions in gels in a way that is scalable remains an open challenge.

Even without cross-link density patterning, shape change may be achieved by grafting a gel with a large swelling response to the surface of a nonspherical core, so that the swollen shell is roughly spherical and the de-swollen shell conforms to the nonspherical hard core (Figure 6e). While a similar effect can be achieved with a polymer brush, gels and other residually-stressed materials that are grafted to rigid surfaces can undergo elastic buckling under changes in the swelling state.[164,165] These buckled states have a reduced symmetry compared with that of the unbuckled states, potentially augmenting the shape design space of these NC materials. Incorporation of buckling—that is, of mechanical instability—has long been of interest to the design of mechanical metamaterials, due in part to the multistability of broken-symmetry, buckled states. Introducing such multistability into NC assembly via the buckling of gel shells may give rise to bulk emergent effects seen in other metamaterials, such as auxeticity,[166,167] as well as a way of actuating transitions between crystal structures.

The deformability of soft shells, which permits the control of NC assembly, also gives rise to several challenging open questions related to the interplay between shape change and many-body interactions. The ability of a particle to change shape in response to confinement by other particles creates effective multivalent NC interactions, especially when the deformation is coupled with the functionalization of the soft shell. An example is when contact-induced deformation or polymer interpenetration leads to the exposure of different binding motifs due to the insertion of ligands within the soft shell. Beyond contact interactions, which involve redistribution of mass within a single NC shell, there is an additional possibility of mass exchange between NCs, which has been shown to play an important role in stabilizing ordered phases in certain assemblies.[168] One example is the exchange of solvent between gel-grafted particles, which is necessary for osmotic equilibrium. Changes in the osmotic equilibrium give rise to variations in the swelling state of the gel. Microgels have been shown to take advantage of solvent or ion exchange to heal lattice defects caused by size polydispersity, and gel swelling or de-swelling.[169] Interestingly, polyNIPAM-based gels can have multiple coexisting swelling states at a single osmotic pressure.[170−172] This permits harnessing multistable osmotic equilibria to stabilize additional crystal structures that are not usually accessible to monodispersed particles (Figure 6g). Examples include complex Frank-Kasper crystal structures, which have been shown to be stabilized by mass exchange between multiple lattice sites in block copolymer systems.[173]

3.3. Ligands with Specific Hydrogen Bonds. The use of ligands with tether groups (Figure 5d) at the end of the ligand chain addresses directional interactions in a way that cannot be achieved by steric, ionic, or van der Waals interactions. Tether interactions often occur by hydrogen bonding of specific sites. These sites present a geometric disposition where bonding is always stronger once meeting its complementary tether. Nevertheless, hydrogen bonds are weak by nature, and therefore bonding of noncomplementary tethers is reversible, permitting structure healing. These interactions lead to the *robust assembly ideal*, based on two universal aspects, (i) preprogrammed heterogeneous nucleation, ensuring that intermediates grow as determined by the current properties of the solution, so growth does not result in a pool of mutually incompatible precursors of the desired superstructure and that there are enough building blocks (NCs) to build it, and (ii) cooperative binding, ensuring that any added building block is guaranteed to bind to its correct spot, thus implementing a form of error correction.

The most prominent ligand that tackles the ideal of robust assembly is deoxyribonucleic acid (DNA), where a sequence of the four nucleobases—namely adenine (A), cytosine (C), guanine (G), and thymine (T), represented by different colors in Figure 5b—bond with their complementary nucleobases. There are however other successful strategies that offer advantages in scalability, lower cost, and operation in organic solvents, such as nanocrystal tectons and interpolymer complexation.

3.3.1. DNA Ligands. Single- and double-stranded DNA chains are widely used as ligands to direct the self-assembly of NCs[16,17,174,175] and permit programming intercomponent interactions via addressable bonds.[176−179] Nonhybridized ACGT nucleobases of DNA dangle at the end of the DNA chains and, once they find their complementary partners, hybridize leading to attractive interactions between NCs. Highly specific molecular-level instructions to direct inter-particle binding also exist in ligands other than DNA. Other classes of biomolecules, including nucleic acids, proteins, and peptides,[180−187] also incur multiple types of orthogonally interacting bonds that can be defined explicitly.[174,175,188−192] DNA ligands are nevertheless attractive in the field of NC assembly due to (i) the chemical stability of DNA and the ability to functionalize DNA with different chemical groups, (ii) its predictable description of sequence-encoded inter-actions, (iii) the ability to control entropic and mechanical properties of DNA chains through its single- and double-stranded composition, and (iv) its structural plasticity.[176,177] Besides DNA used as a ligand shell around the NC core, DNA can also be folded without an NC core to engineer complex 2D and 3D shapes (scaffolds), a technique known as *DNA origami*.[193−211] Recently, both techniques of DNA-grafted NCs and DNA-shaped nanoarchitectures were merged to co-assemble 3D organizations.[212,213]

A fundamental challenge in using DNA ligands regards the collective effect of DNA chains resulting in many-body interactions.[214] Complex DNA shells can lead to intricate assembly pathways that inhibit crystallization, making it difficult to predict the resulting phase. Studies uncovering the phase behavior of DNA-grafted NC assemblies were tackled both theoretically and experimentally.[181,215−218] Recent advances demonstrated that DNA shells of spherical nanoparticles can be rationally designed with prescribed interaction potential by tailoring the rigid and flexible parts of connecting DNA chains and their hybridizing motifs,[219] leading to the assembly of non-closed packed structures. This permits future lattice engineering via DNA shell design. Challenges still remain in (i) prescribing a shape of the interaction potential via DNA motifs and shell composition, (ii) understanding how many-body effects affect local particle

arrangements, and (iii) the results of these factors on the assembled phase.

Interactions between NCs also depend on the placement of DNA at different parts of the NC surface, that is, on the edges or facets of the NC core. This results in complex hybridization behavior of the DNA shells, where the chains seek the maximization of the hybridization area while satisfying entropic effects for both ligand chains and NC cores. The interplay of these effects results in complex phase behaviors of systems with single and binary particle shapes.[40,216,220−225]

While there is significant progress in establishing predictable assembly in DNA-grafted NCs, it is difficult to use this approach broadly for technological applications as particle characteristics (e.g., the habit of the NC core, the DNA shell, and grafting density of DNA ligands) determine the assembled structure, significantly limiting the range of ordered arrays that can be achieved. This can however be overcome by utilizing DNA scaffolds that prescribe placements of NCs. Complex surface scaffolds using DNA tiles and DNA origami[202,226] that self-assemble into desired patterns can provide addressable affinity for NCs at specific locations,[195] although this approach is currently limited to 2D assemblies.

Controlling the behavior of 3D assembly can be achieved by the integration of DNA-grafted NCs and DNA nano-architectures.[213,227−229] In this approach, NCs are provided with defined directional interactions by encapsulating them into polyhedral wireframes made of DNA. This strategy significantly decouples the assembly process from the NC properties thus expanding the range of assembled structures, since NCs act as a nanocargo in a frame, forming a material voxel.[212] Assembly is therefore predominantly driven by directional, interframe hybridization interactions. Such inter-actions are encoded by DNA strands at predefined locations of the frame, such as its vertices. This method drastically expands assembly, since it relies on the valence of the frame. More studies will be required to explore the molecular-level details of the influence of DNA in the crystallization of frames and their phase behavior. Recent work[230] revealed different types of defects in 3D DNA-grafted NC assemblies, and future studies should explore how the occurrence and type of defects depend on the design of assembled components and the assembly pathways.

Selecting a voxel shape and the placement of interframe DNA bonds define the valence and geometry of binding arrangement and, consequently, an assembled DNA frame-work. For example, the 4-, 6-, and 8-fold symmetries of the individual voxel bonds[80,202,212,231−234] result in diamond, simple cubic, and body-centered cubic frameworks, providing different 3D scaffolds to place NCs. By adding a bond identity to the valence when using different sequences, or a composition of a number of sequences for different directional bonds, a higher degree of structural diversity is achieved.[191,232,235] This approach permits (i) coordinating different types of frames, empty or with cargo, to create increasingly complex organizations,[226,232,236] and (ii) establish-ing an inverse design of lattices through the selection of bonds with different identities for a set of voxels. However, the requirements of the bond encoding and their energy distribution for an effective assembly process are unknown. Relevant questions remain on (i) how to reduce the amount of information required for the inverse design of such systems, and (ii) which energy landscape of the bonds provides an

assembly pathway with minimal metastability in such complex systems.

3.3.2. Nanocomposite Tectons and Other Ligands. Hydrogen bonds provide a powerful bonding mechanism between polymer-grafted NCs, being the most prominent example DNA-mediated assembly discussed in the previous section. There are however other successful strategies that offer advantages in scalability, lower cost, and operation in organic solvents.

Nanocomposite tectons[18,19] (NCTs) are one important example that consists of an NC core functionalized with a polymer brush, where each polymer chain terminates in a supramolecular binding group, also called tether (Figure 5d). The highest quality crystals are typically obtained with NCTs that bond via complementary diaminopyridine (DAP) and thymine (Thy) groups that form a hydrogen-bonding pair. The reversible nature of the individual supramolecular interactions is a critical design component to enable crystallization. The use of multivalent interparticle bonding mediated by these supramolecular complexes between particles allows for crystal formation, thus providing an example regarding the rules for robust assembly discussed in the previous section.

NCTs present an interesting tool for assembly, as the composition and length of the polymer brush and the identity of the supramolecular complexes provide design handles to tune the crystallization behavior. The scalability of the polymer system also allows a wider range of experimental variables and conditions to be explored, as well as the investigation of larger-scale effects on nanoscale assembly.[154] Furthermore, passiva-tion of DAP or Thy results in an NC functionalized with a nonspecific polymer brush,[237] thus representing an interpola-tion that may optimize pros and cons of NC bonding by polymer brushes and DNA-mediated assembly discussed in the previous sections.

Another example of polymers interacting through hydrogen bonds is *interpolymer complexation* (IC), where a hydrogen-bond acceptor (e.g., polyethylene oxide) is functionalized to an NC, whereas a hydrogen-bond donor (e.g., polyacrylic acid) is suspended in a water solution providing a bond linker.[20] NCTs and IC however do not yet provide the level of programmability of DNA. Future efforts will require the development of hydrogen-bond polymers that retain the significant advantages of these examples while enabling more sophisticated programmability that can rival the successes achieved in DNA assembly.

3.4. Solvent Effects. *3.4.1. Electrostatic Forces and Ionic Strength.* Long-range Coulomb interactions are screened by the ionic strength of the solvent and controlled through variations in both the salt concentration and the dielectric constant of the solvent. These effects provide a method to finely control NC interactions (Figure 5e). A recent strategy shows that metal (e.g., Au, Pd, Ni) and semiconductor (e.g., PbS, PbSe) NCs assemble into face-centered cubic (fcc) superlattices in the presence of the large ionic strength provided by multivalent salts,[21] with the high dielectric constant of the NC material generating image charges and ionic condensation near the NC surface.[27] A second approach[238] combines charged colloidal NCs and small molecules with multiple opposite charges, e.g., positively-charged Au NCs and negatively charged citrate ions.[238] This approach has recently been generalized to mixtures of positively and negatively charged NCs, leading to the formation of binary NC superlattices. A third approach

consists of NCs functionalized with polyethylene glycol (PEG), including modified PEG with charged end-groups,[239] where the competition between hydrogen bonds and electrostatics leads to 2D and 3D superstructures.[240−242] For μm-sized colloids, organic solvents with a low dielectric constant induce assembly at small salt concentrations.[243,244]

Several effective Yukawa-DLVO-like interaction potentials have been proposed in the literature to model charged NCs/colloids in the presence of monovalent ions.[245−248] Developing accurate potentials to describe NC interactions within implicit solvent models nevertheless remains a challenge. The finite element method (FEM) solves integral equations of the primitive model surrounding a spherical macroion with an arbitrary number of ionic species, including ion correlations, ionic excluded volume effects, and large size and charge dispersities. Nevertheless, there remain critical disagreements between theory and experiment regarding, e.g., interactions between rods, which requests more complex models.[249] For instance, conformational degrees of freedom of ligands are difficult to describe within primitive models. The development of models that explicitly describe water[250] is key to moving beyond primitive models in electrostatic interactions. Machine-learned potentials trained on first-principle computational data may provide a promising path forward, to be discussed later in this article.

3.4.2. Many-Body Interactions of Ligands. Nonadditive[251] and many-body effects[252] exist in a vacuum and can also arise from solvent molecules that remain within assemblies. During the assembly of, e.g., ultra-thin nanowires,[253] they affect the spacing and structure depending on their molecular packing. Ligand fluctuations also lead to anisotropic geometries that influence the apparent physicochemical properties of the ligand shell by exposing different functional groups to the solvent or by increasing the amount of surface area accessible by the solvent.[254,255] In an aqueous solution, disruptions of the hydrogen bond network of water at the interface due to ligand fluctuations can manifest as changes in hydrophobic interactions that are nonadditive and difficult to anticipate from the chemical structure alone.[256−258] Similarly, ion-mediated interactions can drive anisotropic interactions between particles in solution[259] or lead to anisotropic shell structures.[260] It is already possible to account for the effects of molecular transitions in the shell[261,262] and solvent effects including mixtures on the interaction between apolar NCs.[263,264] The quantification of effects related to assembly kinetics on the final free energy minima, and dependence on perturbations of the structure of the ligand shell in complex solvent environments is however yet to be established.

There are important open questions about the spatial distributions of ligands on the NC surface and the role of unbound ligands. In some cases, the dynamic equilibrium between surface-bound ligands and those in solution may become relevant. Some popular families of ligands bind strongly, such as ligands with thiol end-groups on gold NCs[265,266] (Figure 5d). They establish essentially complete surface coverage, with limitations primarily determined by the molecular shape of the ligand species, except in extremely diluted conditions. Other ligand end-groups (e.g., amines) present a weaker binding, with binding free energies on the order of $k_B T$ or less. NC interactions display sensitive dependencies on the NC and ligand concentrations, temperature, and solvent quality[267] in the presence of these weakly binding ligands. In addition, excess ligands in the solution can

play an important role during assembly and remain in the final dried superstructure.[268] Understanding these effects requires joint efforts in molecular simulation and experimental characterization of NC assemblies.

Another challenge is to anticipate the behavior with the increasing complexity of ligand architectures. Most simulation studies focused on molecular shells composed of linear alkanes, which exhibit well-established order-disorder transitions as a function of temperature, alkyl chain length, and particle size. Even in those simple systems, the physics of dispersion at temperatures below the ligand order-disorder transition, where ligands bundle and relaxation times increase, remains to be understood. Significantly more complex ligand structures, such as ligands that include branched groups or many unsaturated bonds, disrupt chain packing in significant ways[255] and critically influence the stability of the NC assembly.[269] Ligands with multiple chemically distinct segments can lead to apparent spatial variations in chemical properties.[270] NC shells can be synthesized with a mixture of multiple ligands (small molecules or polymers),[271−273] enabling tuning of NC-NC interactions, e.g., for the formation of patchy particles.

The interplay between ligand coverage, NC shape, and interparticle interactions is also an open problem. NCs can have facets of different crystallographic directions, each with a distinct affinity to the ligands.[274] This can result in different ligand densities on different facets, even for a single ligand type, and more complex behavior can arise for mixtures of ligands with different binding groups or tail chemistry and molecular structure. There is evidence that such ligand partitioning between NC facets can be exploited to direct assembly via patchy facet-specific interactions, either with a substrate[275] or other NC,[276] but the full extent of this potential remains to be explored.

3.4.3. Liquid Crystal Solvents. Liquid crystal solvent media permits other ways of controlling NC assemblies[23,277−282] (Figure 5f). NCs induce deformations in the liquid crystal described by its multipole expansion.[23] Such a description introduces an analogy with electrostatics, where the molecular alignment (director field) deformations play a role similar to that of electrostatic charge distributions. By controlling NC shape and surface boundary conditions, multipoles ranging from dipoles to hexadecapoles can be obtained experimentally and modeled theoretically.[23] Design rules come from analogy to electrostatics. When (i) the highly anisotropic interactions mediated by nematic orientational elasticity are further supplemented by (ii) electrostatic repulsions and various steric interactions while (iii) taking advantage of anisotropic NC shapes, then (iv) a large variety of molecular-colloidal condensed matter phases can arise, including various low-symmetry crystalline and liquid crystalline nanocolloidal phases such as triclinic crystals and monoclinic nematic liquid crystals.[23,277,278,280−282]

Dispersing NCs in a nematic liquid crystal has already yielded fundamental breakthroughs in realizing condensed matter assemblies. It enables low-voltage electric switching of various nanocolloidal systems, such as silver nanoplates,[283] which promise technological utility in controlling solar gain of smart windows. Current ongoing efforts and challenges in utilizing this liquid crystal-enabled approach of assembly include (i) establishing the relations between shapes/symmetries of NCs and the ensuing mesophases that can arise from their self-assembly in nematic hosts, (ii) the assembly of lowest symmetry chiral and triclinic nematic

phases with uninhibited fluidity, and (iii) the development of robust means for electric or magnetic reconfiguration of orderly NC assemblies within nematic hosts.

The global liquid crystal industry is over one trillion USD per year and is mainly based on electro-optic uses of uniaxial nematics. Its further growth can be propelled by phases and properties designed and realized by combining the different symmetries of partially ordered NC assemblies with that of the anisotropic fluid host, such as the conventional liquid crystals used in displays. The interplay of the ordering of anisotropic NCs and molecules will allow the development of highly orientationally ordered, low-symmetry liquid crystals with emergent physical behavior of facile responses to external stimuli and properties not yet encountered in currently available materials. On the other hand, the topology of diverse solitonic field configurations in low-symmetry nanocolloidal systems permits hierarchical designs enabled by NC assemblies, where topological solitons such as skyrmions and hopfions[284] define spatial configurations of NC orientations.

4. ASSEMBLY PROTOCOLS

The design of assembly protocols includes the optimization of process parameters that determine a desirable superstructure. Of particular importance is controlling dynamics during assembly. NCs must not move too much or interact too weakly; otherwise, assembly does not occur, and the system remains in a disordered, fluid state. NCs must also not interact too strongly, to avoid irreversible aggregation. Strategies to achieve robust and large-scale NC assembly consist of varying temperature (annealing), varying concentration via solvent evaporation, changing the fluid composition, and utilizing interfaces as a means to induce or guide assembly are all valuable. Other techniques employ external fields, like electrophoretic deposition, a combination with top-down approaches, or are inspired by biological systems.

4.1. Controlling NC Kinetics. Slow or non-ergodic dynamics caused by strong NC attractions can be problematic. In particular, the intrinsic sensitivity of effective NC-NC interactions may prevent reaching equilibrium in multivalent ligand suspensions, such as those with DNA-mediated and other valence-limited colloidal interactions driven by temperature,[285] often resulting in arrested aggregates. Another factor that slows kinetics is related to the stickiness of the multivalent interactions. Sticky interactions prevent pairs of NCs from diffusing around each other while remaining bound, which is a key step for the relaxation of crystal defects.

To improve assembly, it is essential to have access to strategies that accelerate NC kinetics. The relative diffusion between bound NCs can be improved using high ligand coating density,[190] which increases the melting temperature (as a result of combinatorial gain) and the rates at which pairs of ligand-receptor bridges form/open.[286,287] General computational approaches optimize interactions for model systems,[288−290] but a comprehensive understanding of how molecular details affect the emerging motility of functionalized particles remains missing and warrants future investigations. The electronic properties of the relevant building blocks may also provide an avenue for further optimization and control. In the case of atomically precise superatomic NCs,[291] the use of dopants can change the electronic character and symmetry of the molecular valence orbitals and thus change the nature of these interactions.[292] Many experimental efforts have now demonstrated the electronic tunability of these building

blocks.[293] The relative motility of NCs is also pivotal to the development of dynamic materials, such as crystals glued by mobile NCs.[120]
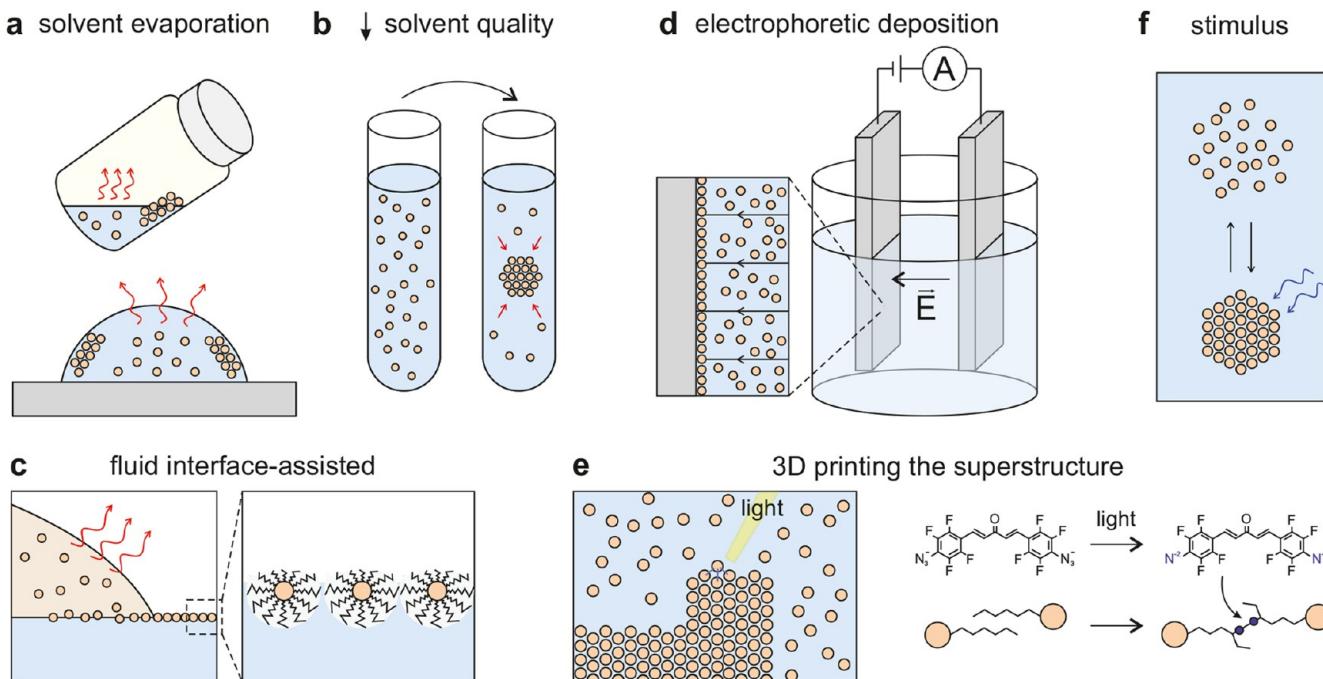
Empirical protocols of NC assembly that slowly decrease and increase temperature have been widely used. It is therefore necessary to understand how to optimize protocols and to identify general principles that guide the choice of cooling rates. At the next level, it would be crucial to embed protocols with on-the-fly feedback to scan parameter spaces autonomously. Advances in this direction have been made, for example, in experiments studying microphase separations in block copolymer systems.[294] Similarly, theoretical work has explored the optimization of experimental protocols for assembly using reinforcement learning.[295,296]

4.2. Varying Solvent Conditions. The most common assembly protocols consist of changing the interaction between NCs by modulating solvent conditions. Solvent-induced self-assembly has been demonstrated in various systems, offering control over NC assembly and disassembly and, in some instances, reversibility.[22,297] Additionally, advances have been made in assembling NCs with complex morphologies, such as Janus NCs.[298] Dynamic self-assembly using solvent gradients and localized solvent addition has also been explored,[299−301] leading to the formation of patterned NC films.[302] To further advance in NC assembly, it is crucial to understand the role of surface ligands,[303] especially in those systems where a single NC can host a multitude of ligands,[304] as well as balancing attractive van der Waals interactions and steric repulsion.

4.2.1. Assembly by Solvent Evaporation. Solvent evaporation is a strategy to assemble at near-equilibrium conditions.[6] The initial state is usually a stable dispersion, and the final state is solvent-free (dry). If solvent evaporation is slow enough, then it may be regarded as a quasi-static process, i.e., a succession of equilibrium states at the particular solvent concentration. This is conceptually similar to hard shape systems, where crystallization occurs as the particle concentration increases, achieving a given packing fraction—approximately 50% for spheres. Long relaxation times might however occur due to activation barriers, and nonequilibrium effects are relevant.

Solvent evaporation starts from a dispersion in which an NC core is stabilized by soluble grafted ligands. Methods include spray drying, evaporation of emulsions ([Figure 7](#)a, top), and drying on solid (superamphiphobic) surfaces[305−310] ([Figure 7](#)a, bottom). When the dispersion dries on a solid substrate, NCs typically assemble into 3D superlattices, which exist as grains in a continuous film or as isolated faceted crystals.[311] Alternatively, solvent evaporation at the air-liquid interface[312] results in extended 2D superlattices, whose width is within 100 nm in a single NC monolayer. With single-component NCs, the structures are fcc or body-centered cubic (bcc),[313,314] although there is evidence for a C14 phase, also named $MgZn_2$,[315] but its stability is not fully characterized. Assembly at the air-liquid interface enables the subsequent exchange of ligands in the NC monolayer, leading to epitaxially-connected NCs.[129,131,316] Including two or more types of NCs leads to a large number of different crystal[317,318] and quasicrystal[319,320] phases. Although most solvent evaporation examples consist of NCs grafted with relatively short ligands, there are examples with dendrimers[321] and long polymers such as polystyrene.[237]

Solvent evaporation is a confined process that involves thermodynamic and transport phenomena of disparate length and time scales, thus requiring the development of theoretical

Figure 7. Assembly protocols for synthesis of superstructures composed of NCs. (a) Assembly by solvent evaporation inside half-opened vials (top) and drop cast (bottom). (b) Assembly by changing the solvent quality. (c) Assembly with the assistance of a fluid interface that induces ordering. (d) Electrophoretic deposition, that is, assembly induced by an electric field. (e) 3D printing of superstructures using NCs as the ink, where a focused light beam activates a reaction that bonds two NCs. (f) Assembly activated by an external stimulus.
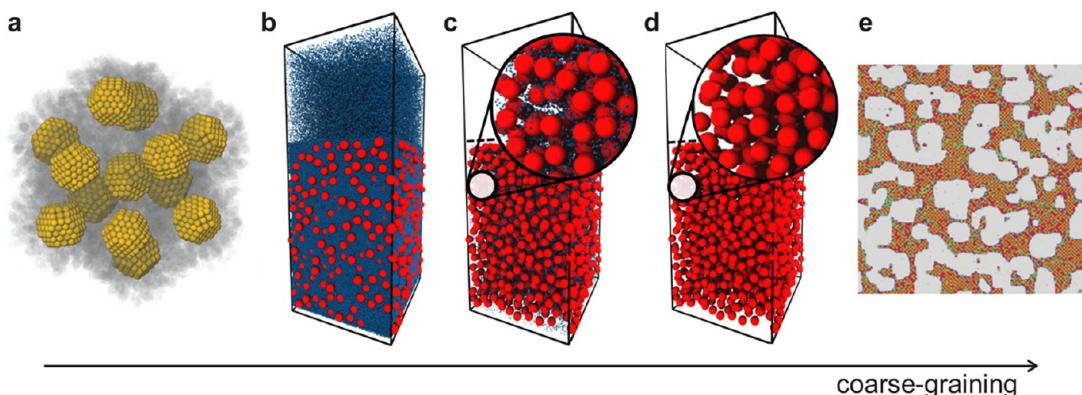
concepts beyond traditional equilibrium frameworks.[322] Additionally, NC interactions can change over time during drying. For example, electrostatic interactions become screened with increasing salt concentration,[323] or the (effective) solvent quality worsens as the composition changes.[324] Depending on processing parameters such as the evaporation rate or the annealing protocol, the emerging structures might get kinetically trapped before reaching equilibrium.[307,325] In NC mixtures, changes in NC interactions can theoretically cause transitions between binary superlattice formation and demixing, which relate to the formation of assemblies of different textures within the same evaporating emulsion.[326]

The case of fast evaporation rates (quantified by large Péclet numbers) is relevant and is encountered in colloidal suspensions[307,308] and during drying.[327] Intricate kinetically trapped structures might emerge, such as composition gradients in multicomponent droplets[308,328] with highly tunable optical properties.[329] Although the driving force behind structure formation remains incompletely understood, recent studies have established that hydrodynamic interactions play an important role in suppressing stratification.[328,330] The open questions include (i) the role of additives such as surfactants, (ii) the impact of surface-stimulated nucleation,[330] and (iii) the effect of macroscopic flow fields within evaporating droplets and films.[331] Another challenge comes with engineering supraparticles using anisotropic NCs, which can become arrested in sparsely packed disordered states,[332,333] including multicomponent cases. Such highly porous assemblies are characterized by large surface-to-volume ratios, making them promising materials for catalysis, as recently demonstrated for the enhanced photocatalytic activity of TiO_2 supraparticles.[334]

As illustrated in Figure 8, bridging the disparate time scales of assembly by solvent evaporation is another challenge.

Within all-atom models,[335,336] timescales are within hundreds of nanoseconds, and length scales in tens of nanometers (Figure 8a). With coarse-grained models coupled to an explicit solvent, the accessible length- and timescales can be extended to microsecond and micrometer scales[337] (Figure 8b), while implicit solvent models can even access time scales on the order of hundreds of milliseconds[308] (Figure 8c,d). Finally, lattice-gas models[338−342] reach time scales of days and virtually infinite spatial resolutions (Figure 8e). However, an inherent challenge of coarse-graining is the softening of interactions and the concomitant (inhomogeneous) acceleration of the dynamics of the system,[343] which can lead to dynamics that overlook intermediate steps and activation barriers that play a relevant role in experiments.

4.2.2. Assembly by Changing Solvent Quality. NCs can be assembled by degradation of solvent quality when, e.g., adding a polar solvent to a stable dispersion of NCs with polystyrene shells.[22] This leads to the formation of a superstructure from a solution of NCs (Figure 7b) and is known as *assembly by changing solvent quality*. It is possible to tune the structure of the resulting assemblies via the length of the polymer chain and the quality of the solvent in, e.g., *N,N*-dimethylformamide (DMF) mixtures with water.[297] The solvent-induced agglomeration of gold NCs with thinner alkylthiol chains leads to an ordered assembly at temperatures above a certain threshold, which is correlated with the order-disorder transition of the shell.[344] Anisotropic particles with sites of different polarity react to changes in solvent quality. For example, Janus particles from organosilica and gold react to changes by forming clusters.[345] Although solvent is often regarded as a catalyst, that is, it allows assembly but does not determine the equilibrium structure, experiments and DFT and MD simulations show that, in some cases, solvent effects determine

Figure 8. Models of solvent evaporation with increasing level of coarse-graining. (a) All-atom simulations showing structure with icosahedron symmetry. Reprinted in part with permission from ref 336. Copyright 2019 Royal Society of Chemistry. (b−d) Simulation snapshots of hard spherical NCs (red) in a drying film, modeled with explicit (b), mesoscale (c), and implicit (d) solvents (blue). The dashed black line in (c, d) indicates the liquid-vapor interface. (e) 2D lattice-gas simulation. Reprinted in part with permission from ref 340. Copyright 2006 John Wiley & Sons - Books.

the geometry and electronic structure,[346] stability,[347] and functionality.[348]

4.2.3. Assembly by Solvent Annealing. Another assembly protocol is *solvent annealing.*[25] Exposure to solvent vapors swells the ligand chains and imparts mobility to the NCs. Solvent annealing can be performed at controlled solvent vapor pressures to attain well-defined NC volume fractions. Starting from a disordered or glassy NC film, the assembly process can be monitored by using in situ X-ray scattering techniques. Fast quenching of solvent-swollen films to the dry state helps to preserve the intermediate structures, allowing their characterization by electron microscopy. Solvent annealing has proven effective in forming one-component[349−351] and more recently, complex multicomponent NC superlattices.[352] It can also be used to improve the degree of ordering or induce structural transition in preformed superstructures.

4.3. Fluid Interface-Assisted Assembly. The absorption of NCs to liquid interfaces is controlled by surface energies. In Pickering emulsions,[353] the oil-water interface is stabilized by adsorbed particles. The adsorption to the interface can be considered an irreversible process with a high energy barrier for desorption from the interface, $E = \gamma_{ow}\pi R^2(1 - |\cos(\theta)|)^2$, where R is the particle radius, γ_{ow} is the oil-water interfacial tension, and θ is the wetting angle.[354] In contrast to the curved interfaces in emulsions, which complicates ordering, adsorption to flat fluid interfaces (e.g., a Langmuir trough) is a strategy for large-area assembly of NCs into monolayers.

Monolayers of polystyrene NCs are easily obtained at the air-water interface.[26] The switch to deformable particles, such as nanogels and microgels,[13] (Figure 6), creates assemblies that depend on the density of NCs at the fluid interface[355] (Figure 7c). In a Langmuir trough, this density can be manipulated through movable barriers.[356,357] Deformable polymer shells also affect the assembly outcome, especially in situations where capillary interactions play a role.[358,359] Furthermore, macroscopically well-ordered, non-close-packed (beyond simplex hexagonal order[360]) monolayers of plasmonic NCs were assembled from plasmonic core-shell microgels at the air-water interface.[355,361]

Microstructural analysis of monolayers prepared via fluid interface-assisted assembly typically relies on microscopy (atomic force and electron microscopy) and scattering (X-ray and light scattering).[362,363] The application of such techniques assumes the microstructure is conserved during transfer to a solid interface and subsequent drying, which might be untrue. Combining ex situ (i.e., after the deposition of the monolayer on the solid substrate) with in situ analysis[364−368] revealed significant changes in the microstructure.[368] This study covers only micron-sized core-shell NCs. In situ measurements are challenging for building blocks below or near the Abbe limit unless markers are used. These however alter the interactions between NCs.

Despite widespread usage of soft and deformable building blocks in fluid interface-assisted assembly and considerable progress in their understanding,[369] many important questions remain. A detailed quantification of interaction forces is necessary, and methods are available, such as using optical tweezers at the interface. An improved understanding of the complex interplay of forces at the interface and upon transfer and drying onto different solid substrates will require better theory and simulations. Additionally, contactless interfacial rheology[370,371] combined with small-angle scattering and/or high-resolution microscopy will provide insights, linking rheological properties to microstructural characteristics. Furthermore, typical Langmuir trough setups operate with uniaxial compression, which can change the isotropy of monolayers made from soft, deformable particles. It is still required to measure and understand such influences and to compare them to radial compression.

4.4. Electrophoretic Deposition. *Electrophoretic deposition* (EPD) involves the use of an electric field to direct the assembly of charge-stabilized NCs onto a solid substrate (Figure 7d). Initially used to assemble gold NCs into densely packed monolayers,[372] it has since assembled rod-shaped NCs with permanent dipoles into dense mono- and multilayer structures.[373] More recently, EPD on patterned substrates was used to control both the position and orientation of individual particles over large areas, including millions of gold nanorods arranged either horizontally or vertically.[374−376] Two important factors comprise (i) using nanoscale lithography to create cavities within an insulating layer deposited on top of the electrode and (ii) optimizing the deposition conditions.

Depositing a wide range of different particle types into well-defined patterns in a scalable way with surface-templated EPD presents some limitations. For example, it is difficult to deposit NCs with diameters below 10 nm due to constraints in surface

charge density and the strength of the applied electric field.[376] Whereas clustering or shelling (e.g., with SiO_2) can be used to deposit smaller quantum dots,[376] finding alternative strategies is desirable. Another open question is how close the NCs can be spaced. Charged NCs approaching the surface pull counterions, creating complex flow patterns near cavities and electro-osmotic effects that still require characterization. Depositing NC mixtures into more complex patterns remains a challenge. Finally, the range and diversity of structures that can be assembled from EPD remain an open question.

4.5. 3D Printing Superstructures. Self-assembly is a bottom-up strategy that can be combined with the top-down strategy 3D printing or additive manufacturing. Research efforts in this direction targeted the creation of 3D-printed nanomaterials using NCs as the ink. To maximally exploit the properties of the NCs in this process without disturbance from the matrix material, usually a polymeric matrix,[377] organic content should be minimal.

A breakthrough was the creation of bulk superstructures by locally controlling NC aggregation (disordered assembly) in solution, triggered by light-induced reactions that connect NCs via shared organic molecules[378] (Figure 7e). This approach initially required specific NC inorganic cores and highly specialized ligands.[379] The concept has since evolved to a stage where the inorganic cores no longer directly contribute to the assembly process. Instead, a light-sensitive additive is added to the particle suspension. Upon irradiation, the additive converts into a molecule terminated with nitrene radicals, which react forming bonds connecting hydrocarbon chains.[380,381] Nitrene radicals can connect (i) ligands of the same NC, locally reducing colloidal stability and bringing the particles closer together, or (ii) ligands of different NCs, thereby creating interparticle links. These developments are promising towards expanding additive manufacturing capabilities to a broad range of NC building blocks.

4.6. Bioinspired Assembly Protocols. *4.6.1. Stimuli-Response Assembly.* To mimic and exploit the intricate functions of natural living systems, research recently focused on systems of NCs that are dynamic and respond to external stimuli by initiating the ordering process (Figure 7f).[382] The challenge is to realize stimuli-responsive NC assembly that is capable of storing information and executing programmed tasks.[383,384] The wealth of available ligands, coupled with the diverse sizes, shapes, and properties of the inorganic cores provides sufficient flexibility to control NC solubility and guides the self-assembly process. Yet, it remains imperative to broaden the scope of NC cores beyond the currently common noble metal cores.

Carefully designed ligand-capped NCs respond to a broad spectrum of stimuli acting on the ligands and/or the cores. Typical stimuli are chemical triggers like solvents, pH levels, metal ions, gases, and biomolecules, as well as physical triggers like temperature, magnetic fields, and electrical fields.[382,385,386] More complex design strategies include (i) employing ligands that react to multiple stimuli, (ii) utilizing multiple ligands, each responsive to distinct stimuli, and (iii) leveraging the inherent properties of the NCs in conjunction with those of the ligands. The goal is to initiate assembly only once all stimuli converge, and the removal of any stimulus prompts disassembly.[382]
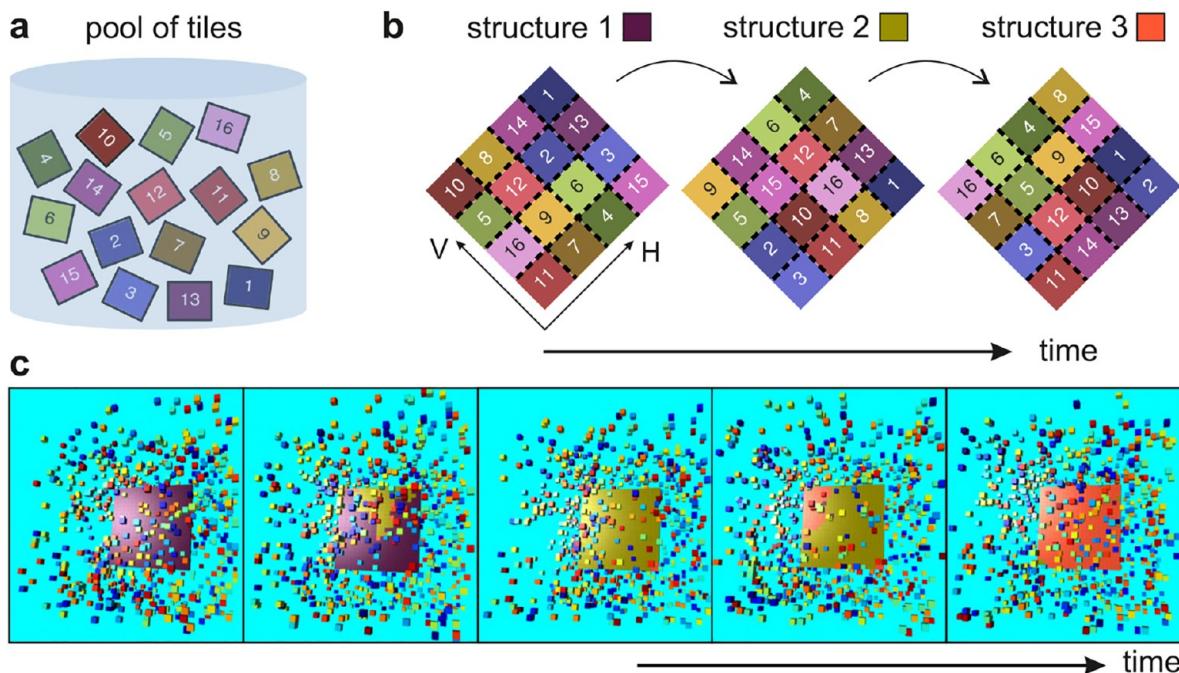
The exploration of practical applications of stimuli-responsive NC assemblies remains largely open. These responsive assemblies might permit delivery systems for drugs, tags, or catalysts, responding to environmental cues for targeted and controlled release. Bioimaging modalities are envisioned utilizing the NCs' ability to alter structures in response to specific biological signals. Furthermore, they could play a crucial role in theranostics, combining therapy and diagnostics by delivering therapeutic agents while offering imaging contrast for monitoring treatment.[387] Beyond healthcare, these NCs have applications in environmental sensing, responsive coatings with functionalities like self-healing, smart textiles that adapt to changing environmental conditions, and even the creation of nanorobots to treat water or remove pollutants,[388] or as soft actuators.[389] Even magnetically responsive colloidal NCs have been used for creating arrays with reversible tunable structural colors that can be exploited as a platform for chromatic applications.[390] Overall, stimuli-responsive self-assembly showcases its versatility and potential for transformative applications in medicine, materials science, and beyond.

4.6.2. Nonreciprocal Multifarious Self-Assembly. Beyond the principle of robust assembly, there is a paradigm termed *multifarious self-assembly*, where a shared set of tiles (i.e., the basic building blocks) is utilized to assemble multiple target structures.[391] This concept draws an analogy to memory formation in matter,[392] where assembly structures are memorized or encoded in tile interactions, akin to learning. Key components include (i) a common pool of tiles, (ii) the desired structures, (iii) an interaction matrix acquired during learning, (iv) and a suitable parameter region in a high-dimensional parameter space of the self-assembly problem.[391,393,394]

A proper design or learning rule defines an interaction matrix between the tiles in a way that the pool functions as an associative memory,[395−397] such that desired structures settle on the minima of the energy landscape of the system. Starting close to those minima, one can stimulate the pool to restore the full structure. Methods of stimulating the pool to assemble the desired structure include introducing a minimal seed extracted from a structure, and changing the concentration of a selection of tiles to lower the nucleation barrier of a specific structure.[391,397] Recent experiments using DNA nanotechnology have demonstrated remarkable promise along these directions .[398,399] Regaining the analogy of NCs with atoms, the multifarious assembly of NCs into superlattices is analogous to the synthesis of atoms into lattices, where the same key components (salts of precursors, ligands, and ions with capping or diffusion-directing effects, and seeds of defined geometry) at different concentrations and synthesis protocols lead to kinetic pathways resulting in diverse NC core habits.

Biological self-assembly utilizes building blocks economically, allowing for disassembly and reassembly of structures in a controlled manner. The nonreciprocal multifarious self-assembly model mimics this behavior synthetically by leveraging nonreciprocal interactions between tiles.[400] Nonreciprocity, breaking action-reaction symmetry, drives systems out of equilibrium,[401−405] enabling the design of time-varying self-assembled structures. A pool of tiles can form various structures (Figure 9a), with the goal of inducing shifts between them in a specific sequence. An example is shown in Figure 9b, where a cyclic sequence of three structures is demonstrated. Proper self-assembly and shifting occur within a limited range of high-dimensional parameter space, and molecular dynamics simulations[400] confirm the feasibility of shape-shifting structures (Figure 9c).

Figure 9. Nonreciprocal multifarious self-assembly. (a) A pool of sixteen distinct tiles can self-assemble into (b) any of three 4 × 4 square-shaped target structures. The goal is to introduce transformations among these structures by introducing nonreciprocal specific interactions between the tiles. (c) Snapshots of molecular dynamics simulation capturing nonreciprocal multifarious self-assembly. The colors correspond to the structures depicted in (b), where structure 1 is colored in purple, structure 2 in dark yellow, and structure 3 in orange. Adapted with permission under a Creative Commons CC BY license from ref 400. Copyright 2022 The Author(s).

Nonreciprocal multifarious self-assembly enhances self-assembly by enabling spontaneous structure formation and transformation without manual intervention. Key questions remain, such as the transition from 2D to 3D structures, that can be addressed by adapting DNA origami techniques.[406] Chemically active colloids providing nonreciprocity through chemical concentration[407] offer another potential solution. Enhancing system capacity, measured by the variety of structures they can remember and transition into, poses a significant challenge.

5. SUPERSTRUCTURE PREDICTION

A general framework that reliably and autonomously predicts the equilibrium superstructure of a given set of building blocks does not yet exist. The development of such a framework is challenging and therefore relies on starting with simple models where superstructure prediction is more tractable. Among the simplest NC descriptions are *hard shape* (HS) models.[408] These models capture many aspects of the equilibrium structure and dynamics of NC assemblies surprisingly well and provide an excellent first level of approximation. However, HS models completely ignore enthalpic (i.e., non-entropic) NC interactions. They also omit the compressibility and conformations of ligands, which are critical for NC assembly as discussed in previous sections.

Whereas HS models have been studied extensively and are generally well-understood, moving beyond HS models is a critical future challenge. Further research is also necessary to advance techniques for (i) estimating free energy at higher precision, (ii) better understanding the role of geometric frustration for superstructure formation, and (iii) advancing the treatment of inverse problems. The latter challenge, inverse problems, is particularly important, as it pushes superstructure prediction into the development of materials with desired functions and properties.

5.1. Hard Shape NCs. Hard shape (HS) models have a long-standing history, in part owing to their elegance and simplicity. Building on the success of analogous models for ionic solids[409] and amphiphiles,[410] the advent of NCs as building blocks for assembly has prompted a flurry of research in this area. Assembly of HS NCs is commonly simulated via Monte Carlo (MC) (Figure 10a,b), and assembly diagrams[411] exist to categorize different polyhedral NC shapes into crystal, liquid crystal, plastic crystal, and glass superstructures (Figure 10c).

Early work on hard tetrahedra showed that instead of a dense packing structure, particles self-assemble into a dodecagonal quasicrystal.[412] It was a big success of the hard tetrahedron model that this highly nontrivial simulation prediction was eventually confirmed in experiments.[413] Other hard shapes self-assemble into a host of mesophases that differ from their densest packing.[414] Many of these mesophases occur in NCs that do not tile space, raising the question of whether mismatches with packing expectations[411,415] were due to some form of geometric frustration. Indeed, many shapes that fill space do not assemble in their densest packing structures.[416,417] The discrepancy between solutions to optimal packing problems and the self-assembled equilibrium structures of HS systems appears to work both ways. Not only do HS generally not form the superstructures in which they pack most densely,[412,–416] materials design of superstructures via digital alchemy also shows a thermodynamic preference for shapes that do not tile them perfectly.[59,417–419]

For systems in which the shapes are approximately hard, more accurate predictions are beginning to emerge from supramolecular chemistry-motivated models. These models are

based on the notion that entropy gives rise to emergent, directional entropic forces among particles[420] that induce a form of bonding.[124,125] This perspective has been corroborated by evidence from the creation of *entropically patchy particles*,[421−423] and by the study of cluster packing,[424] doping simulations,[425] and inverse design.[59] For a given target superstructure, it has been argued that an *eigenshape* should exist—that is, an idealized HS that minimizes the free energy of that structure.[419]

As it relates to NC assembly, the adoption of HS goes back to binary superlattices.[6,317,426] The HS model presents obvious limitations: (i) superlattices exist even at zero pressure, so significant NC attraction (enthalpic contribution) must be present for assembly, and (ii) the shell around the core is usually quite compressible. The HS description can be improved by mapping a given NC to an effective HS eigenshape. For spherical NCs, this is another spherical HS with a diameter that includes the contribution of the ligands. Early studies[6,317,426] defined the HS diameter as the lattice constant of the resulting single component hexagonal lattice, as deposited on a solid substrate. Due to the interactions of the bottom NC with the solid substrate, and the unconstrained ligands at the top of the NC, this definition is relatively inaccurate.[427] One definition is the *optimal packing model* (OPM).[428,429] The HS diameter d_{HS} of a spherical NC with a core radius R and grafting density σ is $\tau = (1 + 3\xi\lambda)^{1/3}$ with $\tau \equiv d_{HS}/2R$, $\xi \equiv \sigma/\sigma_{max}$, and $\lambda \equiv L/R$, where σ_{max} is the maximum grafting density of the core, and L is the extended ligand length. For single-component systems, lattice constants of fcc and bcc are consistent with HS packing with a diameter given by the OPM with some small correction for bcc.[430,431] For *binary NC superlattices* (BNSLs) consisting of two NC types A and B with a ratio of their diameters, $\gamma = d_{HS}^B/d_{HS}^A \leq 1$, where d_{HS}^A and d_{HS}^B represent the diameter of the larger and the smaller HS, respectively. When identifying γ with the same parameter used to characterize the phase diagram of binary HS,[432] there is a correlation between the phases found experimentally and the maximum packing fraction for binary HS. However, there are several significant quantitative deficiencies in the HS description: (i) The measured lattice constant in BNSLs is not generally consistent with HS predictions.[427] (ii) Many phases occur at low packing fractions, where the system is too open to be stable.[427] (iii) Many BNSLs (e.g., $MgZn_2$) have packing fractions below fcc, implying that phase separation into single-component superlattices would incur more efficient packings. (iv) There is a strong dependence of the lattice constant with coordination number[427] (the number of nearest neighbors), suggesting that many-body (nonadditive[251]) effects are of importance. This calls for the development of more advanced and predictive models.

5.2. NC Description beyond HS.

Most NCs are not sufficiently well approximated by HS models and require the introduction of additional enthalpic interaction potentials. Such potentials stem from core-core, core-ligand, or ligand-ligand interactions, which can be short-range (e.g., van der Waals, hydrogen bonding) or long-range (electrostatic). The future success of computer simulations to predict super-structure crucially depends on the quality of the description of the complex energy profile of NC systems.

Models of NC interactions can be pairwise or include many-body terms. Figure 10d,e presents a snapshot of an MD simulation of the assembly of non-HS NCs and the inhomogeneous average ligand density that plays a role in the interaction between NCs.[324] In this simulation, the behavior of the ligands approximates an incompressible elastic medium. Pushing the ligand shell on one side affects the elasticity of the shell on the opposite side. This means that incompressible ligand shells can be modeled only by including a description of many-body effects.
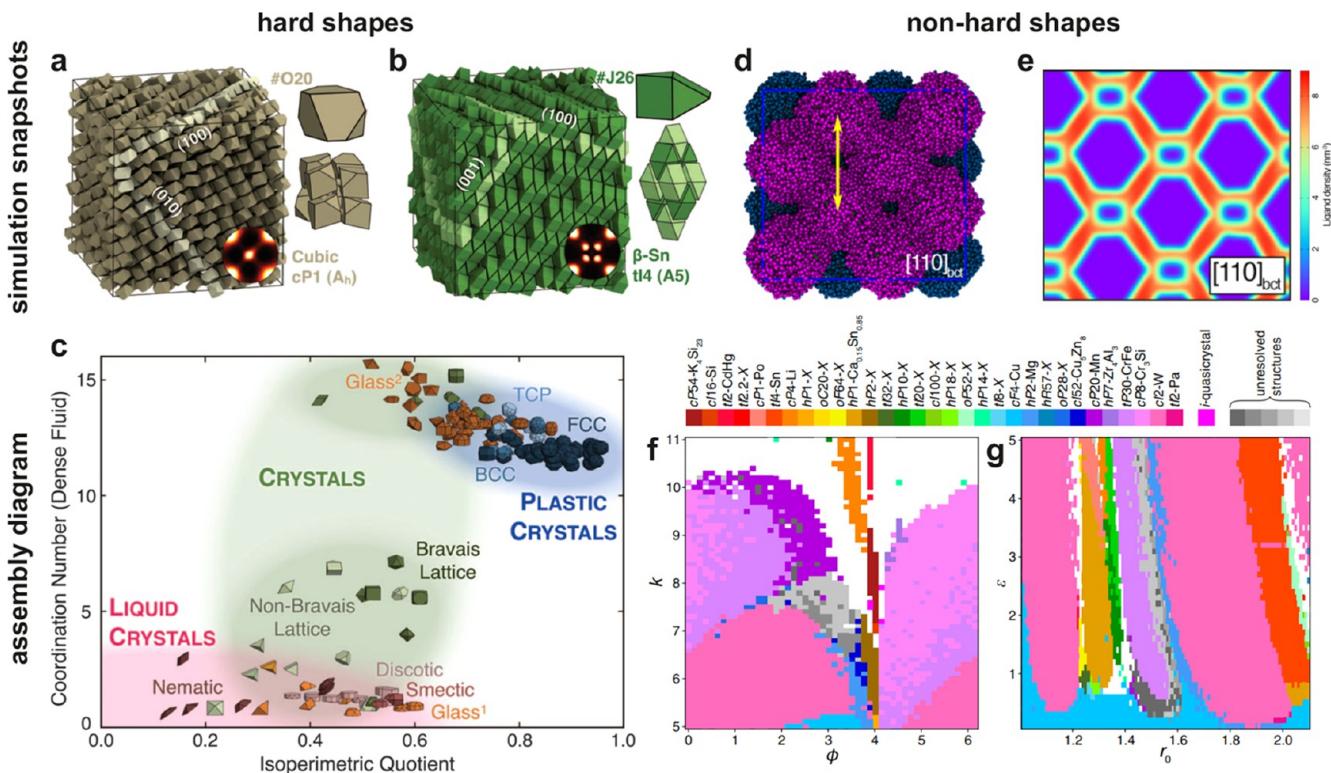
This section briefly explores four strategies beyond the HS approximation that improve specific aspects of the model description. These strategies are (i) quasi-spherical NCs, in which isotropic pair potentials target superstructures by tailoring local order, (ii) the orbifold topological model, which aims to describe the deformability of the ligand shell and resulting many-body effects, (iii) coarse-graining strategies, which aim to understand effective interactions at the mesoscale and describe them via a multiscale modeling approach by reducing model complexity, and (iv) machine-learned interaction potentials, which aim to provide more accurate models trained directly on ab initio data. Beyond these individual strategies, future work may also combine ideas from multiple strategies into an even more comprehensive model.

5.2.1. Quasi-Spherical NCs. We term an NC model as *quasi-spherical* if the spherical shape is a good approximation of the NC. The most obvious modification is a softer potential. A simple ansatz is pair potentials with an appropriately chosen radial dependence. Power-law pair potentials are capable of stabilizing crystal phases,[433] including quasicrystals,[434] depending on the softness of the interaction.

More structural diversity is uncovered when the radial dependence of the potential is varied further by adding a shoulder[435] or multiple wells. An example is the *oscillating pair potential*[126] (OPP), which has the form $V(r) = r^{-15} + r^{-3} \cos(kr + \phi)$ and depends on two parameters k and ϕ. Figure 10f presents the phase diagram of superstructures formed using this model.[126] A comparable level of structural complexity also appears in a different quasi-spherical NC model using the Lennard-Jones-Gauss potential (Figure 10f). A virtue of these multiwell pair potentials lies in the fact that they are minimal models to perform simulations of superlattices of interest characterized only by the crystallographic structure of the superlattice. That the OPP and related potentials were originally designed to model interatomic pair potentials incorporating Friedel oscillations[436] is not an issue because fundamental dynamical and structural processes are universal across scales from atoms to NCs. These quasi-spherical models can successfully reproduce the majority of crystal structures found in the periodic table of elements and beyond.[126] This suggests that simple classical models (i.e., ignoring quantum effects) are fully sufficient for the description of basic dynamic and geometric aspects of NC superstructures, including their formation pathways and defects.

Likewise, generalizations of binary[432,437] or size-disperse[438] HS mixtures make the interaction softer, for example, by using binary Lennard-Jones[439] or power-law[440] potentials, or by adding an attractive term to the potential in the form of an inverse power-law.[440,441] These approaches reproduce most of the binary phases found in experiments and permit studying details of superlattice nucleation and growth.[442,443] Never-theless, just like identical particle counterparts,[126] the binary model systems[444] include many phases in their assembly diagrams not yet observed with NCs. This means there are either more NC superlattices to be discovered or that the models describe interactions that cannot be realized with NCs.

Figure 10. Simulation snapshots and assembly diagrams for hard and non-hard shapes. (a, b) Example snapshots of MC assembly simulations of HS from disordered fluids.[411] The inset shows the NC shapes that form cubic (a) and β-Sn (b) superstructures. (c) Assembly diagram[411] of polyhedral HS assembled into crystals, liquid crystals, plastic crystals, and glasses projected on the parameters of coordination number (the number of nearest neighbors) and isoperimetric quotient (a measure of sphericity). (d) Example snapshot of MD assembly simulation of non-HS, octahedral NCs with C_{14} ligands forming a bct superstructure.[324] (e) Average ligand density in the simulation snapshot shown in (d), in units of ligand beads per nm^3, viewed in the [110] direction.[324] (f, g) Phase diagrams[126] of superstructures formed by NCs modeled as quasi-spherical using (f) the oscillating pair potential and (g) the Lennard-Jones-Gauss potential. Predicted phases, indicated by colors, are described by Pearson symbol and representative compound. (a–c) Reprinted in part with permission from ref 411. Copyright 2012 The American Association for the Advancement of Science. (d, e) Reprinted in part with permission from ref 324. Copyright 2019 American Chemical Society. (f, g) Adapted with permission from ref 126. Copyright 2021 The Author(s).

5.2.2. Orbifold Topological Model. Given the current difficulties in developing a predictive theoretical framework, a more modest problem is to predict the structure of NCs within a given crystal. For the case of spheres, the *orbifold topological model* (OTM)[153,445] provides a solution to this problem, which has been verified through extensive simulations[252,446] and experiments.[447] The OTM describes NCs as pseudotopological objects such that, at low coordination, ligands may show large deformations called *vortices*. The model naturally incorporates many-body effects without adding extra parameters, and predictions of lattice constants and packing fractions agree well with experiments.

One open challenge lies in extending the OTM to describe geometries other than spheres. The case of cubes has already been developed.[318,448,449] Cubes interacting through their faces behave as hard cubes, whereas when interacting through vertices or edges, ligands splay (i.e., form vortices) enabling a closer approach than that of hard cubes. The breakdown of the description of the HS by vortices shows that the previously discussed concept of eigenshape further depends on the environment and NC relative coordination, and it is not a property of the NC alone. However, OTM does not provide free energy. A pressing open problem is in developing a standard NC model with computationally tractable free energy that (i) predicts the phase diagram as found in experiments,

(ii) provides the correct lattice constant, reproducing the OTM predictions, and (iii) systematically accounts for subleading effects. Mean-field models may provide such a description and close this important gap.

5.2.3. Coarse-Grained Models. The idea of coarse-graining is to approximate the essential aspects of a fine-grained model (i.e., a description at high resolution) by reducing the number of degrees of freedom. NCs are comprised of a core and a ligand shell containing a total of many thousands up to millions of atoms that interact while moving in a solvent environment. Coarse-grained models treat all or parts of the ligand shell and/ or the solvent implicitly.

Nearly atomistic MD simulations demonstrated that ligands can show highly collective behavior including order-to-disorder transitions as a function of temperature, facet dimensions, and ligand coverage.[450] Such emergent phenomena are critical for modeling interactions between NC building blocks.[275] We are only beginning to understand the role of the solvent for colloidal solubility and agglomeration.[261,451] Scaling up simulations from pairs of NCs to dozens of NCs, which is necessary to evaluate superlattice stability, requires a coarse-grained description of ligands and solvent effects. Such a coarse-grained description is required to reproduce experimentally observed superstructures[324] and interfacial self-assembly phenomena.[452] Examples of successful coarse-grained

models applied to NCs are the Martini force field[453] and united-atom force fields.[252,264]

Toward even larger NC systems, as necessary for simulating superlattice nucleation from a melt of initially disordered NCs, the degree of coarse-graining has to be even higher. This means the ligand shell must likely be omitted from the model entirely. Reported modelling strategies include machine-learned effective many-body potentials for anisotropic particles using orientation-dependent symmetry functions[454] and tabulated (pre-computed) pair potentials for predicting programmable nanoprism assembly.[9] Research on such highly coarse-grained models is in its infancy, and research strategies are heterogeneous. The optimal resolution and model specifics depend crucially on the scientific question. In the future, it is desirable to develop efficient codes and libraries that standardize and accelerate the modeling process.

An important aspect of developing coarse-grained models for NC interactions is the ability to test them on experimental data. Until a few years ago, NC self-assembly was a black box method, in which only the initial state (solution of dispersed NCs) and the final state (dried NC superlattice) were well characterized. The situation recently changed with the advent of in situ electron microscopy methods. Trajectory sampling of particle motion[455,456] allows direct comparison to and validation of coarse-grained computer simulation models. Even the direct observation of the superlattice formation process itself is becoming directly accessible to these methods.[457,458] It is expected that improved methods of coarse-grained modeling and in situ microscopy must be combined to correlate controlling factors to the resulting structures.[459]

5.2.4. Machine-Learned Interaction Models. Fueled by remarkable achievements in the industrial realm, numerous research initiatives have delved into *data-driven artificial intelligence* (AI) and *machine learning* (ML) methodologies. ML approaches seek to construct a surrogate model by establishing an implicit connection between the structures of chemical or material systems and one or more target properties. The development of a predictive ML model using supervised learning usually entails an iterative training process on a reference ground-truth dataset. This dataset may be comprised of quantum mechanical simulation and/or experimental data for the target properties (or labels) corresponding to all structures. Once adequately trained, the model can function as a black-box tool.

To train and utilize ML models, chemical structures in the form of atomistic or geometric specifications of the NCs are essential inputs. These specifications can be represented as arrays of atomic numbers, which are then converted into a format readable by machines. For instance, employing a chemical structure as input and aiming to predict energy as output forms the basis of designing ML interatomic potentials for conducting large-scale molecular dynamics simulations.[460,461] Training machine learning models hinges on the automated tuning of hyperparameters to attain optimal accuracy for a given dataset, typically with little to no human intervention. This parameter adjustment is achieved by minimizing a cost function that quantifies the error of the model by comparing the reference value to the ML-predicted average across all training data points.

A significant category of ML algorithms falls under the umbrella of *kernel methods*.[460] In these methods, the ML practitioner defines a kernel function, which acts as a metric for assessing the similarity between two inputs, such as two local atomic environments. The higher the degree of similarity measured by this function, the better the outputs of the model are expected to be. In techniques like *kernel ridge regression* and the *related Gaussian process regression*, the complexity of the model inherently increases with the size of the dataset. Another extensive category of methods comprises models based on *neural networks* (NN). NNs are immensely flexible, nonlinear functions characterized by thousands to millions of parameters. These parameters are fine-tuned to match a dataset. The substantial number of parameters offers numerous degrees of freedom, enabling an optimization algorithm to determine the most effective transformation that converts the input into an estimation of the desired property.[461−463]

Machine-learned models for non-HS interactions between NCs require a training set comprising the geometry of NCs and their corresponding reference energies. A critical concept in ML is the generalization error. ML models can be susceptible to overfitting. This occurs when the model becomes proficient at fitting the training data but fails to make extrapolations. The process of choosing and expanding the training dataset is a pivotal concern during the development of predictive machine learning models. These method-ologies offer the potential for automated, iterative enhancement of the training dataset. Active learning algorithms[464,465] achieve this by incorporating additional data points within the underrepresented phase space through uncertainty quantification, all while minimizing human bias in the data selection process.

There is a clear current trend of replacing traditional force fields with models derived using ML methodologies, which are now gradually making their way to a variety of molecular dynamics codes.[460−462] This progress potentially facilitates large-scale molecular dynamics simulations, for example, predicting equilibrium structures of NCs or even describing the growth and formation of the NCs. An example is ML interatomic potentials based on DFT simulations of gold.[466] This framework was then used to model the melting dynamics of gold NCs and characterize their liquid atomic arrangements.

Despite these advancements, several challenges still need to be addressed before ML models can fully realize their potential for simulating NCs and their assemblies. An accurate description of long-range interactions encompassing both electrostatic and dispersive forces is of paramount importance. In contrast, the majority of ML potentials rely on a locality approximation, often constrained by a specific distance cut-off for characterizing the local chemical environment, as commonly employed in NN models. Development of various charge equilibration schemes and explicit integration of electronic charges and spins into ML architectures accurately describe molecular charged species, long-range electron transfer, and dispersive forces.[462,467]

Another critical feature of NC assemblies is their immense structural and conformational diversity. This complexity poses challenges when implementing active learning techniques to generate training databases, often requiring a trade-off between the generality and specificity of the resulting models.

5.3. Free Energy Estimations. The equilibrium nature of binary nanocrystal superlattices (BNSL) observed in the literature remains uncertain. It is not yet established whether they represent stable configurations or metastable states that should eventually phase separate into two single-component superlattices.[6] The fact that different experimental strategies—

including microfluidics,[468] evaporation of a solvent on solid support,[317,469,470] and emulsification of the solvent[309,310,471] into large micelles—lead to the same BNSL phases corroborates with the argument that BNSLs are equilibrium states. Methods consisting of tuning hydrophobic interactions by solvent quality[22,472,473] predict interesting structures for a small number of NCs[474,475] but are unsuccessful in assembling BNSLs and always lead to single-component phase-separated systems.[476]

Free energy calculations with all-atom models could settle the question of whether BNSLs are equilibrium or metastable states. Unfortunately, the few free energy calculations available using all-atom[446] or coarse-grained models[477] have shown a difference in free energy between the BNSL and a phase-separated single component of a few k_BT per NC, which is within the accuracy of free energy estimations. Despite these calculations being somewhat inconclusive, the free energy estimations show that regardless of what is the equilibrium state, it is only marginally stable. Therefore, interactions that may appear as subleading (e.g., dipole-dipole and van der Waals forces between NC cores) may ultimately be critical in stabilizing the superstructure. It remains an outstanding challenge to quantify these subtle free-energy balances.

5.4. Geometric Frustration. Geometric frustration is a cooperative phenomenon where the pairwise interactions in a structure cannot be all simultaneously minimized. Whenever the locally favored relative arrangement of the building blocks cannot be realized globally, the resulting structure will inevitably be frustrated. In some cases, frustration can be resolved locally at the scale of a single or a few unit cells (for example, through the proliferation of defects), leading to a uniform strain. However, if the mechanisms for locally resolving frustration are energetically unfavorable, frustration will build up and manifest as a nonuniform strain that grows in magnitude as the assembly grows in size. The associated elastic energy grows super extensively and, in its early stages, follows one of a handful of universal growth exponents. This phenomenon was recently termed as *cumulative geometric frustration*.[31] However, the super-extensive growth of the elastic energy cannot persist indefinitely, and different systems show different mechanisms for frustration saturation. Thus, systems that exhibit cumulative geometric frustration are typically small in size and are associated with weak frustration. Moreover, their building blocks (or their interactions) are soft enough to allow for the required relative strains. If l_g is a geometric length scale associated with the frustration, and l_s is the typical linear dimension of the system, then $l_s \ll l_g$ is necessary for frustration accumulation.

Frustration has been shown to play an important role in determining the shape, residual stress profile, and response properties in a wide variety of assemblies including liquid crystals,[478] filament bundles,[479] twisted molecular crystals,[480–482] and frustrated *xy*-like lattice spin models.[483,484] A recently introduced framework aimed at the continuous description of frustrated assemblies[31] has enabled the quantification and classification of the different types of frustration. Consequently, the super-extensive energy exponent $\lambda > 1$, which satisfies $E \propto M^\lambda$, where M is the mass of the system, can assume only a handful of values according to $\lambda = 1 + 2\eta/d$, where $d = 1, 2, 3$ is the dimensionality of the system, and $\eta = 0, 1, 2, 3, \ldots$ denotes the first non-homogeneous order in the expansion of the compatibility conditions.[31] The rate at which the strain energy builds up in an assembly as it grows predicts if a given

assembly will saturate at a finite size[485] or determines the spacing between the packing defects that absorb growing strains.

While it is possible to tile a plane with equilateral triangles, it is not possible to tile the 3D space with regular tetrahedra,[486] which is the analog of an equilateral triangle in 3D. However, tetrahedra can tile certain types of curved spaces. Such curved spaces represent the ideal ground state for general crystals, and the actual crystal state in 3D is just a frustrated version that is unattainable due to the lack of curvature.[486] *Frank-Kasper phases*,[487] which are quite common in NC assemblies,[33] are phases in which the frustration inherent in regular tetrahedra is relieved by topological defects (disclinations). Frustration in tetrahedral (also known as topologically closed-packed) networks also connects to theories of the glass state.[488–490] There are examples of the role of tetrahedral order (and closely related icosahedral) in NC assemblies.[32,33] The role of geometric frustration is ubiquitous in NC assemblies, and its systematical study is important to design frustrated interactions to produce desired complex structures.

5.5. Mean-Field Theory. *Self-consistent field theory* (SCFT), a type of mean-field theory, has been successful in the study of ordered phases self-assembled from polymeric systems such as block copolymers.[491] Recently, SCFT and other mean-field approaches have been applied to the assembly of NCs by solvent evaporation[492–494] and to NCs dispersed in polymer melts.[495,496] Existing approaches can be categorized into two types. In the first type, the cores, the ligands, and the solvent are all described in terms of density fields.[496] A major challenge in this strategy is to capture core-core excluded volume correlations. In this context, *fundamental measure theory* (FMT, a hard-sphere functional) stands out as a promising solution to predict the thermodynamic stability of hard-sphere superlattices.[494] FMT has also been combined with SCFT to model ligand-coated NCs[497,498] and was applied to single-component and binary mixtures of hard spheres.[499] It remains a challenge to combine these breakthroughs into a theory of ligand-coated NC superlattices.

The second type of mean-field approach to model NC assembly keeps a field-based representation of the ligands and the solvent but adopts a particle-based representation for the NC cores—i.e., the cores are modeled as regions inaccessible for the ligands and solvents.[492,493,495] The diffusion timescale of NCs is much larger than the characteristic timescales of molecular motion. Therefore, in a classical analogy to the Born-Oppenheimer approximation, the solvent/ligand degrees of freedom can be integrated for fixed core positions. A hybrid simulation scheme based on this approach was developed,[495] in which the interparticle forces obtained by solving the solvent/ligand problem were used to evolve the position of the cores in a small-time step. This strategy does not require any a priori knowledge of the final structure, but its long equilibration time may preclude its use to model the formation of superlattices.

Alternatively, the NC cores can be fixed to the lattice positions of different candidate crystalline structures. The free energy resulting from integrating the ligand/solvent degrees of freedom for fixed NC cores can then be used to choose the equilibrium structure. While the direct free energy estimation of superlattices is a great advantage of this method, its range of applicability remains small compared to molecular dynamics (MD) simulation. Consequently, future work should expand its scope to other relevant problems in the field including binary

systems and different ligand chemistries and eventually couple it to MD.

Mean field models also account for the presence of the solvent and its evaporation. The fcc-to-bct-to-bcc sequence of phase transitions in dry lattices of alkanethiol-coated NCs was shown both experimentally[314] and theoretically[428,430,492,500] to depend on the dimensionless parameter $\lambda = L/R$, where L is the fully extended ligand chain and R is the NC radius. A mean-field molecular theory for superlattices has recently shown that this transition can also be triggered by changing the amount of solvent in the system,[492,493] i.e., swelling of superlattice by solvent, both in spherical and nonspherical (cuboctahedral) NCs. Interestingly, decreasing the solvent content during the last steps of assembly induced by evaporation[349,501] or lowering the quality of the solvent in wet NC superlattices by the addition of a nonsolvent[155] leads to a transition from fcc to bcc. This observation suggests that the underlying mechanisms may share similarities, although a detailed understanding would require improving the description of the solvent in mean-field theories of NC assembly to address vapor-liquid phase equilibrium and solvent-nonsolvent mixtures.

5.6. Inverse Methods. An important open question is the definition of valence of NCs. The definition of valence of NCs would imply an a priori prediction of the NC superlattice with accuracy as high as that accomplished for molecular bonding and crystallization of atoms in chemistry. The challenge is that the building blocks composed of NCs and ligands vary continuously in the parameter space, as opposed to the discreteness of the periodic table coming from quantum scales. Recent efforts apply a reverse strategy that starts from a target structure and works backward to design building blocks that assemble the target structure best.[59,419] This inverse design approach has two key virtues, (i) it starts from the target structure of the material, which is closer to the ultimate goal of the materials development process, and (ii) it introduces means by which superstructures can reveal their preferred building blocks, thus providing clues about optimal building block features.

An example of inverse design in HS models is the *alchemical Monte Carlo* method,[59] which takes a set of target structures and generates billions of associated preferred shapes of the building blocks. These sets of preferred shapes can differ along hundreds of anisotropy dimensions, and then machine learning or other big data classification methods can be used to construct heuristic associations among building block features and structures.[502] In addition to applications in hard particle models, inverse-design approaches have also been applied to design enthalpic interactions.[418,503−506] Challenges remain in describing the nonconvexity of shapes and the effects of ligands. However, the fact that high-dimensional parameter spaces can be reduced to a handful of key parameters suggests that combinations of inverse design and big data approaches provide a promising way forward.

6. DYNAMICS OF NC ASSEMBLIES

The assembly of NCs undergoes the basic steps of crystallization comprising (i) nucleation, which can be either classical or nonclassical depending on the assembly protocol and conditions, and (ii) growth, determining the size, shape, and surface morphology of the final superstructure. The involved kinetic pathways of assembly are determined by the free energy landscape of the system, where certain paths can lead to the formation of defects and grain boundaries that might kinetically trap superstructures in local minima. The consideration of metastable superstructures in simulations greatly enhances assembly prediction. If those metastable states are sufficiently long-lived, then they are as relevant and practical as equilibrium superstructures. The theories for crystal nucleation and growth of atomic crystals have served as inspirations for understanding the assembly of NC-based superstructures. As already discussed in the section about NC cores, there are many examples of useful metastable states of NC habits that are not the equilibrium Wulff shape. One could therefore expect the analogous for metastable superstructures.
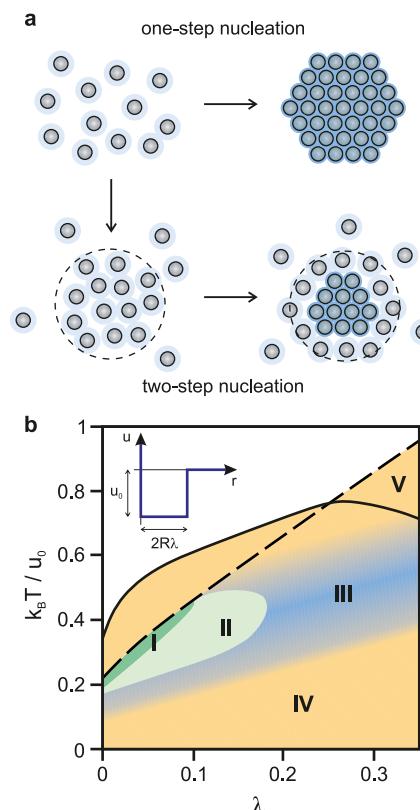
6.1. Nucleation of NC Clusters. Even if the predicted superstructures are confirmed to be thermodynamically stable, kinetic effects may render them inaccessible. Disorder-order transitions are often first-order phase transitions and proceed through nucleation and growth mechanisms. During nucleation, a sufficiently large nucleus of the ordered phase emerges within the disordered phase, which then grows to reach thermodynamic equilibrium during the growth stage. At sufficiently small driving forces (i.e., close to co-existence), nucleation is generally the rate-limiting step, since the free energy barrier for the formation of a critical nucleus, also known as the nucleation barrier, generally exceeds k_BT considerably. Although nucleation is generally a single-step process in most pure systems (i.e., nucleation from within the melt), it may as well comprise multiple steps when dealing with NC assemblies.[27] Characterizing the kinetics, free energies, and the mechanism of nucleation provides a natural way of determining the kinetic pathways that are actually accessible to a disordered system under different conditions and can assist in identifying the structures that are not kinetically accessible. Moreover, understanding the nucleation kinetics and mechanism can help devise pathways that lead to structures that are thermodynamically metastable but possess superior functional properties.

The principles that determine the kinetic accessibility of NC superlattices remain addressed primarily computationally, despite rapid advances in in situ electron microscopy. Advanced sampling techniques, such as *umbrella sampling,*[507] *metadynamics,*[508] *transition path sampling,*[509] *transition interface sampling,*[510] and *forward flux sampling,*[511] are an excellent toolkit to study kinetics and mechanism of nucleation over a wide range of timescales. There is a rich history of using such techniques to study the nucleation of NC model systems, such as hard spheres[512−516] and hard polyhedra.[517−519] A significant challenge consists of harnessing this body of work into computational methods to predict the nucleation of NC clusters, where quantities like the chemical potential and the liquid-solid interfacial energy are not easily accessible.

Another challenge pertains to formulating proper descriptions of heterogeneous nucleation, which often constitutes the dominant pathway for the formation of NCs. Experimentally, it is fairly challenging to predict heterogeneous nucleation rates due to uncertainties in the types of impurities present within a solution.[520] Moreover, it has been recently demonstrated that traditional definitions of crystallinity break down in describing the physics of heterogeneous nucleation even on the simplest surfaces,[516] even when nucleation is still a single-step process. This highlights the importance of devising more robust descriptions of structure and its interplay with the outcome of heterogeneous nucleation. It is also imperative to understand situations in which heterogeneous nucleation exhibits

deviations from the classical picture provided by Turnbull and Vonnegut.[521] These explorations are critical for constructing predictive models that can be used for estimating the rate of heterogeneous nucleation as a function of operational variables under different experimental conditions.

An important case for models that go beyond critical nucleation is the two-step nucleation mechanism introduced for globular proteins.[522] It involves the formation of an intermediate disordered phase with a high concentration of particles, so nucleation occurs within the intermediate phase (Figure 11a), with a lowered nucleation barrier. Computational

Figure 11. Nucleation of NC assemblies. (a) Schematic representation of one-step and two-step nucleation processes. (b) Probability of superlattice nucleation represented by color gradients, where green is high, blue is intermediate, and yellow is a low probability. The axes represent the depth u_0 and range λ of a square-well potential, as represented in the inset, for colloidal particles with radius R and a volume fraction of 0.1. The diagram shows the regions of (I) one-step nucleation, (II) two-step nucleation, (III) the coexistence of two metastable fluids with a slow nucleation rate, (IV) gel formation, and (V) a thermodynamically stable colloidal fluid. The dashed line is the metastable fluid-fluid binodal curve. The solid black curve is the thermodynamic boundary for the stability of an fcc crystal. Adapted with permission from ref 27. Copyright 2022 The American Association for the Advancement of Science. Based on data of ref 21.
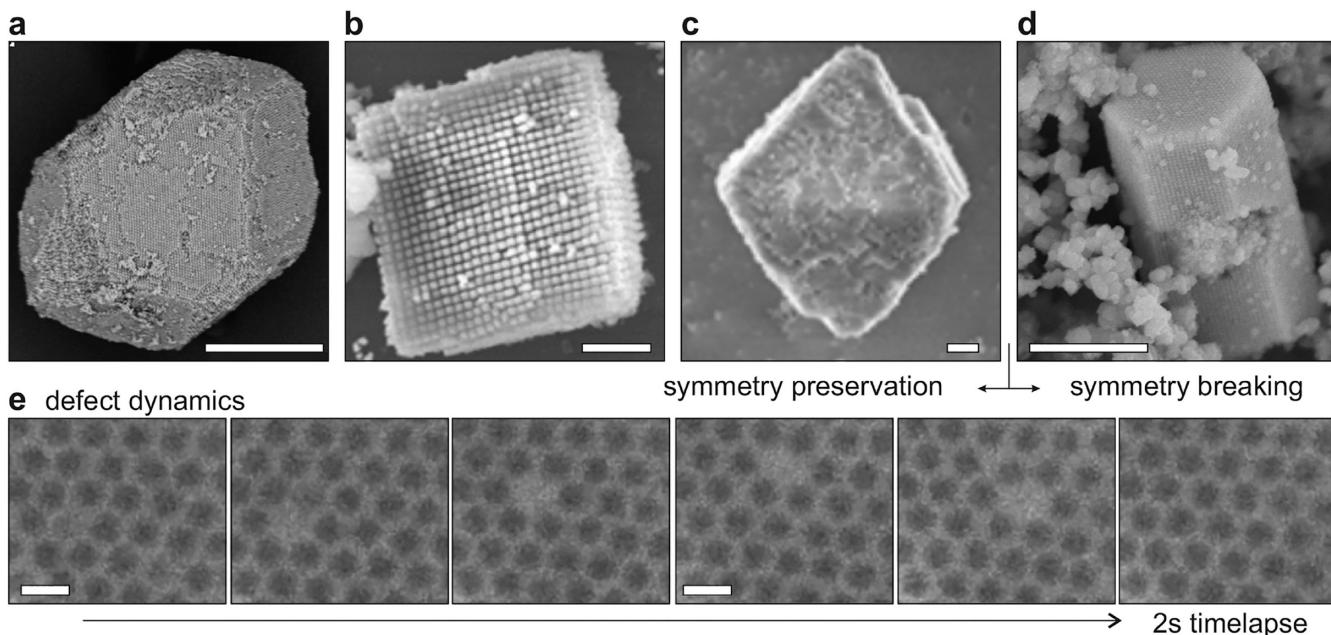
studies predicted two-step nucleation for spherical colloids with short-ranged attractive potentials (Figure 11b).[21] More recently, simulations considering complex hard polyhedral shapes showed a two-step nucleation process where nucleation occurs from a high-density precursor fluid phase with prenucleation motifs in the form of clusters, fibers and layers, and networks.[518] In addition to these computational efforts, advanced in situ characterization methods allow experimental

observations of nucleation. Two-step nucleation of NC superlattices was observed by transmission electron microscopy (TEM) and small angle X-ray scattering (SAXS) studies of NC assemblies,[27,523,524] where crystalline structures grow from amorphous aggregates. While SAXS provides bulk ensemble characterization of structural evolution in reciprocal space, liquid-phase TEM—sealing solution samples against the high vacuum of TEM for imaging at the nanometer and millisecond resolution—resolves NC dynamics, interaction, and crystallization pathways in real space with single-particle tracking.

6.2. Superstructure Growth. The length and energy scales associated with NC assembly are dramatically different than those in atoms or simple molecules. The larger timescales and sizes of NCs make direct, real-space observation of these assembly processes more feasible than their atomic counterparts, permitting detailed experimental verification. Nevertheless, the length scale has a major effect during crystal growth. For example, larger crystalline clusters of NCTs[154] are associated with (i) slower cooling rates, consistent with classical nucleation theory, but also (ii) higher concentration of NCTs, opposing classical nucleation theory. This unexpected behavior was explained as a function of the significantly lower diffusion constants and concentrations of NCs in solution compared to atoms in a melt or in solution. Additionally, while the size of the NCT crystallites increased with slower cooling rates, the degree of crystallinity was equally high for all systems regardless of the thermal assembly path. The ability to form high-quality crystals at rapid cooling rates was attributed to (i) the highly dynamic nature of the supramolecular bonding that permits fast reorganization of NCs upon binding, and (ii) the softness of the polymer coating that enables particles to easily accommodate deviations in suboptimal binding. Yet, it remains an open question to assess the generality of these statements and to develop actual quantitative methods that can be experimentally verified.

In addition to the length scale effect due to the larger size of NCs compared to atoms, NCs also present different growth behaviors due to the extended interaction range. As shown in both liquid-phase TEM observations and KMC simulations,[525] inter-NC interactions can significantly modulate in-plane and step-edge diffusion barriers. This gives rise to four growth modes for NC assemblies, permitting wide control over the surface morphology and bulk defect densities in superstructures. These observations call for comprehensive modeling considerations of inter-NC interactions and mass transport dynamics to enable crystal engineering.

Wulff construction models[89,90] capture the assembly of NCs, giving rise to superstructures with habits (superhabits) composed of cubes,[526] octahedra,[526] and rhombic dodecahedra[28] (Figure 12a–c). These superhabits comply with the symmetry of the superlattice. *Plane multiplicity* in alloys of NCs—that is, the existence of planes of the same crystalline orientation with different compositions of NCs—can lead to symmetry breaking.[29] KMC was able to show the existence of nucleation barriers in the crystallographic directions that contain plane multiplicity when a layer of NCs that present a higher surface energy grows over a layer of NCs with a lower surface energy, leading to the suppression of some crystalline growth directions and the formation of superstructures with rod-like superhabits[29] (Figure 12d). The analogy between atoms and NCs helps understand the growth process. Just like certain NC core habits break the symmetry of the underlying

a

b

c symmetry preservation ← → **d** symmetry breaking

e defect dynamics

2s timelapse

Figure 12. Microscopy of superstructures formed of NCs. (a−d) Scanning electron microscopy of superhabits formed by the assembly of DNA-functionalized NCs. Superhabits can preserve the symmetry of the superlattice, forming (a) rhombic dodecahedra,[28] (b) cubes,[526] and (c) and octahedra;[526] or break symmetry as shown in (d) via the formation of energetic barriers in certain crystallographic directions due to plane multiplicity of the AB₂ superlattice formed by an NC alloy.[29] **(e)** Liquid cell TEM showing a vacancy diffusion in a superstructure, evidencing the dynamics of superstructure defects.[457] Scale bars, 1 μm (a−d) and 100 nm (e). (a) Reprinted in part with permission from ref 28. Copyright 2014 Springer Nature BV. (b, c) Reprinted in part with permission under a Creative Commons CC BY license from ref 526. Copyright 2016 American Chemical Society. (d) Adapted with permission under a Creative Commons CC BY license from ref 29. Copyright 2018 Springer Nature. (e) Reprinted in part with permission from ref 457. Copyright 2022 American Chemical Society.
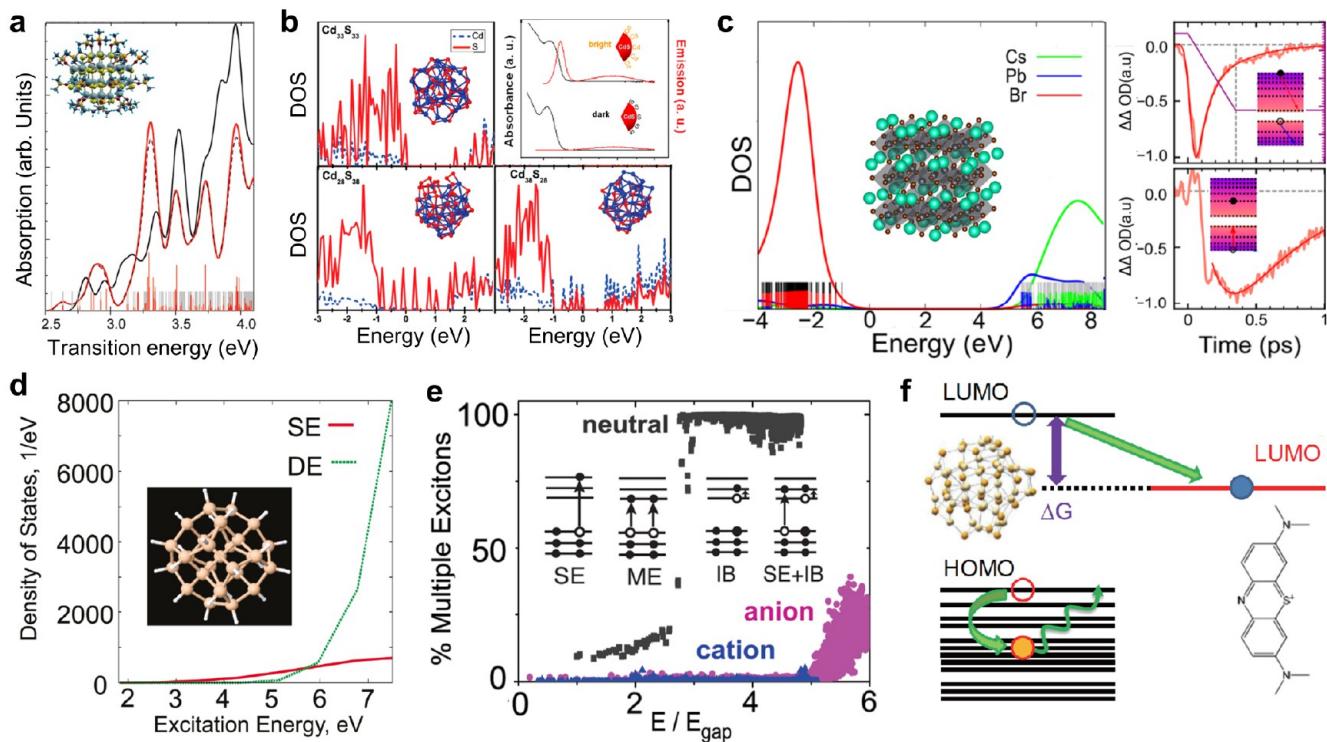
atomic lattice, supraparticles' superhabits can preserve[28,526] or break[29] the symmetry of the superlattice. The synthesis strategies of non-Wulff NC shapes can therefore potentially be utilized in the future to assemble NC superstructures of nonconventional shapes and properties. For example, one can expect to use (i) superseeds, that is, small clusters of NC assemblies, to initiate the superstructure growth, and (ii) diffusion-limited growth environments to guide the formation of spikes or NC snowflakes.

Strain accumulation is also an important factor changing the dynamics of NC assemblies, and there is an increasing body of evidence on the microstructural features and defects within NC assemblies.[30,457] They can even be processed into larger polycrystalline systems that exhibit grain boundaries, dislocations, voids, and vacancies at length scales larger than the individual NCs or superlattice unit cells. Figure 12e evidences the dynamics of the diffusion of a vacancy defect in a superstructure, in the timescale of seconds. Modeling the dynamics of (super)defects is an important but difficult challenge, as the stability of microstructural features can be affected by the inherent size of the system being studied. As experimental techniques continue to improve, and synthetic and fabrication routes generate larger quantities of NC assemblies, the role of these microstructural features becomes increasingly important. Wafer-scale 2D films are regularly produced via evaporative assembly,[312] and NCTs can be processed into cm-scale in fully 3D polycrystalline materials with complex geometries at the nano-, micro-, and macro-scales.[154,527]

Computational tools and models that can properly treat such large systems of particles without relying on periodic boundary conditions will be required to better understand these levels of structural hierarchy. The frameworks to predict the kinetic pathway of the assembly of NC into superstructures nevertheless present similar challenges to the ones to crystallize atoms into NCs, already discussed in a previous section. Such frameworks need to (i) be multiscale, coupling building blocks to superstructures, the latter commonly composed of tens to hundreds of millions of building blocks, (ii) allow introduction/removal of building blocks through grandcanonical or semi-Gibbs ensembles,[106] and (iii) be computationally efficient. These three aspects are, however, incompatible in the common simulation conundrum of physics description vs. computational cost. Whereas Brownian dynamics (BD) presents a better description of trajectories, inherently important for describing the kinetic of assemblies, MC and KMC approaches are computationally more efficient, thus upscaling the systems in size and time at the cost of reduced physical descriptions. Compared to the crystallization of atoms into NC, the assembly of NC into superlattices further presents the already-discussed challenges in modeling interactions between NCs. Another complication comes from the anisotropy of interactions between NC cores, which requires Derjaguin approximation, that is, integration of forces over the surface of two interacting bodies, and the consideration of potential ligand vortices in the edges of the NCs.

First-principles calculations of atomic clusters have generally been limited to small crystallites on the order of hundreds up to thousands of atoms. Despite the small cluster sizes, these calculations were conducted for atoms across the periodic table with diverse quantum mechanical interactions. Calculations at the atomic scale highlight the importance of unpacking the relative and specific strengths of different types of physical interactions during the growth process as well as their
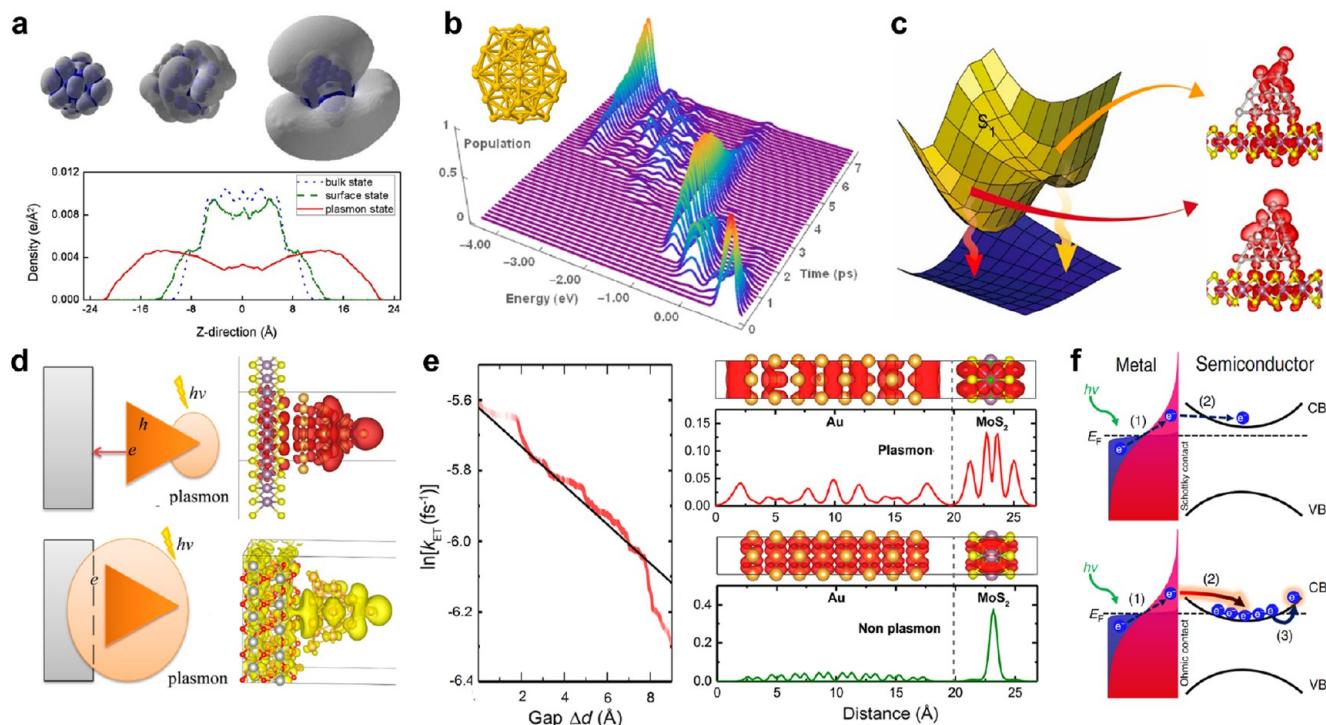
Figure 13. Electronic properties of semiconducting NCs. (a) Optical absorption of $Cd_{33}Se_{33}$ with (red) and without (black) -$OP(CH_3)_3$ ligands. The electronic spectrum is dense even for this small NC. Each peak includes multiple states (vertical bars). Adapted with permission from ref 543. Copyright 2009 American Chemical Society. (b) Density of states (DOS) of the stoichiometric $Cd_{33}Se_{33}$ NC, and the non-stoichiometric $Cd_{28}Se_{38}$ and $Cd_{38}Se_{28}$ NCs. Excess Se creates traps across the band gap, facilitating fast nonradiative relaxation without light emission. In contrast, excess Cd forms a trap sub-band, and the NC emits at the main peak and from the sub-band. Se is a non-metal and needs directional bonds to heal traps, while Cd is a metal and creates bonds more easily. Adapted with permission from ref 544. Copyright 2012 American Chemical Society. (c) DOS and charge carrier dynamics in $CsPbBr_3$ NCs. The valence band is denser than the conduction band, and photo-excitation deposits energy primarily into electrons. Electrons transfer energy to holes within 200 fs. Holes relax by depositing energy into phonons. Adapted with permission from ref 545. Copyright 2023 American Chemical Society. (d) DOS of single excitons (SE) and double excitons (DE) in the $Si_{29}H_{24}$ NC. The DE DOS rises rapidly and exceeds SE DOS at energies above 2.7 times the band gap. Quantum confinement enhances Coulomb interactions, and SEs evolve into DEs at energies above the threshold. Electron-vibrational relaxation brings electronic energy below the threshold, and DEs recombine to form SEs. Adapted with permission from ref 546. Copyright 2012 American Chemical Society. (e) Optical excitations in small neutral and charged PbSe NCs. Multiple excitons (MEs) dominate in neutral NCs at energies above 2.7 band gaps.[34] MEs couple to and borrow optical intensity from SEs. Charged NCs exhibit intraband (IB) excitations. In combination with SEs they form trions. Trions dominate at energies up to 5 band gaps, and few MEs are generated. Adapted with permission from ref 34. Copyright 2009 American Chemical Society. (f) Auger-assisted charge transfer from NC to molecule. Electron transfer from NC to molecular LUMO is accompanied by hole excitation. The hole rapidly relaxes by coupling to phonons. Hole participation accelerates electron transfer and eliminates the Marcus inverted regime in the dependence of the transfer rate on driving force (ΔG). Adapted with permission from ref 547. Copyright 2013 American Chemical Society.

contribution to emergent physical properties. For example, whereas van der Waals forces were almost entirely responsible for the cohesive energy of a certain NC assembly,[428] more complex electronic interactions may be present as well in other systems. As discussed in the coming section about electronic properties, sustaining charge transfer between NCs in assemblies in the presence of dominant van der Waals bonding[528] remains an open challenge.

6.3. Towards Nanoscale Active Matter. Establishing a close-knit loop between computation and advanced experimental measurements permits understanding the dynamics of NC assemblies. Liquid-phase TEM has been utilized to map inter-NC interactions[456,529,530] and liquid-solid interfacial stiffness[531] in NC assemblies, both of which can be fed as inputs into simulations to predict self-assembly pathways or even guide the selection of polymorphs or microstructures for experimental systems of practical NCs. NCs are a potential system for understanding phase transitions and transition path

sampling. The diverse parameter space due to shape anisotropy and interaction potential leads to exotic phases that are chiral, multicomponent, topologically regulated, and even swarming (if out of equilibrium), whose formation mechanisms and reconfiguration dynamics are of fundamental importance for condensed matter physics and the design of complex phases. Notably, the reconfiguration dynamics of NC assemblies[382,532] are barely studied both experimentally and computationally, despite their huge potential as rewritable, self-healing, and self-evolving devices. Fundamental understandings of the effects of multiple length scales, from inter-NC interactions to hydrodynamic flows and other effects due to external fields, are lacking when it comes to nanoscale building blocks. More efforts are required to establish the field of nanoscale active matter, where external energy drives the actions of NCs near or far from thermodynamic equilibrium.

Figure 14. Electronic properties of metallic NCs. (a) Bulk, surface, and plasmon states in Ag₁₀₄. Plasmons extend far beyond NC, providing strong coupling to other NCs, substrates, molecules, and light. Plasmon states couple to vibrations more weakly than bulk and surface states. Adapted with permission from ref 579. Copyright 2010 American Physical Society. (b) Evolution of hot electron energy in Au₅₅.[570] Metallic NCs have no band gap, in contrast to semiconducting NCs ([Figure 13](#)). Nevertheless, smaller gaps do appear, giving rise to excited states that remain populated for a picosecond. Adapted with permission from ref 570. Copyright 2016 American Chemical Society. (c) Surface atoms of metallic NCs can undergo slow fluctuations, creating longer-lived states and (photo-) catalytic sites. Adapted with permission from ref 571. Copyright 2020 American Chemical Society. (d) Active absorbers of light, surface plasmons are collective electronic excitations that lose coherence within femtoseconds. Hot charges need to be extracted prior to electron-hole recombination (top). If metallic NCs are strongly coupled to charge acceptors, plasmon excitations produce charge-separated states immediately, enhancing charge extraction (bottom). Adapted with permission under a Creative Commons CC BY license from ref 572. Copyright 2014 American Chemical Society. (e) By extending far away from metal, plasmons enable efficient coupling to substrates over long distances, facilitating charge and energy transport. Adapted with permission from ref 573. Copyright 2020 American Chemical Society. (f) Metallic NCs support ensembles of hot charges, but simultaneous transfer of many charges are forbidden (top). Instead, hot electrons can transfer energy by scattering with substrate electrons (bottom), enabling energy transport devices. Adapted with permission from ref 574. Copyright 2021 Springer Nature BV.

7. FUNCTIONS AND APPLICATIONS

The diversity of NC cores with different shapes, sizes, chemical compositions, and capping ligands defines a staggering design space for materials. The obvious challenge is identifying the regions of this space that contain NC assemblies with given properties or superior performance compared to traditional materials structured solely at the atomic and molecular scale. There are many strategies for expanding the inventory of NC assemblies. For example, so far only superstructures containing up to three NC species (ternary systems) have been considered,[449,476,533] yet analogues to high entropy alloys[534] may soon be investigated. Adding active NCs to the system during synthesis or operation, in which the environment supplies energy or momentum, further expands the design space.

Significant potential with open challenges exists for NC assemblies in the application fields of thermoelectric materials, batteries, plasmonics, high mobility semiconductors, flexible electronics, and light-emitting devices.[60] Assembled QD solids permit solution-processed functional optoelectronic nanomaterials.[535] Phononics has recently been identified as an as-of-yet untapped area.[536] Bridging the scales from functional nanocomposites to robust macroscale devices, such as smart windows, flexible sensors, displays, and efficient catalysts,[537] and assisted by 3D nanoprinting,[379] will be key. Given the breadth of the field, we do not attempt an exhaustive description of all phenomena that have been proposed or are under investigation. Instead, we highlight a few selected examples, for which nanoscale structural order plays a central role in achieving desired functional properties.

7.1. Electronic Properties. The rational design of electronic NC-based materials is a formidable task due to the complex structural motifs and the intricate electronic processes involved, which requires a detailed understanding of the evolution of energy and charge following photo-excitation or charge injection. In principle, the multiscale nature of NCs offers great potential for fine-tuning their electronic properties. However, achieving accurate and reliable results at reasonable computational cost necessitates tailored-modeling approaches that account for the complexity of the NC electronic structure and the diversity of materials and chemical motifs. Conceived as artificial atoms based on the *effective mass theory* (EMT) of finite-size semiconductors,[538] colloidal NCs often exhibit contradictory or disparate physical and chemical properties at the atomistic, molecular, and bulk scale, which can lead to differing viewpoints about the behavior of NCs.[539] For

example, the molecular view suggests strong electron-hole and charge-phonon interactions, as well as slow energy relaxation due to the mismatch between electronic energy gaps and phonon frequencies.[540] In contrast, the bulk view advocates that (i) the kinetic energy of quantum confinement is greater than electron-hole interactions, (ii) the charge-phonon coupling is weak, and (iii) the energy relaxation through quasi-continuous bands is rapid.

The reality often falls somewhere in between these extremes. An atomistic description of electronic properties and electron-vibrational dynamics in NCs can help to elucidate which viewpoint—artificial atoms, molecules, or bulk—is more suitable for understanding a particular application, depending on NC size and composition, energy range, and type of process. The atomistic description can capture realistic properties of NCs, such as defects, surface passivation with shells and ligands, and coupling between NCs and substrates. The size of NCs is the main challenge for an atomistic description. Realistic NCs are notably larger than those amenable to an ab initio calculation, and the number of electronic states involved is enormous, apart from special situations within small energy ranges.[539] Modern machine learning methods allow addressing size and timescale challenges of atomistic modeling by providing reduced models of electronic Hamiltonians[463] and force fields of ab initio quality.[460]

Semiconducting and metallic NCs share many commonalities, while there exist qualitative differences. Most notably, semiconducting NCs have a large energy gap in the electronic spectrum, enabling long-lived excited states whose excess energy can be utilized in optoelectronic and solar energy applications. Metallic NCs have no gap between occupied and vacant electronic states, but they exhibit collective electronic excitations—*localized surface plasmon resonances* (LSPR), or *plasmons*—at energies that are relevant for many applications. Plasmons respond strongly to electromagnetic fields and spatially extend far outside NCs, enabling electronic interactions with substrates and surface species. Figures 13 and 14 provide illustrations of important electronic properties and electron-vibrational dynamics in semiconducting and metallic NCs, respectively. We should also point to an enormous variety of semiconducting NC structures produced to date. For example, in terms of materials, this includes conventional (e.g., Si) and binary (e.g., II-VI materials such as CdSe, InP, ZnS) as well as more complex hybrid structures. Recently, quantum dots made of halide perovskite materials (e.g., $CsPbI_3$) have attracted wide attention worldwide.[541] Explored architectures include various shapes and sizes as well as more complex architectures (e.g., core-shell structures). Finally, significant work has been done on hybrid semiconducting and metallic NC structures, taking advantage of semiconducting and metallic properties of constituents.[542]

7.1.1. Semiconducting NCs. Semiconducting NCs are usually composed of thousands of atoms, and correspondingly, they contain an enormous number of discrete electronic states. For example, if each atom (e.g., Si) provides four valence electrons, there are 4000 valence band (VB) in a 1000 Si NC. An even larger number of states is available in the conduction band (CB), and therefore there are millions of single excitons (4000^2) and many more trions (three charges) and double excitons[546,548] (two electrons and two holes). Despite their seeming complexity, these electronic manifolds can be treated at various modeling levels. The optical-electronic spectra

appear atom-like (Figure 13a) because (i) the density of states (DOS) is sparse at low energies, and (ii) the large number of excitations follows optical selection rules of the EMT[538] that provides s-type, p-type, etc. envelope functions, each containing multiple excitations. Furthermore, there exist exciton states below the quasi-continuum of excitations across the band gap. Pseudopotential[549] and stochastic wave function[550] approaches exhibit favorable scaling with system size. Alternatively, one can consider combining periodic solid-state physics treatments of bulk NC regions with explicit consideration of surfaces by using, e.g., embedding methods.[551] Excitonic effects are typically treated by the Bethe-Salpeter theory, which is computationally demanding. Simpler descriptions involving approximations to the dielectric function[552] and stochastic sampling[553] are valuable.

The main function of ligands is to enable various synthetic routes for manufacturing colloidal NCs, passivate the electronic defects, and protect the NC surface. Moreover, ligands interact strongly with NC surfaces leading to substantial charge redistribution and polarization effects on the surface.[543] Hybridized states form, in which the electronic density is spread over the NC and the ligands. In fully passivated NCs, neither the ligand-localized nor hybridized molecular orbitals appear as trap states inside or near the band gap. Instead, being mostly optically dark, dense hybridized states open channels of relaxation of high-energy electronic excitations (Figure 13a). Loss of passivating ligands leads to either optically dark or bright additional states inside of the band gap, depending on the position of the leaving ligand. Mid-gap trap states are eliminated by surface reconstruction in certain magic-size NCs, such as $Cd_{33}S_{33}$ (Figure 13b). However, surface passivation is typically required.[554,555] Modeling of electronic properties of passivated NCs requires proper placement of ligands on NC surfaces to satisfy charge neutrality and realistic synthesis conditions.

Achieving precise control over the placement of molecular ligands remains an outstanding synthetic challenge. It often brings forward properties and applications, such as chiroptical features, which is of interest to structure determination, polarized photo-detectors, sensing, and spintronics. Typically, semiconducting NCs are nonchiral structures with significant optical activity in the UV-Vis range. In contrast, chiral molecular systems generally have a significant band gap. One approach to induce chiroptical signatures in semiconducting NC is by creating chirality in their surrounding environment, often referred to as *chirality transfer*. This can be achieved by embedding inorganic NCs within chiral superstructures or by using achiral molecular ligands to passivate the semiconductor surfaces. While some experimental and theoretical reports are encouraging,[556−558] understanding of the physical processes underpinning chirality transfer is yet to be achieved. For example, structural templating, state hybridization, and long-range dipolar interactions were proposed as mechanisms to be employed by fabrication strategies.[559−562]

NC composition is often not fully stoichiometric, and the NC surface can be rich in a particular element. Metal-rich surfaces behave differently from non-metal-rich surfaces.[544] The stoichiometric CdS NC maintains a large band gap. However, an S-rich surface creates a larger number of defect states with energies everywhere inside the band gap (lower-left panel of Figure 13b), leading to rapid electron-vibrational relaxation and impeding light emission. In contrast, defect states created by a Cd-rich surface form a sub-band inside the

bandgap (lower-right panel of Figure 13b), leaving a large energy gap between the CB minimum and the defect band. The nonradiative energy relaxation is limited, and the NC emits both at the main peak corresponding to the band-gap transition and broadly at lower energy corresponding to transitions into and out of the defect sub-band.[544] The differences arise due to the bonding properties of metals and non-metals. S, Se, and other non-metals require directional covalent bonds, and all the bonding requirements cannot be satisfied on the S-rich surface. Metals, such as Cd and Pb, can form bonds more easily and in a less directional manner, reducing the number of defect levels. Such general chemical bonding principles, as reflected in the covalent bond classification scheme and charge-orbital balance model,[554,563] guide NC synthesis, passivation, and stabilization toward attaining desirable electronic features.

NCs simultaneously exhibit molecular and bulk properties. Sufficiently high above the band gap, the NC electronic DOS is high, similar to that in bulk. At the same time, charge-charge interactions are strong in NCs, due to quantum confinement, resembling molecules. Such a combination opens channels for efficient Auger-type processes, such as multiple exciton generation,[540] electron-hole energy exchange,[538,545] and Auger-assisted charge transfer[547] (Figure 13c−f). The VB DOS is higher than the CB DOS in many materials (Figure 13b−c), and therefore, photo-excitation at energies above the band gap places the excess energy mostly into electrons. The Coulomb interaction between electrons and holes results in a rapid (100 fs) energy exchange between electrons and holes, with most of the energy transferred to holes, due to the larger hole DOS. Subsequently, the holes relax to the band edge by coupling to vibrations on a 1 ps timescale[545] (Figure 13c).

The electronic DOS rises rapidly with energy, and there is a universal crossover between the DOS of *single excitons* (SE) and *double excitons* (DE) at energies of about 2.7 band gaps[546,564,565] (Figure 13d−e). At energies above the threshold, reached by photo-excitation or electron-hole injection, SEs transform rapidly to DEs, a process known as *carrier multiplication*[564] and *multiple exciton generation* (MEG).[540] MEG and closely related singlet fission[566] can be used to increase solar cell efficiencies by creating more than one electron-hole pair per absorbed photon. Electronic energy relaxes by coupling to vibrations on the timescale of picoseconds, and as the energy drops below the SE/DE DOS crossover threshold, DEs recombine to form SEs.[546] Coulomb coupling in semiconducting NCs couples SE and DE states. Photo-excitation of superpositions of SEs and DEs leads to the instantaneous generation of multiple electron-hole pairs per absorbed photon. This process is particularly efficient in small NCs.[565] NCs are known to blink, and the blinking is attributed to charge trapping by surface defects or ligands.[567] The complementary charge remains in the NC core, creating trions (three-particle states) arising as a combination of intraband (IB) transitions and SEs (Figure 13e). The trion states dominate statistically over DEs at intermediate energies, and the threshold for MEG is shifted to much higher energies. A similar effect arises if a charge is trapped by a mid-gap state inside the NC core. These multielectron-charged states may also be of relevance to photocatalytic reactions.[568] Thus, attaining robust control over the formation and dynamics of such multiparticle natural and charged excitations remains an important avenue toward enabling applications particularly relevant to the clean energy realm.

The electron-hole energy exchange in NCs is responsible for unconventional mechanisms of charge transfer from an NC to a molecule, a substrate, or another NC. In molecular systems, the excess electronic energy between the *lowest unoccupied molecular orbitals* (LUMO) of the donor and acceptor species is deposited to vibrations, giving rise to a characteristic Marcus theory parabolic dependence of the charge transfer rate on the LUMO-LUMO energy gap.[569] The latter is known as the driving force ΔG (Figure 13f). In NCs, the excess electronic energy can be transferred to another charge, eliminating the Marcus inverted region, in which the rate decreases with increasing ΔG.[547] The intermediate hole-excited states are populated transiently in the timescale of picoseconds. However, their participation changes the transfer rate by orders of magnitude. Such Auger-type charge transfer is not possible in molecules, due to low electronic DOS, or bulk semiconductors, due to weak charge-charge interactions.

7.1.2. Metallic NCs. There are two major differences in the electronic properties of metallic NCs compared to their semiconducting counterparts. First, there is no energy gap separating occupied and empty electronic states. Second, metallic NCs support plasmon excitations at practically relevant energies. Plasmons are collective excitations of multiple electrons, and their wave functions extend many angstroms outside the NCs.[575−578] Figure 14a shows representative bulk, surface, and plasmon states in an Ag_{104} NC.[579] As demonstrated by the projection in the bottom panel, the plasmon orbital extends over a nanometer beyond the NC. Plasmon excitation is a superposition of many such orbitals. The superposition dephases[575] into independent electron-hole pairs in the timescale of tens of femtoseconds (Figure 14d). The collective nature of plasmon excitations and their significant spatial delocalization result in an intense optical response and strong coupling to substrates[573] (Figure 14e). Because plasmons are localized significantly away from the atoms, they couple more weakly to NC phonons compared to the bulk and surface states.[579] Consequently, electron-vibrational relaxation of plasmonic excitations is slower than that of electronic excitations in the bulk.[580]

Since metallic NCs have no energy gap separating occupied and vacant electronic states, electrons and holes recombine fast in metals, within the timescale of picoseconds, while in semiconductors they can live in the timescale of nanoseconds. The strong optical response of plasmons allows generating many electron-hole pairs. If energetic charge carriers can be utilized before they relax by transferring electronic energy to heat, important applications can be envisioned, including photochemical reactions and solar energy, ultrafast electro-optical and photonic devices, photodetection and sensing, and bioscience.[575−581] For example, the use of plasmons to mediate heterogeneous catalysis of adsorbates on metallic surfaces holds the promise of achieving high photoelectric conversion efficiency and controllable reaction selectivity.

Although metallic NCs exhibit a (quasi-) continuous electronic spectrum, some special states can be populated for relatively long periods of time. This can happen if the electronic DOS of an NC exhibits gaps[570] (Figure 14b), or if an electronic state is decoupled from the rest of the structure due to a structural fluctuation[571] (Figure 14c). In the Ag_{104} NC shown in Figure 14b, the state 1 eV below the plasmon excitation energy is energetically separated from the lower energy states and survives for 0.8 ps. The state is above the TiO_2 CB edge, and therefore, hot electrons in that state can be

efficiently extracted.[570] The top atom of the Pt_{20} NC pyramid adsorbed on the MoS_2 substrate undergoes structural fluctuations on the timescale of 50 ps.[571] When the atom fluctuates out of its equilibrium location, its coupling to the rest of the structure decreases, and the lifetime of the corresponding electronic state grows to 0.6 ps. Unsaturated chemical bonds are created, and the catalytic activity of the site increases. The energy of the state is close to the MoS_2 CB edge, such that catalysis can be performed both optically by plasmon excitation of the NC, and electrically by injection of charge from the MoS_2 substrate to the NC. Although 0.6−0.8 ps excited state lifetimes appear short, they still embrace multiple periods of molecular vibrations, which may be sufficient to break chemical bonds. Accurate description and identification of chemically active electronic resonances within electronic state continua in metals are challenging. It is also challenging to identify the mechanism by which electrons propagating in substrates over micrometers get localized to a metallic NC, and then break and form bonds on the Å-scale.[578]

Collective plasmon excitations dephase into electron-hole pairs in the timescale of 10 fs, and the hot carriers should be extracted within the timescale of picoseconds before they recombine nonradiatively[575−578] (top panel of Figure 14d). However, if coupling to a substrate is strong, photo-excitation of the plasmon resonance generates charge-separated states, in which one of the charges is already extracted from the metallic NC (bottom panel of Figure 14d). This theoretical prediction[572] was confirmed experimentally.[582] The strength of the NC-substrate interaction depends on the condition of the substrate surface. If the surface is smooth and chemically saturated, as in MoS_2 and other layered materials, the interaction is weak, largely van der Waals, and the extent of instantaneous charge separation is small.[583] If the surface is chemically unsaturated and the NC-substrate interaction involves chemical bonding, the charge-separated character of the photo-excited state is as large as 20% or more.[572,582] Even if there is no chemical bonding between a metallic NC and the substrate, plasmon states generate efficient electronic coupling across large distances in the nanometer scale (Figure 14e), because they extend far outside the metal (Figure 14a). This was confirmed by the spatially and time-resolved experiments performed on interfaces of Au films with MoS_2.[573] Even if charge transfer across metal NC-substrate interfaces is inhibited by intermediate insulation layers or off-resonance excitations, energy transduction remains possible. Hot electrons in the metal can transfer their energy to pre-existing free electrons in the semiconductor, whose concentration can be controlled by doping.[574] By proper system design and tuning the interfacial interactions at the atomistic level, one can achieve directional energy flow to produce thermal diodes and cool down electronic devices.

The modeling of metallic NCs and their interfaces with molecules and substrates is particularly challenging, because of the wide ranges of size, time, and energy scales involved. Plasmon excitations involve many electrons and extend over tens of nanometers along the NC surface, while plasmon-driven photo-catalysis occurs on the atomic scale (Å) and involves one or a few electrons. It is important to know how the energy of the plasmon wave of the electron ensemble is funneled to perform a localized single electron process. Surface scattering, electron-phonon coupling, and electron-electron interactions are the major mechanisms that determine the final state of the hot electron and its ability to perform a specific
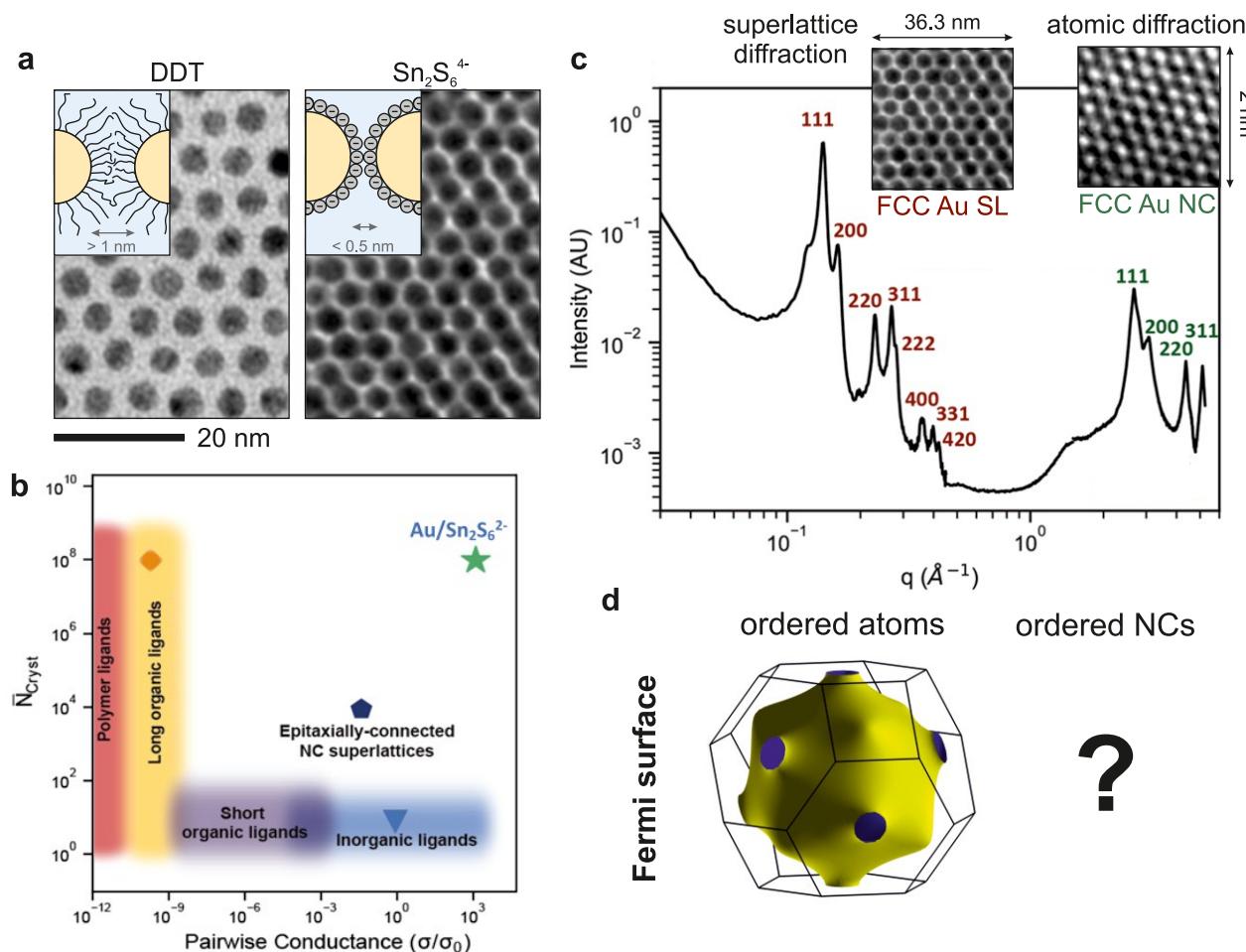
reaction. An accurate atomistic description of localized interactions of excited electrons with molecules and substrates, together with proper models of collective plasmon excitations in metallic NCs, requires a combination of theories developed in different fields. Subsequently, such models need to relate to engineers who work on device design and applications.

7.2. Optoelectronic Coupling. Tuning NC parameters such as the size, composition, and shell thickness, provides access to a variety of heterostructured artificial molecules with potential for emerging applications. In fused-dimer CQDMs, differences in core sizes can create dual-color emission from a single quantum system.[584] Color emission is also highly tunable and switchable by tailoring NC core sizes and compositions. This is relevant for display applications that utilize switchable pixels, and in tunable photon sources.[584] The possibility to adjust tunneling barriers by changing the ligand shell thickness makes fused NC molecules ideal candidates for probes of the coupling mechanism and underlying photo-physics. At larger core separations, resonance energy transfer can dominate the photophysical process, while at shorter separations charge tunneling prevails.[127] The local electric field and effect of external perturbation depend greatly on the degree and mode of coupling. Photogenerated excitons can tunnel and switch between dots driven by the modulation of the electric field, making CQDM candidates for electric-field sensors.

Numerous bright multiexcitonic configurations may form in NC molecules,[585] which, unlike the multiexcitons in single-NC semiconductors, are not necessarily dimmed by strong nonradiative Auger recombination processes.[586] Localized vs. segregated (delocalized) states are possible and can be manipulated by the neck barrier characteristics. The coupling regime can be identified by distinct optical signatures, such as the photoluminescence quantum yield, intensity time traces, lifetimes, and spectra of the neutral-exciton, charged-exciton, and biexciton states. In the weak-coupling regime, the emitted photons are bunched, unlike in the monomer NCs, because they behave akin to two weakly interacting emission centers. The anti-bunching characteristic of a single-photon emitter could be partially regained at the strong coupling regime, due to the facile coupling of electrons and holes, leading to a more efficient nonradiative Auger interaction of the biexciton states.[585] The attributes of CQDMs, with excellent absorbing and bright tunable excitonic and multiexcitonic states, equip them with single- and two-photon emission properties relevant to light-emitting applications.

Controlling the core/shell semiconductor band offsets of the composing NC monomers is also important. In type II core/shell semiconductor NCs, the staggered band alignment allows extensive delocalization of the carrier type to the shell.[587] A higher degree of delocalization can facilitate the transfer of charge carriers to neighboring NCs. This could facilitate color switching under the application of an external electric field. Furthermore, a long-lived charge carrier that is of relevance for light-harvesting applications can be designed and achieved by staggered band alignment of the two cores. Because the electron and hole wave functions are in two different dots, their overlap is reduced, increasing charge carrier lifetimes.

The description of the electronic and optical properties of single NCs is a great challenge, even to modern computers. Accurate techniques developed to study small molecules or solids are limited to small system sizes and computationally too expensive to be applicable to NCs.[34,35] Early work utilized

Figure 15. Conductivity and electronic coupling of NCs assembled by ligands. (a) TEM images comparing interparticle spacing for self-assembled Au NCs of 5 mm in size, capped with 1-dodecanethiol (DDT) and $Sn_2S_6^{4-}$ ligands. (b) Order-coupling diagram for existing NC assemblies. The data points correspond to superlattices of DDT-capped Ag NCs[600] (orange diamond), film of inorganically capped HgTe NCs[601] (blue triangle), and epitaxially connected PbSe superlattice by oriented attachment[268] (navy blue pentagon). (c) X-ray scattering patterns of superlattices of Au NCs with $Sn_2S_6^{4-}$ ligands, showing crystalline order at both the supercrystal and atomic length scales for a superlattice of Au NCs of size 5 mm. (d) In the strong coupling regime, NC assemblies are expected to develop a hierarchical band structure, but their Fermi surface remains to be understood. (a−c) Adapted with permission from ref 27. Copyright 2022 The American Association for the Advancement of Science.

continuum approaches based on the effective mass model and its multiband generalization for realistic-sized NCs.[2,538,588] Atomistic models based on semiempirical pseudopotentials[589−591] were developed for NC inhomogeneities that cannot be captured by continuum models. These atomistic models can be applied to describe electronic couplings, alloys, heterostructures, and vibronic and polaritonic effects,[592] but are still limited to single NC properties. Moreover, understanding surface effects, defects, and the inclusion of passivation of dangling bonds remains a challenge even for a single NC.

The description of the electronic and optical properties of NC assemblies is even more daunting. Ideally, an accurate description should (i) cover the atomistic scale of a single NC including electrons, holes, excitons, and their coupling to lattice vibrations, while (ii) bridging the time and length scales relevant for the emergent properties of NC assemblies. A promising bottom-up approach is coarse-grained electronic structure models, which utilize linear-scaling techniques at the single-particle level and then use them to parameterize a coarse-grained model for NC assembly. Along this line, it was

recently shown that electron transfer in a NC dimer can be driven from the damped nonadiabatic limit to the coherent adiabatic limit even at room temperature, thereby increasing the transfer rate by orders of magnitude.[593] This was achieved by carefully designing the interface between the NCs that act as donors and acceptors, resulting in the discovery of large differences in coupling strength between NC molecules and bulk assemblies. Finally, moving beyond dimers requires accounting for collective phenomena and coupling between the NCs, as well as the inclusion of superlattice modes,[536] superradiance, and other many-body effects.

7.3. Conductivity. Ordered NC assemblies are candidates for the bottom-up design of materials with hierarchically engineered electronic structures. Traditional approaches[8,311,317,319,594,595] require NCs with bulky organic ligands or DNA strands, making these materials electrical insulators (Figure 15a). Although some collective effects can still develop via coupling of plasmonic excitations,[596] transition dipoles,[38] or magnetic dipoles,[597] it is the free movement of electrons that is the prerequisite for electronic bands.

The coupling strength in NC assemblies can be described using the Landauer formula $\sigma = 2e^2/h \sum_{i,j} T_{i,j}$, where $T_{i,j}$ is the transmission of the conductance channel between state i on one particle and state j on the other particle, and $2e^2/h \equiv \sigma_0$ is the quantum conductance unit. A normalized conductance is defined as $\sigma^* = \sigma/\sigma_0$. The transmission for each channel can be approximated as $T = e^{-\beta l}$, where β is the attenuation length of the wave function, and l is the edge-to-edge separation between two neighboring particles.[598] For hydrocarbon ligands,[599] $\beta \approx 1.1$ Å^{-1} and $\sigma^* \approx 1.8 \times 10^{-10}$ at an interparticle separation of 2 nm. This corresponds to an fcc array of 5 mm-sized NCs capped with 1-dodecanethiol ligands.

The conductivity of NC assemblies, σ_{SL}, can be further analyzed by modeling the NC array as a resistive network with defined resistances between nearest neighbors. Applying such a model to the simple cubic lattice, gives $\sigma_{SL} = (Rd)^{-1}$, where $R = \sigma^{-1}$ is the interparticle resistance and d is the center-to-center distance between two neighboring NCs.[602] The physics of the metal-insulator transition in granular materials and NC arrays[603,604] predicts the transition between the weak to strong coupling regimes when σ^* is on the order of unity.

The realization of strong coupling in ordered NC assemblies requires ligands different from those present after synthesis. NCs with compact, typically inorganic, surface ligands show much stronger coupling[601,605] (Figure 15a). Strong electronic coupling between neighboring NCs is achieved through a combination of the short interparticle distances, greater polarizabilities, and lower tunneling barriers afforded by the inorganic infill compared to those of analogous organic ligands. An alternative approach to creating strongly coupled NC solids involves post-assembly removal of the insulating organic ligands.[129,131,268]

Figure 15b highlights the current trade-off between order and electronic coupling strength in NC assemblies. For a long time, materials with good electronic coupling showed no long-range order, whereas ordered arrays used highly insulating ligands. Only recently have examples of strongly coupled NC superlattices been reported, following the development of an understanding of the phase behavior of electrostatically stabilized colloidal NCs.[27] This work is nevertheless far from complete. For example, current strategies are successful only for NC cores with high dielectric constants, such as cores composed of metals (Au, Pd, Ni) and lead chalcogenide (PbS, PbSe). This behavior relates to the dielectric mismatch between the NCs and the surrounding medium, which creates an attraction between surface ions and image charges.[606]
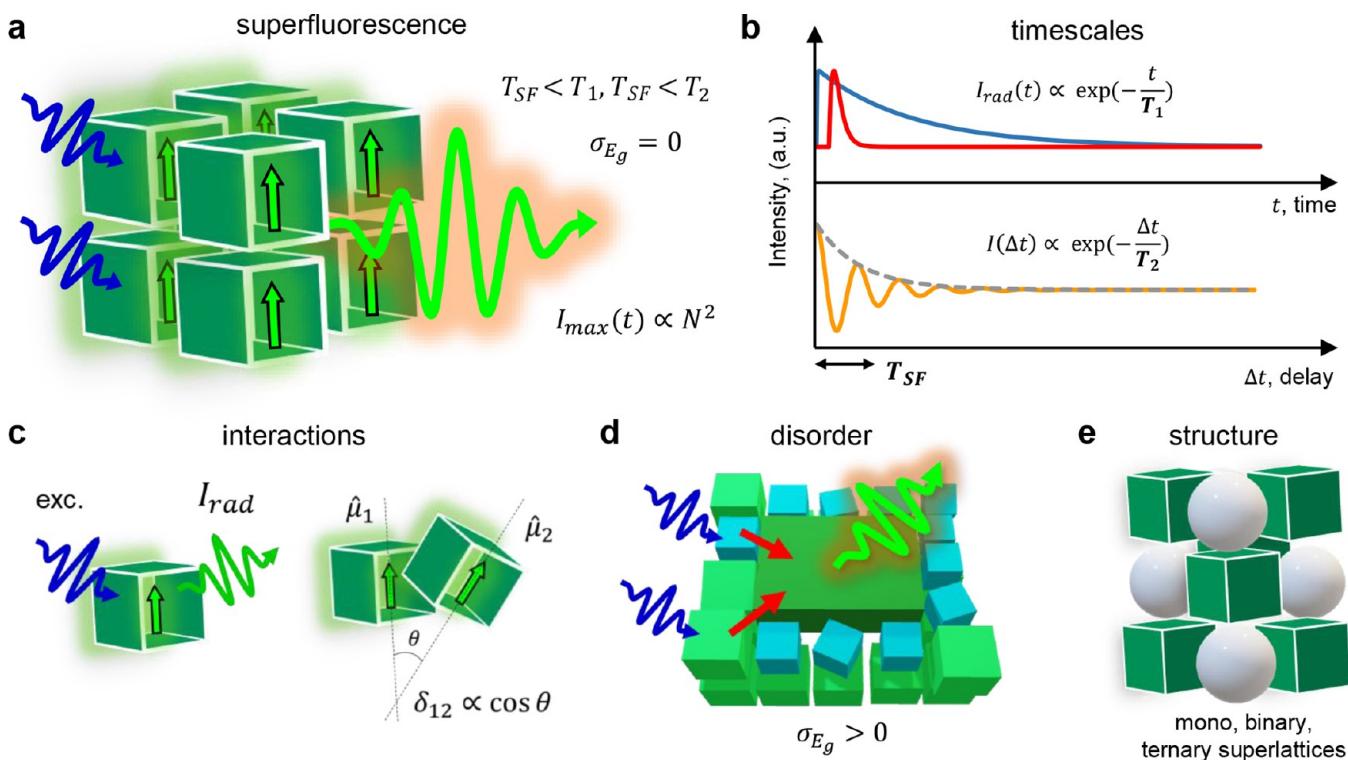
The properties of strongly-coupled NC assemblies have not yet been studied systematically. In the few available examples, the optical reflectance spectrum measured for arrays of weakly-coupled Au NCs shows signatures of LSPR, whereas the reflection spectrum of similar NCs with inorganic ligands approaches the behavior of bulk metals.[27] The temperature-dependent resistivity of strongly-coupled metal NC assemblies follows the predictions of the Boltzmann transport theory, as for typical metallic solids.[27] NC assemblies with simultaneous strong electronic coupling and long-range order have a hierarchical structure with two distinct scales of translation symmetry (Figure 15c). It is reasonable to expect that a similar hierarchy in the electronic structure, superlattice minibands convoluted with the band structure defined by the atomic lattices of individual NCs, should exist for strongly-coupled NC assemblies (Figure 15d).

7.4. Surface Lattice Resonances.

Noble metal NCs, such as gold and silver, support LSPRs in the visible wavelength range,[607] making these attractive for (i) sensing applications, (ii) use as nanoscale cavities to manipulate emitters, and (iii) as optical metamaterials. Due to the high intrinsic absorption losses that are most prominent at the lower wavelength end of visible light, such LSPRs are short-lived leading to pronounced resonance broadening.[608] The challenge of overcoming this damping, needed for future nanophotonic applications, is ongoing in the field of plasmonics. A suitable concept to enhance plasmon lifetimes and thus reduce resonance line width is the arrangement of plasmonic nanostructures into periodic superstructures.[609] In such arrangements, LSPRs of individual plasmonic constituents interact with different modes of diffraction, leading to narrow line-width resonances.[39] These *surface lattice resonances* (SLRs) result from collective electromagnetic and plasmonic-diffractive coupling. Given sufficient spectral overlap, the spectral position of the diffractive mode determines the spectral appearance of the SLR. In other words, altering the periodicity of an NC lattice shifts the position of the SLR.

Periodic plasmonic NC arrays are typically prepared by top-down approaches such as electron beam lithography. While such fabrication schemes lead to arrays with near-perfect structures, control over the shape, size, and morphology of the individual NC constituents is limited, typically leading to amorphous structures. Furthermore, superstructures prepared by lithography are often limited in total array size, and the fabrication is not scalable, requiring expensive equipment. Alternative preparation schemes using an assembly of plasmonic NCs have attracted significant interest in recent years.[157] While literature offers many robust wet-chemical protocols for the synthesis of noble metal NCs with excellent control over particle size, shape, and size distribution, their assembly into periodic, non-close-packed superstructures with precise lattice parameters (symmetry, periodicity) is a remaining scientific challenge.

In this sense, two assembly protocols have been proven suitable: (i) template-assisted assembly, where topographic templates are used to guide NC assembly[610,611] and (ii) polymer-guided (template-free) self-assembly of NCs that are encapsulated in sufficiently thick polymer shells.[361] While the symmetry and periodicity of the template control the final array structure in template-assisted assembly, template-free self-assembly of polymer-encapsulated NCs typically yields hexagonally ordered superstructures. In the latter, the periodicity of the lattice can be controlled by the thickness of the polymer shell and its degree of compression in the 2D confinement.[355] Another direction is superstructures that provide chiral SLRs. Chiral SLRs can be realized by fabricating superlattices with chiral plasmonic nanostructures[612,613] or by inducting optical chirality into otherwise achiral super-structures using chiral molecules.[614]

Challenges regarding SLRs comprise (i) the fabrication of non-close-packed superstructures that are periodic in all directions, (ii) understanding the role of defects and structural imperfections on the quality factor of coupled, collective resonances, (iii) improving quality factors of SLRs from self-assembled periodic plasmonic arrays, (iv) use of chiral SLRs in advanced biodetection, (v) manipulating SLRs by external parameters such as mechanic deformation of the lattice and (reversible) changes of the refractive index in the dielectric environment (substrate or superstrate), and (vi) coupling of

Figure 16. Superfluorescence in NC assemblies. (a) Collective superfluorescence is achieved when NC properties fulfill criteria for identical and coherent emitters. (b−e) Relevant degrees of freedom for superfluorescence. (b) Timescales of radiative decay, T_1, first-order coherence, T_2, and accelerated decay, T_{SF}, are of correct relative order to favor superfluorescence, for example, $T_{SF} < T_1$, $T_{SF} < T_2$. (c) Dipole-dipole interactions between close-packed NCs contribute to radiative coupling, where $\hat{\mu}_1$ and $\hat{\mu}_2$ are unit vectors of transition electric dipole, and δ_{12} is the orientation-dependent interaction energy. (d) Disorder leading to energetic inhomogeneity shall be minimized as it leads to excitation localization as opposed to the collective state. For example, size dispersion results in the energy transfer between NCs with different E_g. (e) Mixing NC building blocks is a strategy to tune cooperative emission.

SLRs to gain media (emitter) to produce plasmonic nanolasers or sources of chiral light in the case of chiral SLRs.

7.5. Superradiance and Superfluorescence.

The fast pace of improvements in the synthesis and optimization of highly luminescent and uniform colloidal NCs[615,616] permits the engineering of cooperative light emission in NC assemblies. Photoluminescence of NCs in an ensemble is typically expected to add up. However, N identical NCs tightly packed in a volume λ^3 (where λ is the emission wavelength) can create a macroscopic polarization after photo-excitation, in the absence of decoherence (such as in low-temperature experiments). This macroscopic polarization decays with a peak intensity proportional to N^2 and an accelerated radiative lifetime (Figure 16a). Such collective phenomena have been theoretically considered for ensembles of two-level systems and are known as (i) *superradiance*, an accelerated radiative decay following a coherent excitation,[36] and (ii) *superfluorescence*, an accelerated radiative decay preceded by a spontaneous build-up of coherence after an incoherent excitation.[37] Experimental observations of superfluorescence came from dilute atomic and molecular gases,[617,618] and achieving it in a solid state has been challenging due to fast electronic dephasing and energetic inhomogeneities.[619]

Lead halide perovskite NCs with an unusual electronic structure[620,621] and assembling into highly ordered super-lattices[622] appear to provide a combination of characteristics favorable for the realization of both superradiance and superfluorescence. The report of superfluorescence in single-component CsPbBr₃ NC superlattices[38] was followed by

reports of collective emission in multicomponent NC super-lattices.[318,449] Interestingly, not all perovskite NC superlattices show collective emission behavior. For example, square-shaped superlattices made of oleate/oleylammonium capped $CsPbBr_3$ NCs and NCs capped with sulfobetaine showed super-fluorescence,[38,623] whereas square-shaped superlattices made from oleate-capped $CsPbBr_3$ NCs and rhombic superlattices made of quarternary ammonium-capped $CsPbBr_3$ NCs did not.[624,625] The spread of experimental observations indicates a need for systematic investigations of structure-property relations in perovskite NC superlattices.

If reproducibly achieved, superfluorescence in NC super-lattices[626,627] and bulk perovskites[628,629] might lead to low-cost and miniature coherent light sources for applications in micro-LEDs, laser printing, and, in a longer term, elements of optical information processing circuits and sources of entangled photons. A holy grail of this research direction is the realization of robust, color-tunable superfluorescence at temperatures that are suitable for device integration. This requires control over several design dimensions (Figure 16b−e), each constituting an open challenge for further research. (i) Characteristic superfluorescence rate, which includes a buildup of coherence between NCs and collective decay, shall be shorter than radiative decay (T_1) and dephasing (T_2) to sustain the collective state in an NC assembly (Figure 16b). (ii) Understanding and tuning radiative coupling in NC assemblies (short-range dipole-dipole interactions, coupling to the common light field, phonons) is crucial for controlling superfluorescence and for generalizing to other nanoscale

emitters (Figure 16c). (iii) Variations in energy between neighboring NCs caused by disorder ($\delta_{E_g} > 0$, where E_g is a NC bandgap energy) should be minimized to avoid excitation localization (e.g., energy transfer[625]), a problem that is directly related to engineering narrow emitters from colloidal NCs[616] (Figure 16d). And (iv) the nature of superfluorescence in lead halide perovskites, be it bulk or nanostructured, and the necessity and role of the superstructure and its complexity (single-component, binary or ternary superlattice) is yet to be understood (Figure 16e). Parallel theoretical and experimental efforts are desirable to make progress towards the application of cooperative light emission in NC assemblies.

7.6. Computer-Assisted Determination of Properties.
Machine learning (ML) was discussed in a previous section as a method to upscale molecular dynamics simulations beyond hard-shape interactions between NCs. ML models are, however, not limited to energy predictions and molecular dynamics. In principle, they can be formulated for any property or process of interest, such as electronically excited states and spectra,[630,631] chemical reactivity and catalysis,[632,633] drug discovery,[634] and energy storage materials.[635] Simulations of the electronic properties in NCs were shown to be accelerated with ML models,[636] where plasmonic oscillations in silver NCs were predicted using neural networks trained on ab initio molecular dynamics data. Other important developments include structural analyses of NCs with unsupervised learning algorithms, which rapidly navigate and cluster large datasets.[637]

Data science methodologies to identify trends and relationships in nanostructured materials is a rapidly developing area.[638] Artificial intelligence-guided NC synthesis[639] represents another significant stride in materials discovery towards accelerating nanomaterial synthesis and uncovering the correlations between chemical composition and desired properties. All these developments lay the groundwork for future advancements in the NC assembly field.

7.7. Biological Applications.
The methods described for NC assemblies have many applications to systems that reach far more disciplines. In the following, we briefly discuss two examples of such applications in the fields of molecular biology and biomedicine.

7.7.1. Amyloid Fibrils in Neurodegenerative Diseases.
Amyloid fibrils consist of individual protein molecules assembled into a repeating pattern along a single axis. They are associated with major neurodegenerative diseases, including Alzheimer's disease, Parkinson's disease, and prion diseases. The underlying one-dimensional arrangement is referred to as a *cross-β structure* because the β-strands of the protein molecules are stacked perpendicular to the fibril axis. Like many other 1D crystals, amyloid fibrils possess a highly ordered arrangement along one dimension, forming a repeating pattern. However, they are not as regular or perfect as traditional 3D crystals and can exhibit structural polymorphism.[640]

Despite significant advances in understanding the assembly and disassembly pathways of amyloid fibrils,[641,642] several open problems and challenges persist. One major area of research focuses on the factors that contribute to the structural polymorphism observed in amyloid fibrils and its implications for disease pathology.[642] Additionally, the mechanisms underlying nucleation and the rate-limiting step in fibril formation are still not fully elucidated. Especially important is understanding how molecular chaperones prevent the initiation and propagation of fibril formation and how this ability is lost in disease states. Furthermore, while clearance mechanisms exist to eliminate amyloid fibrils,[643−645] the efficiency and effectiveness of these mechanisms in different cell types and disease contexts are not yet fully understood. Identifying ways to enhance the clearance of fibrils or develop interventions that promote their disaggregation is an ongoing challenge.

7.7.2. Nanocrystalline Complexes of Innate Immune Ligands.
As discussed in the previous section, pathological self-assembly is a concept that has been associated with amyloids, such as amyloid-β (Aβ) in Alzheimer's disease and α-synuclein in Parkinson's disease. While the oligomeric forms of amyloids are thought to be responsible for their cytotoxicity via membrane permeation, their fibrillar forms have been known to interact with the innate immune system to induce inflammation. Furthermore, both eukaryotic and prokaryotic amyloids can self-assemble and organize nucleic acids into nanocrystalline complexes, thereby enabling amplification of *toll-like receptor* (TLR) signaling from the innate immune system. In a more general compass, recent work has shown that *antimicrobial peptides* (AMPs) from the host innate immune system follow a strikingly similar pattern. AMPs have historically been considered essential components of the host innate immune system and play critical roles in defense against microbes, such as preferential permeation of microbial membranes rather than eukaryotic membranes, and sound the proverbial alarm to activate cellular-mediated immune responses.[646,647] Consistent with this perspective, many AMPs are facially amphiphilic and can facilitate membrane remodeling processes such as pore formation. In fact, in the last ten years, the lines of demarcation between amyloids and AMPs have blurred drastically. Like amyloids, it turns out that AMPs are low symmetry objects that can assemble into protofibrils that organize nucleic acids into nanocrystalline structures that amplify TLR mediated immune responses.[648−651] Like AMPs, amyloids have recently been shown capable of antimicrobial activity in addition to their cytotoxic properties, suggesting a function in host defense.[652,653]

One question is why the assembly of innate immune ligands like dsDNA or dsRNA into a nanocrystalline organization by AMPs or amyloids leads to amplified immune activation in the host. To answer this question, it is helpful to assess how the innate immune system functions. The innate immune system is capable of fast decision-making because it works via a form of molecular profiling. TLRs do not sense and respond to chemical individuality. Rather, the innate immune system goes through a more streamlined decision-making process to recognize and respond to a relatively small number of the so-called *pathogen-associated molecular patterns* (PAMPs), conserved molecular ligands derived from microbes. In microbial defense, AMPs can permeate microbial membranes and co-assemble with free microbial ligands from lysed microbes into nanocrystalline complexes that differentially activate TLRs. Depending on the precise assembled supramolecular crystalline structure of the complex, the TLR response from immune cells can vary from nonactivation up to massively amplified activation at about 100 times basal levels.[648] This system is fast and efficient, but the profiling can go wrong. For example, nonmicrobial self-nucleic acids can erroneously activate TLRs (TLR9 for dsDNA, TLR3 for dsRNA) via this AMP-based multivalent amplification mechanism in autoimmune diseases such as lupus, rheumatoid arthritis, and psoriasis.[648,649,651] The reason for this drastic

amplification is a statistical mechanical effect known as *superselectivity*, which was originally formulated to understand the assembly of multivalent NCs.[654] The crystalline face of an NC with the right lattice spacing commensurate with the steric size of TLRs can mediate successful multivalent binding between immune ligands and immune receptors.[648] More importantly, the system presents a vulnerability that allows innate immune machinery to be exploited by microbes, such as enterotoxins from *Clostridioides difficile*,[655] and coronaviruses such as SARS-CoV-2, the causative agent for COVID-19.[656]

8. CONCLUSIONS AND PERSPECTIVES

Although NC-based materials have been used (inadvertently) for more than 3 millennia,[657] the subject, as a field, was basically nonexistent three decades ago. Recent spectacular progress in chemical synthesis and characterization, coupled with rapid advancements in theoretical understanding of fundamental processes, is what motivated the KITP workshop and conference in Santa Barbara entitled "Nanoparticle Assemblies: A New Form of Matter with Classical Structure and Quantum Function". This paper is a result of this event and attempts to categorize and summarize the most promising directions as identified by the workshop participants. Several challenges were elucidated in this study, and it is our expectation that their accomplishment will push the boundaries of the field.

The ability to assemble more complex and diverse structures will continue to be a major area of interest. Increasingly, the effort will be driven by the goal of assembling materials with given functions. Here, it should be expected that theory will increasingly play a leading role. Yet, many important functions are related to electronic properties, so general methods that combine the assembly part, which is more often described by classical statistical mechanics, and the electronic component, which almost entirely requires quantum calculations, will need to be further developed.

Nonequilibrium effects have been arguably under-investigated but present ways of controlling equilibrium and metastable assembly, as well as in developing nanoscale active systems. Furthermore, the ability to design materials that perform many different functions requires a precise understanding of nonequilibrium effects. Insights from biological self-assembly, where complex structures are made from a shared set of building blocks (for example, a variety of protein structures arising from the same set of amino acids), have given rise to the growing field of multifarious self-assembly. An apparently unrelated but equally intriguing question pertains to the dynamic nature of structures. If a structure is constantly changing over time, can it break free from kinetic traps that have long hindered the more widespread adoption of self-assembly processes? Recent advancements hold great promise, offering not only potential applications within the self-assembly field but also insights into the statistical mechanics of systems characterized by rugged landscapes.[658]

The exploration and engineering of optical and electronic interactions between NCs suggest potential avenues for practical applications. QD-OLED TVs, which utilize the NC photoluminescence, are a promising step in this direction. In this example, a fundamental discovery—the synthesis of quantum dots (QD), for which the Nobel Prize in Chemistry 2023 was awarded to Moungi G. Bawendi, Louis E. Brus, and Aleksei Yekimov—was combined with engineering advances to realize controlled QD self-assembly. As microelectronics continues to integrate optical elements, NCs will play an increasingly relevant role. The development of photonic integrated circuits and the emergence of quantum computing could benefit from the low-cost and solution-processable nature of NC assemblies. Incorporating printable electronic and optoelectronic elements into products, from smart fabrics to consumer devices such as smartphones and virtual reality headsets, hints at a future where NC assemblies will enhance many device functionalities.

AUTHOR INFORMATION

Corresponding Author

Alex Travesset — *Iowa State University and Ames Lab, Ames, Iowa 50011, USA;* ● orcid.org/0000-0001-7030-9570; Email: trvsst@ameslab.gov

Authors

Carlos L. Bassani — *Institute for Multiscale Simulation, Friedrich-Alexander-Universität Erlangen-Nürnberg, 91058 Erlangen, Germany;* ● orcid.org/0000-0003-2451-2476

Greg van Anders — *Department of Physics, Engineering Physics, and Astronomy, Queen's University, Kingston, Ontario K7L 3N6, Canada;* ● orcid.org/0000-0002-9746-2484

Uri Banin — *Institute of Chemistry and the Center for Nanoscience and Nanotechnology, The Hebrew University of Jerusalem, Jerusalem 91904, Israel;* ● orcid.org/0000-0003-1698-2128

Dmitry Baranov — *Division of Chemical Physics, Department of Chemistry, Lund University, SE-221 00 Lund, Sweden;* ● orcid.org/0000-0001-6439-8132

Qian Chen — *University of Illinois, Urbana, Illinois 61801, USA;* ● orcid.org/0000-0002-1968-441X

Marjolein Dijkstra — *Soft Condensed Matter & Biophysics, Debye Institute for Nanomaterials Science, Utrecht University, 3584 CC Utrecht, The Netherlands;* ● orcid.org/0000-0002-9166-6478

Michael S. Dimitriyev — *Department of Polymer Science and Engineering, University of Massachusetts, Amherst, Massachusetts 01003, USA; Department of Materials Science and Engineering, Texas A&M University, College Station, Texas 77843, USA;* ● orcid.org/0000-0001-6384-3644

Efi Efrati — *Department of Physics of Complex Systems, Weizmann Institute of Science, Rehovot 76100, Israel; James Franck Institute, The University of Chicago, Chicago, Illinois 60637, USA*

Jordi Faraudo — *Institut de Ciencia de Materials de Barcelona (ICMAB-CSIC), E-08193 Bellaterra, Barcelona, Spain;* ● orcid.org/0000-0002-6315-4993

Oleg Gang — *Department of Chemical Engineering and Department of Applied Physics and Applied Mathematics, Columbia University, New York, New York 10027, USA; Center for Functional Nanomaterials, Brookhaven National Laboratory, Upton, New York 11973, USA;* ● orcid.org/0000-0001-5534-3121

Nicola Gaston — *The MacDiarmid Institute for Advanced Materials and Nanotechnology, Department of Physics, The University of Auckland, Auckland 1142, New Zealand;* ● orcid.org/0000-0001-8049-3295

Ramin Golestanian — *Max Planck Institute for Dynamics and Self-Organization (MPI-DS), 37077 Göttingen, Germany; Rudolf Peierls Centre for Theoretical Physics, University of*

Oxford, Oxford OX1 3PU, UK; ![orcid] orcid.org/0000-0002-3149-4002

G. Ivan Guerrero-Garcia − *Facultad de Ciencias de la Universidad Autónoma de San Luis Potosí, 78295 San Luis Potosí, México;* ![orcid] orcid.org/0000-0002-3174-2643

Michael Gruenwald − *Department of Chemistry, University of Utah, Salt Lake City, Utah 84112, USA;* ![orcid] orcid.org/0000-0003-2186-1662

Amir Haji-Akbari − *Department of Chemical and Environmental Engineering, Yale University, New Haven, Connecticut 06511, USA;* ![orcid] orcid.org/0000-0002-2228-6957

Maria Ibáñez − *Institute of Science and Technology Austria (ISTA), 3400 Klosterneuburg, Austria;* ![orcid] orcid.org/0000-0001-5013-2843

Matthias Karg − *Heinrich-Heine-Universität Düsseldorf, 40225 Düsseldorf, Germany;* ![orcid] orcid.org/0000-0002-6247-3976

Tobias Kraus − *INM − Leibniz-Institute for New Materials, 66123 Saarbrücken, Germany; Saarland University, Colloid and Interface Chemistry, 66123 Saarbrücken, Germany;* ![orcid] orcid.org/0000-0003-2951-1704

Byeongdu Lee − *X-ray Science Division, Argonne National Laboratory, Lemont, Illinois 60439, USA;* ![orcid] orcid.org/0000-0003-2514-8805

Reid C. Van Lehn − *Department of Chemical and Biological Engineering, University of Wisconsin-Madison, Madison, Wisconsin 53717, USA;* ![orcid] orcid.org/0000-0003-4885-6599

Robert J. Macfarlane − *Department of Materials Science and Engineering, Massachusetts Institute of Technology, Cambridge, Massachusetts 02142, USA;* ![orcid] orcid.org/0000-0001-9449-2680

Bortolo M. Mognetti − *Center for Nonlinear Phenomena and Complex Systems, Université Libre de Bruxelles, 1050 Brussels, Belgium;* ![orcid] orcid.org/0000-0002-7960-8224

Arash Nikoubashman − *Leibniz-Institut für Polymerforschung Dresden e.V., 01069 Dresden, Germany; Institut für Theoretische Physik, Technische Universität Dresden, 01069 Dresden, Germany;* ![orcid] orcid.org/0000-0003-0563-825X

Saeed Osat − *Max Planck Institute for Dynamics and Self-Organization (MPI-DS), 37077 Göttingen, Germany*

Oleg V. Prezhdo − *Department of Chemistry, University of Southern California, Los Angeles, CA 90089, USA; Department of Physics and Astronomy, University of Southern California, Los Angeles, California 90089, USA;* ![orcid] orcid.org/0000-0002-5140-7500

Grant M. Rotskoff − *Department of Chemistry, Stanford University, Stanford, California 94305, USA;* ![orcid] orcid.org/0000-0002-7772-5179

Leonor Saiz − *Department of Biomedical Engineering, University of California, Davis, California 95616, USA;* ![orcid] orcid.org/0000-0002-6866-9400

An-Chang Shi − *Department of Physics & Astronomy, McMaster University, Hamilton, Ontario L8S 4M1, Canada;* ![orcid] orcid.org/0000-0003-1379-7162

Sara Skrabalak − *Department of Chemistry, Indiana University, Bloomington, Indiana 47405, USA;* ![orcid] orcid.org/0000-0002-1873-100X

Ivan I. Smalyukh − *Department of Physics and Chemical Physics Program, University of Colorado, Boulder, Colorado 80309, USA; International Institute for Sustainability with Knotted Chiral Meta Matter, Hiroshima University, Higashi-Hiroshima City 739-0046, Japan;* ![orcid] orcid.org/0000-0003-3444-1966

Mario Tagliazucchi − *Universidad de Buenos Aires, Ciudad Universitaria, Buenos Aires 1428, Argentina*

Dmitri V. Talapin − *Department of Chemistry, James Franck Institute and Pritzker School of Molecular Engineering, The University of Chicago, Chicago, Illinois 60637, USA; Center for Nanoscale Materials, Argonne National Laboratory, Argonne, IL 60439, USA;* ![orcid] orcid.org/0000-0002-6414-8587

Alexei V. Tkachenko − *Center for Functional Nanomaterials, Brookhaven National Laboratory, Upton, New York 11973, USA;* ![orcid] orcid.org/0000-0003-1291-243X

Sergei Tretiak − *Theoretical Division and Center for Integrated Nanotechnologies, Los Alamos National Laboratory, Los Alamos, New Mexico 87545, USA;* ![orcid] orcid.org/0000-0001-5547-3647

David Vaknin − *Iowa State University and Ames Lab, Ames, Iowa 50011, USA;* ![orcid] orcid.org/0000-0002-0899-9248

Asaph Widmer-Cooper − *ARC Centre of Excellence in Exciton Science, School of Chemistry, University of Sydney, Sydney, New South Wales 2006, Australia; The University of Sydney Nano Institute, University of Sydney, Sydney, New South Wales 2006, Australia;* ![orcid] orcid.org/0000-0001-5459-6960

Gerard C. L. Wong − *Department of Bioengineering and Department of Chemistry and Biochemistry, University of California, Los Angeles, California 90095, USA; Department of Microbiology, Immunology & Molecular Genetics, University of California, Los Angeles, CA 90095, USA; California NanoSystems Institute, University of California, Los Angeles, CA 90095, USA;* ![orcid] orcid.org/0000-0003-0893-6383

Xingchen Ye − *Department of Chemistry, Indiana University, Bloomington, Indiana 47405, USA;* ![orcid] orcid.org/0000-0001-6851-2721

Shan Zhou − *Department of Nanoscience and Biomedical Engineering, South Dakota School of Mines and Technology, Rapid City, South Dakota 57701, USA;* ![orcid] orcid.org/0000-0002-6476-3280

Eran Rabani − *Department of Chemistry, University of California and Materials Sciences Division, Lawrence Berkeley National Laboratory, Berkeley, California 94720, USA; The Raymond and Beverly Sackler Center of Computational Molecular and Materials Science, Tel Aviv University, Tel Aviv 69978, Israel;* ![orcid] orcid.org/0000-0003-2031-3525

Michael Engel − *Institute for Multiscale Simulation, Friedrich-Alexander-Universität Erlangen-Nürnberg, 91058 Erlangen, Germany;* ![orcid] orcid.org/0000-0002-7031-3825

Complete contact information is available at:
https://pubs.acs.org/10.1021/acsnano.3c10201

Notes

The authors declare no competing financial interest.

ACKNOWLEDGMENTS

VOCABULARY

assembly protocol, the conditions (thermodynamic conditions, concentrations, rates of cooling, that is, the protocol) to assemble nanocrystals/building blocks into superstructures; **building block,** a nanocrystal (core) with a given shape (habit), functionalized by polymers (shell), that serves as a building block to assemble a (super)structure; **plasmonic nanocrystal,** a conductor nanocrystal; **quantum dot,** a semiconductor nanocrystal; **self-assembly,** the process of spontaneous association of individual units (atoms, building blocks) to form a highly arranged pattern or ordered structure; **superstructure,** the meso-/macroscale structure formed by the assembly of nanocrystals/building blocks; **surface functionalization/ligand shell,** the addition of small molecules or polymers (ligands) that attach to the nanocrystal surface and create interactions between nanocrystals.

REFERENCES

(1) Nozik, A. J. Photoelectrochemistry: Applications to Solar Energy Conversion. *Annual Review of Physical Chemistry* **1978**, *29*, 189−222.

(2) Efros, A. Interband absorption of light in a semiconductor sphere. *Soviet Physics: Semiconductors* **1982**, *66*, 772−775.

(3) Brus, L. E. Electron-electron and electron-hole interactions in small semiconductor crystallites: The size dependence of the lowest excited electronic state. *The Journal of Chemical Physics* **1984**, *80*, 4403−4409.

(4) Murray, C. B.; Norris, D. J.; Bawendi, M. G. Synthesis and Characterization of Nearly Monodisperse CdE (E = S, Se, Te) Semiconductor Nanocrystallites. *Journal of the American Chemical Society* **1993**, *115*, 8706−8715.

(5) Glotzer, S. C.; Solomon, M. J. Anisotropy of building blocks and their assembly into complex structures. *Nature Materials* **2007**, *6*, 557−562.

(6) Boles, M. A.; Engel, M.; Talapin, D. V. Self-Assembly of Colloidal Nanocrystals: From Intricate Structures to Functional Materials. *Chemical Reviews* **2016**, *116*, 11220−11289.

(7) Poon, W. Colloids as Big Atoms. *Science* **2004**, *304*, 830−831.

(8) Macfarlane, R. J.; Lee, B.; Jones, M. R.; Harris, N.; Schatz, G. C.; Mirkin, C. A. Nanoparticle Superlattice Engineering with DNA. *Science* **2011**, *334*, 204−208.

(9) Liu, Y.; Klement, M.; Wang, Y.; Zhong, Y.; Zhu, B.; Chen, J.; Engel, M.; Ye, X. Macromolecular Ligand Engineering for Programmable Nanoprism Assembly. *Journal of the American Chemical Society* **2021**, *143*, 16163−16172.

(10) Heuer-Jungemann, A.; Feliu, N.; Bakaimi, I.; Hamaly, M.; Alkilany, A.; Chakraborty, I.; Masood, A.; Casula, M. F.; Kostopoulou, A.; Oh, E.; Susumu, K.; Stewart, M. H.; Medintz, I. L.; Stratakis, E.; Parak, W. J.; Kanaras, A. G. The Role of Ligands in the Chemical Synthesis and Applications of Inorganic Nanoparticles. *Chemical Reviews* **2019**, *119*, 4819−4880.

(11) Ohno, K.; Morinaga, T.; Takeno, S.; Tsujii, Y.; Fukuda, T. Suspensions of Silica Particles Grafted with Concentrated Polymer Brush: Effects of Graft Chain Length on Brush Layer Thickness and Colloidal Crystallization. *Macromolecules* **2007**, *40*, 9143−9150.

(12) Green, P. F. The structure of chain end-grafted nanoparticle/homopolymer nanocomposites. *Soft Matter* **2011**, *7*, 7914.

(13) Karg, M.; Pich, A.; Hellweg, T.; Hoare, T.; Lyon, L. A.; Crassous, J. J.; Suzuki, D.; Gumerov, R. A.; Schneider, S.; Potemkin, I. I.; Richtering, W. Nanogels and Microgels: From Model Colloids to Applications, Recent Developments, and Future Trends. *Langmuir* **2019**, *35*, 6231−6255.

(14) Zhang, Z.; Glotzer, S. C. Self-Assembly of Patchy Particles. *Nano Letters* **2004**, *4*, 1407−1413.

(15) Glotzer, S. C. Some Assembly Required. *Science* **2004**, *306*, 419−420.

(16) Mirkin, C. A.; Letsinger, R. L.; Mucic, R. C.; Storhoff, J. J. A DNA-based method for rationally assembling nanoparticles into macroscopic materials. *Nature* **1996**, *382*, 607−609.

(17) Alivisatos, A. P.; Johnsson, K. P.; Peng, X.; Wilson, T. E.; Loweth, C. J.; Bruchez, M. P.; Schultz, P. G. Organization of 'nanocrystal molecules' using DNA. *Nature* **1996**, *382*, 609−611.

(18) Zhang, J.; Santos, P. J.; Gabrys, P. A.; Lee, S.; Liu, C.; Macfarlane, R. J. Self-Assembling Nanocomposite Tectons. *Journal of the American Chemical Society* **2016**, *138*, 16228−16231.

(19) Wang, Y.; Santos, P. J.; Kubiak, J. M.; Guo, X.; Lee, M. S.; Macfarlane, R. J. Multistimuli Responsive Nanocomposite Tectons for Pathway Dependent Self-Assembly and Acceleration of Covalent Bond Formation. *Journal of the American Chemical Society* **2019**, *141*, 13234−13243.

(20) Nayak, S.; Horst, N.; Zhang, H.; Wang, W.; Mallapragada, S.; Travesset, A.; Vaknin, D. Interpolymer Complexation as a Strategy for Nanoparticle Assembly and Crystallization. *The Journal of Physical Chemistry C* **2019**, *123*, 836−840.

(21) Haxton, T. K.; Hedges, L. O.; Whitelam, S. Crystallization and arrest mechanisms of model colloids. *Soft Matter* **2015**, *11*, 9307−9320.

(22) Sánchez-Iglesias, A.; Grzelczak, M.; Altantzis, T.; Goris, B.; Pérez-Juste, J.; Bals, S.; Van Tendeloo, G.; Donaldson, S. H.; Chmelka, B. F.; Israelachvili, J. N.; Liz-Marzán, L. M. Hydrophobic interactions modulate self-assembly of nanoparticles. *ACS Nano* **2012**, *6*, 11059−11065.

(23) Smalyukh, I. I. Liquid Crystal Colloids. *Annual Review of Condensed Matter Physics* **2018**, *9*, 207−226.

(24) Koley, S.; Cui, J.; Panfil, Y. E.; Banin, U. Coupled Colloidal Quantum Dot Molecules. *Accounts of Chemical Research* **2021**, *54*, 1178−1188.

(25) Cheng, X.; Böker, A.; Tsarkova, L. Temperature-Controlled Solvent Vapor Annealing of Thin Block Copolymer Films. *Polymers* **2019**, *11*, 1312.

(26) Vogel, N.; Goerres, S.; Landfester, K.; Weiss, C. K. A Convenient Method to Produce Close- and Non-close-Packed Monolayers using Direct Assembly at the Air-Water Interface and Subsequent Plasma-Induced Size Reduction. *Macromolecular Chemistry and Physics* **2011**, *212*, 1719−1734.

(27) Coropceanu, I.; Janke, E. M.; Portner, J.; Haubold, D.; Nguyen, T. D.; Das, A.; Tanner, C. P. N.; Utterback, J. K.; Teitelbaum, S. W.; Hudson, M. H.; Sarma, N. A.; Hinkle, A. M.; Tassone, C. J.; Eychmuller, A.; Limmer, D. T.; Olvera de la Cruz, M.; Ginsberg, N. S.; Talapin, D. V. Self-assembly of nanocrystals into strongly electronically coupled all-inorganic supercrystals. *Science* **2022**, *375*, 1422−1426.

(28) Auyeung, E.; Li, T. I. N. G.; Senesi, A. J.; Schmucker, A. L.; Pals, B. C.; de la Cruz, M. O.; Mirkin, C. A. DNA-mediated nanoparticle crystallization into Wulff polyhedra. *Nature* **2014**, *505*, 73−77.

(29) Seo, S. E.; Girard, M.; de la Cruz, M. O.; Mirkin, C. A. Nonequilibrium anisotropic colloidal single crystal growth with DNA. *Nature Communications* **2018**, *9*, 1−8.

(30) Ondry, J. C.; Alivisatos, A. P. Application of Dislocation Theory to Minimize Defects in Artificial Solids Built with Nanocrystal Building Blocks. *Accounts of Chemical Research* **2021**, *54*, 1419−1429.

(31) Meiri, S.; Efrati, E. Cumulative geometric frustration in physical assemblies. *Physical Review E* **2021**, *104*, No. 054601.

(32) De Nijs, B.; Dussi, S.; Smallenburg, F.; Meeldijk, J. D.; Groenendijk, D. J.; Filion, L.; Imhof, A.; Van Blaaderen, A.; Dijkstra, M. Entropy-driven formation of large icosahedral colloidal clusters by spherical confinement. *Nature Materials* **2015**, *14*, 56−60.

(33) Travesset, A. Nanoparticle Superlattices as Quasi-Frank-Kasper Phases. *Physical Review Letters* **2017**, *119*, No. 115701.

(34) Prezhdo, O. V. Photoinduced dynamics in semiconductor quantum dots: Insights from time-domain ab initio studies. *Accounts of Chemical Research* **2009**, *42*, 2005−2016.

(35) Yazdani, N.; Andermatt, S.; Yarema, M.; Farto, V.; Bani-Hashemian, M. H.; Volk, S.; Lin, W. M.; Yarema, O.; Luisier, M.; Wood, V. Charge transport in semiconductors assembled from nanocrystal quantum dots. *Nature Communications* **2020**, *11*, 1−9.

(36) Dicke, R. H. Coherence in spontaneous radiation processes. *Physical Review* **1954**, *93*, 99−110.

(37) Bonifacio, R.; Lugiato, L. A. Cooperative radiation processes in two-level systems: Superfluorescence. *Physical Review A* **1975**, *11*, 1507−1521.

(38) Rainò, G.; Becker, M. A.; Bodnarchuk, M. I.; Mahrt, R. F.; Kovalenko, M. V.; Stöferle, T. Superfluorescence from lead halide perovskite quantum dot superlattices. *Nature* **2018**, *563*, 671−675.

(39) Kravets, V. G.; Kabashin, A. V.; Barnes, W. L.; Grigorenko, A. N. Plasmonic Surface Lattice Resonances: A Review of Properties and Applications. *Chemical Reviews* **2018**, *118*, 5912−5951.

(40) Li, Y.; Zhou, W.; Tanriover, I.; Hadibrata, W.; Partridge, B. E.; Lin, H.; Hu, X.; Lee, B.; Liu, J.; Dravid, V. P.; Aydin, K.; Mirkin, C. A. Open-channel metal particle superlattices. *Nature* **2022**, *611*, 695−701.

(41) Shi, Y.; Lyu, Z.; Zhao, M.; Chen, R.; Nguyen, Q. N.; Xia, Y. Noble-Metal Nanocrystals with Controlled Shapes for Catalytic and Electrocatalytic Applications. *Chemical Reviews* **2021**, *121*, 649−735.

(42) Zhang, L.; Zhou, M.; Wang, A.; Zhang, T. Selective Hydrogenation over Supported Metal Catalysts: From Nanoparticles to Single Atoms. *Chemical Reviews* **2020**, *120*, 683−733.

(43) Seh, Z. W.; Kibsgaard, J.; Dickens, C. F.; Chorkendorff, I.; Nørskov, J. K.; Jaramillo, T. F. Combining theory and experiment in electrocatalysis: Insights into materials design. *Science* **2017**, *355*. DOI: 10.1126/science.aad4998

(44) Zhang, F.; Luo, J.; Chen, J.; Luo, H.; Jiang, M.; Yang, C.; Zhang, H.; Chen, J.; Dong, A.; Yang, J. Interfacial Assembly of Nanocrystals on Nanofibers with Strong Interaction for Electro-catalytic Nitrate Reduction. *Angewandte Chemie International Edition* **2023**, *62*, No. e202310383.

(45) Kamyshny, A.; Magdassi, S. Conductive Nanomaterials for Printed Electronics. *Small* **2014**, *10*, 3515−3535.

(46) Talapin, D. V.; Lee, J.-S.; Kovalenko, M. V.; Shevchenko, E. V. Prospects of Colloidal Nanocrystals for Electronic and Optoelectronic Applications. *Chemical Reviews* **2010**, *110*, 389−458.

(47) Fiedler, C.; Kleinhanns, T.; Garcia, M.; Lee, S.; Calcabrini, M.; Ibáñez, M. Solution-Processed Inorganic Thermoelectric Materials: Opportunities and Challenges. *Chemistry of Materials* **2022**, *34*, 8471−8489.

(48) Meseguer, F. Colloidal crystals as photonic crystals. *Colloids and Surfaces A: Physicochemical and Engineering Aspects* **2005**, *270-271*, 1−7.

(49) Quan, L. N.; Kang, J.; Ning, C.-Z.; Yang, P. Nanowires for Photonics. *Chemical Reviews* **2019**, *119*, 9153−9169.

(50) Rycenga, M.; Cobley, C. M.; Zeng, J.; Li, W.; Moran, C. H.; Zhang, Q.; Qin, D.; Xia, Y. Controlling the Synthesis and Assembly of Silver Nanostructures for Plasmonic Applications. *Chemical Reviews* **2011**, *111*, 3669−3712.

(51) Jones, M. R.; Osberg, K. D.; Macfarlane, R. J.; Langille, M. R.; Mirkin, C. A. Templated Techniques for the Synthesis and Assembly of Plasmonic Nanostructures. *Chemical Reviews* **2011**, *111*, 3736−3827.

(52) Jasieniak, J.; MacDonald, B. I.; Watkins, S. E.; Mulvaney, P. Solution-Processed Sintered Nanocrystal Solar Cells via Layer-by-Layer Assembly. *Nano Letters* **2011**, *11*, 2856−2864.

(53) Jiang, X.; Ding, Y.; Zheng, S.; Ye, Y.; Li, Z.; Xu, L.; Wang, J.; Li, Z.; Loh, X. J.; Ye, E.; Sun, L. In-Situ Generated CsPbBr₃ Nanocrystals on O-Defective WO₃ for Photocatalytic CO₂ Reduction. *ChemSusChem* **2022**, *15*, No. e202102295.

(54) Li, L.; Wang, Y.; Wang, X.; Lin, R.; Luo, X.; Liu, Z.; Zhou, K.; Xiong, S.; Bao, Q.; Chen, G.; Tian, Y.; Deng, Y.; Xiao, K.; Wu, J.; Saidaminov, M. I.; Lin, H.; Ma, C.-Q.; Zhao, Z.; Wu, Y.; Zhang, L.; Tan, H. Flexible all-perovskite tandem solar cells approaching 25% efficiency with molecule-bridged hole-selective contact. *Nature Energy* **2022**, *7*, 708−717.

(55) Jana, A.; Meena, A.; Patil, S. A.; Jo, Y.; Cho, S.; Park, Y.; Sree, V. G.; Kim, H.; Im, H.; Taylor, R. A. Self-assembly of perovskite nanocrystals. *Progress in Materials Science* **2022**, *129*, No. 100975.

(56) Tang, Z.; Wang, Y.; Podsiadlo, P.; Kotov, N. Biomedical Applications of Layer-by-Layer Assembly: From Biomimetics to Tissue Engineering. *Advanced Materials* **2006**, *18*, 3203−3224.

(57) Yang, X.; Yang, M.; Pang, B.; Vara, M.; Xia, Y. Gold Nanomaterials at Work in Biomedicine. *Chemical Reviews* **2015**, *115*, 10410−10488.

(58) Pelaz, B.; Alexiou, C.; Alvarez-Puebla, R. A.; Alves, F.; Andrews, A. M.; Ashraf, S.; Balogh, L. P.; Ballerini, L.; Bestetti, A.; Brendel, C.; Bosi, S.; Carril, M.; Chan, W. C. W.; Chen, C.; Chen, X.; Chen, X.; Cheng, Z.; Cui, D.; Du, J.; Dullin, C.; Escudero, A.; Feliu, N.; Gao, M.; George, M.; Gogotsi, Y.; Grunweller, A.; Gu, Z.; Halas, N. J.; Hampp, N.; Hartmann, R. K.; Hersam, M. C.; Hunziker, P.; Jian, J.; Jiang, X.; Jungebluth, P.; Kadhiresan, P.; Kataoka, K.; Khademhosseini, A.; Kopecek, J.; Kotov, N. A.; Krug, H. F.; Lee, D. S.; Lehr, C.-M.; Leong, K. W.; Liang, X.-J.; Ling Lim, M.; Liz-Marzan, L. M.; Ma, X.; Macchiarini, P.; Meng, H.; Mohwald, H.; Mulvaney, P.; Nel, A. E.; Nie, S.; Nordlander, P.; Okano, T.; Oliveira, J.; Park, T. H.; Penner, R. M.; Prato, M.; Puntes, V.; Rotello, V. M.; Samarakoon, A.; Schaak, R. E.; Shen, Y.; Sjoqvist, S.; Skirtach, A. G.; Soliman, M. G.; Stevens, M. M.; Sung, H.-W.; Tang, B. Z.; Tietze, R.; Udugama, B. N.; VanEpps, J. S.; Weil, T.; Weiss, P. S.; Willner, I.; Wu, Y.; Yang, L.; Yue, Z.; Zhang, Q.; Zhang, Q.; Zhang, X.-E.; Zhao, Y.; Zhou, X.; Parak, W. J. Diverse Applications of Nanomedicine. *ACS Nano* **2017**, *11*, 2313−2381.

(59) Geng, Y.; van Anders, G.; Dodd, P. M.; Dshemuchadse, J.; Glotzer, S. C. Engineering entropy for the inverse design of colloidal crystals from hard shapes. *Sci. Adv.* **2019**, *5*. DOI: 10.1126/sciadv.aaw0514

(60) Kovalenko, M. V.; Manna, L.; Cabot, A.; Hens, Z.; Talapin, D. V.; Kagan, C. R.; Klimov, V. I.; Rogach, A. L.; Reiss, P.; Milliron, D. J.; Guyot-Sionnnest, P.; Konstantatos, G.; Parak, W. J.; Hyeon, T.; Korgel, B. A.; Murray, C. B.; Heiss, W. Prospects of Nanoscience with Nanocrystals. *ACS Nano* **2015**, *9*, 1012−1057.

(61) Xia, Y.; Xiong, Y.; Lim, B.; Skrabalak, S. Shape-Controlled Synthesis of Metal Nanocrystals: Simple Chemistry Meets Complex Physics? *Angewandte Chemie International Edition* **2009**, *48*, 60−103.

(62) de Arquer, F. P. G.; Talapin, D. V.; Klimov, V. I.; Arakawa, Y.; Bayer, M.; Sargent, E. H. Semiconductor quantum dots: Technological progress and future challenges. *Science* **2021**, *373*. DOI: 10.1126/science.aaz8541

(63) Xia, X.; Zeng, J.; Zhang, Q.; Moran, C. H.; Xia, Y. Recent developments in shape-controlled synthesis of silver nanocrystals. *Journal of Physical Chemistry C* **2012**, *116*, 21647−21656.

(64) Ahn, H.-Y.; Lee, H.-E.; Jin, K.; Nam, K. T. Extended gold nano-morphology diagram: synthesis of rhombic dodecahedra using CTAB and ascorbic acid. *Journal of Materials Chemistry C* **2013**, *1*, 6861.

(65) Sun, M.; Cheng, Z.; Chen, W.; Jones, M. Understanding Symmetry Breaking at the Single-Particle Level via the Growth of Tetrahedron-Shaped Nanocrystals from Higher-Symmetry Precursors. *ACS Nano* **2021**, *15*, 15953−15961.

(66) Langille, M. R.; Zhang, J.; Personick, M. L.; Li, S.; Mirkin, C. A. Stepwise Evolution of Spherical Seeds into 20-Fold Twinned Icosahedra. *Science* **2012**, *337*, 954−957.

(67) Ye, X.; Zheng, C.; Chen, J.; Gao, Y.; Murray, C. B. Using Binary Surfactant Mixtures To Simultaneously Improve the Dimensional Tunability and Monodispersity in the Seeded Growth of Gold Nanorods. *Nano Letters* **2013**, *13*, 765−771.

(68) Ye, X.; Jin, L.; Caglayan, H.; Chen, J.; Xing, G.; Zheng, C.; Doan-Nguyen, V.; Kang, Y.; Engheta, N.; Kagan, C. R.; Murray, C. B. Improved Size-Tunable Synthesis of Monodisperse Gold Nanorods through the Use of Aromatic Additives. *ACS Nano* **2012**, *6*, 2804−2817.

(69) Wang, D.; Kang, Y.; Ye, X.; Murray, C. B. Mineralizer-Assisted Shape-Control of Rare Earth Oxide Nanoplates. *Chemistry of Materials* **2014**, *26*, 6328−6332.

(70) Choi, B. K.; Kim, J.; Luo, Z.; Kim, J.; Kim, J. H.; Hyeon, T.; Mehraeen, S.; Park, S.; Park, J. Shape Transformation Mechanism of Gold Nanoplates. *ACS Nano* **2023**, *17*, 2007−2018.

(71) Ma, X.; Lin, F.; Chen, X.; Jin, C. Unveiling Growth Pathways of Multiply Twinned Gold Nanoparticles by in Situ Liquid Cell Transmission Electron Microscopy. *ACS Nano* **2020**, *14*, 9594−9604.

(72) Yang, T.-H.; Shi, Y.; Janssen, A.; Xia, Y. Surface Capping Agents and Their Roles in Shape-Controlled Synthesis of Colloidal Metal Nanocrystals. *Angewandte Chemie International Edition* **2020**, *59*, 15378−15401.

(73) Balankura, T.; Qi, X.; Zhou, Y.; Fichthorn, K. A. Predicting kinetic nanocrystal shapes through multi-scale theory and simulation: Polyvinylpyrrolidone-mediated growth of Ag nanocrystals. *Journal of Chemical Physics* **2016**, *145*, No. 144106.

(74) Nguyen, Q. N.; Wang, C.; Shang, Y.; Janssen, A.; Xia, Y. Colloidal Synthesis of Metal Nanocrystals: From Asymmetrical Growth to Symmetry Breaking. *Chemical Reviews* **2023**, *123*, 3693.

(75) Manna, L.; Milliron, D. J.; Meisel, A.; Scher, E. C.; Alivisatos, A. P. Controlled growth of tetrapod-branched inorganic nanocrystals. *Nature Materials* **2003**, *2*, 382−385.

(76) Chen, S.; Wang, Z. L.; Ballato, J.; Foulger, S. H.; Carroll, D. L. Monopod, Bipod, Tripod, and Tetrapod Gold Nanocrystals. *Journal of the American Chemical Society* **2003**, *125*, 16186−16187.

(77) Chandra, K.; Culver, K. S.; Werner, S. E.; Lee, R. C.; Odom, T. W. Manipulating the Anisotropic Structure of Gold Nanostars using Good's Buffers. *Chemistry of Materials* **2016**, *28*, 6763−6769.

(78) Deka, S.; Miszta, K.; Dorfs, D.; Genovese, A.; Bertoni, G.; Manna, L. Octapod-Shaped Colloidal Nanocrystals of Cadmium Chalcogenides via "One-Pot" Cation Exchange and Seeded Growth. *Nano Letters* **2010**, *10*, 3770−3776.

(79) Zhang, G.; Wang, D.; Möhwald, H. Decoration of Microspheres with Gold Nanodots—Giving Colloidal Spheres Valences. *Angewandte Chemie International Edition* **2005**, *44*, 7767−7770.

(80) Sun, S.; Yang, S.; Xin, H. L.; Nykypanchuk, D.; Liu, M.; Zhang, H.; Gang, O. Valence-programmable nanoparticle architectures. *Nature Communications* **2020**, *11*, 2279.

(81) Roh, K.-H.; Martin, D. C.; Lahann, J. Biphasic Janus particles with nanoscale anisotropy. *Nature Materials* **2005**, *4*, 759−763.

(82) Leonardi, A.; Engel, M. Particle Shape Control via Etching of Core@Shell Nanocrystals. *ACS Nano* **2018**, *12*, 9186−9195.

(83) Chen, L.; Leonardi, A.; Chen, J.; Cao, M.; Li, N.; Su, D.; Zhang, Q.; Engel, M.; Ye, X. Imaging the kinetics of anisotropic dissolution of bimetallic core−shell nanocubes using graphene liquid cells. *Nature Communications* **2020**, *11*, 3041.

(84) Suzuki, N.; Wang, Y.; Elvati, P.; Qu, Z. B.; Kim, K.; Jiang, S.; Baumeister, E.; Lee, J.; Yeom, B.; Bahng, J. H.; Lee, J.; Violi, A.; Kotov, N. A. Chiral Graphene Quantum Dots. *ACS Nano* **2016**, *10*, 1744−1755.

(85) Ma, W.; Xu, L.; De Moura, A. F.; Wu, X.; Kuang, H.; Xu, C.; Kotov, N. A. Chiral Inorganic Nanostructures. *Chemical Reviews* **2017**, *117*, 8041−8093.

(86) Googasian, J. S.; Lewis, G. R.; Woessner, Z. J.; Ringe, E.; Skrabalak, S. E. Seed-directed synthesis of chiroptically active Au nanocrystals of varied symmetries. *Chemical Communications* **2022**, *58*, 11575−11578.

(87) González, E.; Arbiol, J.; Puntes, V. F. Carving at the Nanoscale: Sequential Galvanic Exchange and Kirkendall Growth at Room Temperature. *Science* **2011**, *334*, 1377−1380.

(88) Ham, S.; Jang, H.-J.; Song, Y.; Shuford, K. L.; Park, S. Octahedral and Cubic Gold Nanoframes with Platinum Framework. *Angewandte Chemie International Edition* **2015**, *54*, 9025−9028.

(89) Wulff, G. Zur Frage der Geschwindigkeit des Wachstums und der Auflösung der Krystallflagen. *Zeitschrift für Krystallographie und Mineralogie* **1901**, *34*, 449−530.

(90) Marks, L. D.; Peng, L. Nanoparticle shape, thermodynamics and kinetics. *Journal of Physics: Condensed Matter* **2016**, *28*, No. 053001.

(91) Rahm, J. M.; Erhart, P. WulffPack: A Python package for Wulff constructions. *Journal of Open Source Software* **2020**, *5*, 1944.

(92) Roosen, A. R.; McCormack, R. P.; Carter, W. C. A tool for the calculation and display of crystal shapes. *Computational Materials Science* **1998**, *11*, 16−26.

(93) Winterbottom, W. Equilibrium shape of a small particle in contact with a foreign substrate. *Acta Metallurgica* **1967**, *15*, 303−310.

(94) De Coninck, J.; Fruttero, J.; Ziermann, A. Non-typical Wulff shapes in a corner: A microscopic derivation. *Physica A: Statistical Mechanics and its Applications* **1993**, *196*, 320−334.

(95) Ringe, E.; Van Duyne, R. P.; Marks, L. D. Wulff Construction for Alloy Nanoparticles. *Nano Letters* **2011**, *11*, 3399−3403.

(96) Fichthorn, K. A.; Balankura, T.; Qi, X. Multi-scale theory and simulation of shape-selective nanocrystal growth. *CrystEngComm* **2016**, *18*, 5410−5417.

(97) Broughton, J. Q.; Gilmer, G. H.; Jackson, K. A. Crystallization Rates of a Lennard-Jones Liquid. *Physical Review Letters* **1982**, *49*, 1496−1500.

(98) Grossi, J.; Pisarev, V. Two-temperature molecular dynamics simulations of crystal growth in a tungsten supercooled melt. *Journal of Physics: Condensed Matter* **2023**, *35*, No. 015401.

(99) Wang, Y.; Peng, H. C.; Liu, J.; Huang, C. Z.; Xia, Y. Use of reduction rate as a quantitative knob for controlling the twin structure and shape of palladium nanocrystals. *Nano Letters* **2015**, *15*, 1445−1450.

(100) Qi, X.; Chen, Z.; Yan, T.; Fichthorn, K. A. Growth Mechanism of Five-Fold Twinned Ag Nanowires from Multiscale Theory and Simulations. *ACS Nano* **2019**, *13*, 4647−4656.

(101) Fichthorn, K. A. Atomic-Scale Theory and Simulations for Colloidal Metal Nanocrystal Growth. *Journal of Chemical & Engineering Data* **2014**, *59*, 3113−3119.

(102) Qi, X.; Balankura, T.; Zhou, Y.; Fichthorn, K. A. How Structure-Directing Agents Control Nanocrystal Shape: Polyvinylpyrrolidone-Mediated Growth of Ag Nanocubes. *Nano Letters* **2015**, *15*, 7711−7717.

(103) Goudeli, E.; Pratsinis, S. E. Crystallinity dynamics of gold nanoparticles during sintering or coalescence. *AIChE Journal* **2016**, *62*, 589−598.

(104) Kim, M. J.; Alvarez, S.; Yan, T.; Tadepalli, V.; Fichthorn, K. A.; Wiley, B. J. Modulating the Growth Rate, Aspect Ratio, and Yield of Copper Nanowires with Alkylamines. *Chemistry of Materials* **2018**, *30*, 2809−2818.

(105) Xia, Y.; Nelli, D.; Ferrando, R.; Yuan, J.; Li, Z. Y. Shape control of size-selected naked platinum nanocrystals. *Nature Communications* **2021**, *12*, 3019.

(106) Boerrigter, S. X. M.; Josten, G. P. H.; van de Streek, J.; Hollander, F. F. A.; Los, J.; Cuppen, H. M.; Bennema, P.; Meekes, H. MONTY: Monte Carlo crystal growth on any crystal structure in any crystallographic orientation; Application to fats. *Journal of Physical Chemistry A* **2004**, *108*, 5894−5902.

(107) Ye, X.; Jones, M. R.; Frechette, L. B.; Chen, Q.; Powers, A. S.; Ercius, P.; Dunn, G.; Rotskoff, G. M.; Nguyen, S. C.; Adiga, V. P.; Zettl, A.; Rabani, E.; Geissler, P. L.; Alivisatos, A. P. Single-particle mapping of nonequilibrium nanocrystal transformations. *Science* **2016**, *354*, 874−877.

(108) Anderson, M. W.; Gebbie-Rayet, J. T.; Hill, A. R.; Farida, N.; Attfield, M. P.; Cubillas, P.; Blatov, V. A.; Proserpio, D. M.;

Akporiaye, D.; Arstad, B.; Gale, J. D. Predicting crystal growth via a unified kinetic three-dimensional partition model. *Nature* **2017**, *544*, 456−459.

(109) Li, X.; Zhu, B.; Qi, R.; Gao, Y. Real-Time Simulation of Nonequilibrium Nanocrystal Transformations. *Advanced Theory and Simulations* **2019**, *2*, No. 1800127.

(110) Hill, A. R.; Cubillas, P.; Gebbie-Rayet, J. T.; Trueman, M.; de Bruyn, N.; al Harthi, Z.; Pooley, R. J.; Attfield, M. P.; Blatov, V. A.; Proserpio, D. M.; Gale, J. D.; Akporiaye, D.; Arstad, B.; Anderson, M. W. CrystalGrower: a generic computer program for Monte Carlo modelling of crystal growth. *Chemical Science* **2021**, *12*, 1126−1146.

(111) Witten, T. A.; Sander, L. M. Diffusion-Limited Aggregation, a Kinetic Critical Phenomenon. *Physical Review Letters* **1981**, *47*, 1400.

(112) Ortellado, L.; Gómez, L. R. Phase Field Modeling of Dendritic Growth on Spherical Surfaces. *Frontiers in Materials* **2020**, *7*, 163.

(113) Bassani, C. L.; Sum, A. K.; Herri, J. M.; Morales, R. E.; Cameirão, A. A Multiscale Approach for Gas Hydrates Considering Structure, Agglomeration, and Transportability under Multiphase Flow Conditions: II. Growth Kinetic Model. *Industrial & Engineering Chemistry Research* **2020**, *59*, 2123−2144.

(114) Zhu, C.; Zeng, J.; Tao, J.; Johnson, M. C.; Schmidt-Krey, I.; Blubaugh, L.; Zhu, Y.; Gu, Z.; Xia, Y. Kinetically controlled overgrowth of Ag or Au on Pd nanocrystal seeds: From hybrid dimers to nonconcentric and concentric bimetallic nanocrystals. *Journal of the American Chemical Society* **2012**, *134*, 15822−15831.

(115) Xia, X.; Xia, Y. Symmetry Breaking during Seeded Growth of Nanocrystals. *Nano Letters* **2012**, *12*, 6038−6042.

(116) Al-Saidi, W. A.; Feng, H.; Fichthorn, K. A. Adsorption of polyvinylpyrrolidone on Ag surfaces: Insight into a structure-directing agent. *Nano Letters* **2012**, *12*, 997−1001.

(117) Schneider, N. M.; Norton, M. M.; Mendel, B. J.; Grogan, J. M.; Ross, F. M.; Bau, H. H. Electron−Water Interactions and Implications for Liquid Cell Electron Microscopy. *The Journal of Physical Chemistry C* **2014**, *118*, 22373−22382.

(118) Pitzer, K. S.; Mayorga, G. Thermodynamics of electrolytes. II. Activity and osmotic coefficients for strong electrolytes with one or both ions univalent. *Journal of Physical Chemistry* **1973**, *77*, 2300−2308.

(119) Chen, C.-C.; Song, Y. Generalized electrolyte-NRTL model for mixed-solvent electrolyte systems. *AIChE Journal* **2004**, *50*, 1928−1941.

(120) Girard, M.; Wang, S.; Du, J. S.; Das, A.; Huang, Z.; Dravid, V. P.; Lee, B.; Mirkin, C. A.; de la Cruz, M. O. Particle analogs of electrons in colloidal crystals. *Science* **2019**, *364*, 1174−1178.

(121) Filion, L.; Hermes, M.; Ni, R.; Vermolen, E. C. M.; Kuijk, A.; Christova, C. G.; Stiefelhagen, J. C. P.; Vissers, T.; van Blaaderen, A.; Dijkstra, M. Self-Assembly of a Colloidal Interstitial Solid with Tunable Sublattice Doping. *Physical Review Letters* **2011**, *107*, No. 168302.

(122) Poon, W. C. K. The physics of a model colloid polymer mixture. *Journal of Physics: Condensed Matter* **2002**, *14*, R859−R880.

(123) Schacht, J.; Gaston, N. Cluster assemblies as superatomic solids: a first principles study of bonding & electronic structure. *Physical Chemistry Chemical Physics* **2018**, *20*, 6167−6175.

(124) Harper, E. S.; van Anders, G.; Glotzer, S. C. The entropic bond in colloidal crystals. *Proc. Natl. Acad. Sci. U.S.A.* **2019**, *116*, 16703−16710, DOI: 10.1073/pnas.1822092116.

(125) Vo, T.; Glotzer, S. C. A theory of entropic bonding. *Proc. Natl. Acad. Sci. U.S.A.* **2022**, *119*, No. e2116414119, DOI: 10.1073/pnas.2116414119.

(126) Dshemuchadse, J.; Damasceno, P. F.; Phillips, C. L.; Engel, M.; Glotzer, S. C. Moving beyond the constraints of chemistry via crystal structure discovery with isotropic multiwell pair potentials. *Proc. Natl. Acad. Sci. U.S.A.* **2021**, *118*, No. e2024034118, DOI: 10.1073/pnas.2024034118.

(127) Cui, J.; Panfil, Y. E.; Koley, S.; Shamalia, D.; Waiskopf, N.; Remennik, S.; Popov, I.; Oded, M.; Banin, U. Colloidal quantum dot molecules manifesting quantum coupling at room temperature. *Nature communications* **2019**, *10*, 5401.

(128) Cui, J.; Koley, S.; Panfil, Y. E.; Levi, A.; Ossia, Y.; Waiskopf, N.; Remennik, S.; Oded, M.; Banin, U. Neck Barrier Engineering in Quantum Dot Dimer Molecules via Intraparticle Ripening. *Journal of the American Chemical Society* **2021**, *143*, 19816−19823.

(129) Boneschanscher, M. P.; Evers, W. H.; Geuchies, J. J.; Altantzis, T.; Goris, B.; Rabouw, F. T.; Van Rossum, S. A. P.; Van Der Zant, H. S. J.; Siebbeles, L. D. A.; Van Tendeloo, G.; Swart, I.; Hilhorst, J.; Petukhov, A. V.; Bals, S.; Vanmaekelbergh, D. Long-range orientation and atomic attachment of nanocrystals in 2D honeycomb super-lattices. *Science* **2014**, *344*, 1377−1380.

(130) Ondry, J. C.; Philbin, J. P.; Lostica, M.; Rabani, E.; Alivisatos, A. P. Resilient Pathways to Atomic Attachment of Quantum Dot Dimers and Artificial Solids from Faceted CdSe Quantum Dot Building Blocks. *ACS Nano* **2019**, *13*, 12322−12344.

(131) Whitham, K.; Yang, J.; Savitzky, B. H.; Kourkoutis, L. F.; Wise, F.; Hanrath, T. Charge transport and localization in atomically coherent quantum dot solids. *Nature Materials* **2016**, *15*, 557−563.

(132) Hasegawa, R.; Aoki, Y.; Doi, M. Optimum Graft Density for Dispersing Particles in Polymer Melts. *Macromolecules* **1996**, *29*, 6656−6662.

(133) Ferreira, P. G.; Ajdari, A.; Leibler, L. Scaling Law for Entropic Effects at Interfaces between Grafted Layers and Polymer Melts. *Macromolecules* **1998**, *31*, 3994−4003.

(134) Balazs, A. C.; Emrick, T.; Russell, T. P. Nanoparticle polymer composites: Where two small worlds meet. *Science* **2006**, *314*, 1107−1110.

(135) Alexander, S. Adsorption of chain molecules with a polar head a scaling description. *Journal de Physique France* **1977**, *38*, 983−987.

(136) De Gennes, P.G. Scaling theory of polymer adsorption. *Journal de Physique* **1976**, *37*, 1445−1452.

(137) Milner, S. T.; Witten, T. A.; Cates, M. E. A Parabolic Density Profile for Grafted Polymers. *EPL (Europhysics Letters)* **1988**, *5*, 413.

(138) Ball, R. C.; Marko, J. F.; Milner, S. T.; Witten, T. A. Polymers grafted to a convex surface. *Macromolecules* **1991**, *24*, 693−703.

(139) Belyi, V. A. Exclusion zone of convex brushes in the strong-stretching limit. *The Journal of Chemical Physics* **2004**, *121*, 6547−6554.

(140) Dimitriyev, M. S.; Grason, G. M. End-exclusion zones in strongly stretched, molten polymer brushes of arbitrary shape. *Journal of Chemical Physics* **2021**, *155*, No. 224901.

(141) Midya, J.; Rubinstein, M.; Kumar, S. K.; Nikoubashman, A. Structure of Polymer-Grafted Nanoparticle Melts. *ACS Nano* **2020**, *14*, 15505−15516.

(142) Akcora, P.; Liu, H.; Kumar, S. K.; Moll, J.; Li, Y.; Benicewicz, B. C.; Schadler, L. S.; Acehan, D.; Panagiotopoulos, A. Z.; Pryamitsyn, V.; Ganesan, V.; Ilavsky, J.; Thiyagarajan, P.; Colby, R. H.; Douglas, J. F. Anisotropic self-assembly of spherical polymer-grafted nano-particles. *Nature Materials* **2009**, *8*, 354−359.

(143) Chremos, A.; Panagiotopoulos, A. Z. Structural transitions of solvent-free oligomer-grafted nanoparticles. *Physical Review Letters* **2011**, *107*, No. 105503.

(144) Bilchak, C. R.; Jhalaria, M.; Huang, Y.; Abbas, Z.; Midya, J.; Benedetti, F. M.; Parisi, D.; Egger, W.; Dickmann, M.; Minelli, M.; Doghieri, F.; Nikoubashman, A.; Durning, C. J; Vlassopoulos, D.; Jestin, J.; Smith, Z. P.; Benicewicz, B. C.; Rubinstein, M.; Leibler, L.; Kumar, S. K. Tuning Selectivities in Gas Separation Membranes Based on Polymer-Grafted Nanoparticles. *ACS Nano* **2020**, *14*, 17174−17183.

(145) Bilchak, C. R.; Jhalaria, M.; Adhikari, S.; Midya, J.; Huang, Y.; Abbas, Z.; Nikoubashman, A.; Benicewicz, B. C.; Rubinstein, M.; Kumar, S. K. Understanding Gas Transport in Polymer-Grafted Nanoparticle Assemblies. *Macromolecules* **2022**, *55*, 3011−3019.

(146) Midya, J.; Cang, Y.; Egorov, S. A.; Matyjaszewski, K.; Bockstaller, M. R.; Nikoubashman, A.; Fytas, G. Disentangling the Role of Chain Conformation on the Mechanics of Polymer Tethered Particle Materials. *Nano Letters* **2019**, *19*, 2715−2722.

(147) Gao, B.; Arya, G.; Tao, A. R. Self-orienting nanocubes for the assembly of plasmonic nanojunctions. *Nature Nanotechnology* **2012**, *7*, 433−437.

(148) Milner, S. T.; Witten, T. A.; Cates, M. E. Effects of polydispersity in the end-grafted polymer brush. *Macromolecules* 1989, 22, 853−861.

(149) Birshtein, T.; Liatskaya, Y.; Zhulina, E. Theory of super-molecular structures of polydisperse block copolymers: 1. Planar layers of grafted chains. *Polymer* 1990, 31, 2185−2196.

(150) Minko, S.; Luzinov, I.; Luchnikov, V.; Müller, M.; Patil, S.; Stamm, M. Bidisperse Mixed Brushes: Synthesis and Study of Segregation in Selective Solvent. *Macromolecules* 2003, 36, 7268−7279.

(151) Romeis, D.; Sommer, J.-U. Binary and Bidisperse Polymer Brushes: Coexisting Surface States. *ACS Applied Materials & Interfaces* 2015, 7, 12496−12504.

(152) Santos, P. J.; Cheung, T. C.; Macfarlane, R. J. Assembling Ordered Crystals with Disperse Building Blocks. *Nano Letters* 2019, 19, 5774−5780.

(153) Travesset, A. Soft Skyrmions, Spontaneous Valence and Selection Rules in Nanoparticle Superlattices. *ACS Nano* 2017, 11, 5375−5382.

(154) Santos, P. J.; Gabrys, P. A.; Zornberg, L. Z.; Lee, M. S.; Macfarlane, R. J. Macroscopic materials assembled from nanoparticle superlattices. *Nature* 2021, 591, 586−591.

(155) Yee, D. W.; Lee, M. S.; An, J.; Macfarlane, R. J. Reversible Diffusionless Phase Transitions in 3D Nanoparticle Superlattices. *Journal of the American Chemical Society* 2023, 145, 6051−6056.

(156) Plamper, F. A.; Richtering, W. Functional Microgels and Microgel Systems. *Accounts of Chemical Research* 2017, 50, 131−140.

(157) Karg, M.; König, T. A.; Retsch, M.; Stelling, C.; Reichstein, P. M.; Honold, T.; Thelakkat, M.; Fery, A. Colloidal self-assembly concepts for light management in photovoltaics. *Materials Today* 2015, 18, 185−205.

(158) Karg, M. Functional Materials Design through Hydrogel Encapsulation of Inorganic Nanoparticles: Recent Developments and Challenges. *Macromolecular Chemistry and Physics* 2016, 217, 242−255.

(159) de Aguiar, I. B.; van de Laar, T.; Meireles, M.; Bouchoux, A.; Sprakel, J.; Schroën, K. Deswelling and deformation of microgels in concentrated packings. *Scientific Reports* 2017, 7, No. 10223.

(160) Conley, G. M.; Aebischer, P.; Nöjd, S.; Schurtenberger, P.; Scheffold, F. Jamming and overpacking fuzzy microgels: Deformation, interpenetration, and compression. *Science Advances* 2017, 3, No. e1700969.

(161) Lyon, L. A.; Fernandez-Nieves, A. The Polymer/Colloid Duality of Microgel Suspensions. *Annual Review of Physical Chemistry* 2012, 63, 25−43.

(162) Guillermo, A.; Addad, J. P. C.; Bazile, J. P.; Duracher, D.; Elaissari, A.; Pichot, C. NMR investigations into heterogeneous structures of thermosensitive microgel particles. *Journal of Polymer Science Part B: Polymer Physics* 2000, 38, 889−898.

(163) Wang, Z. J.; Zhu, C. N.; Hong, W.; Wu, Z. L.; Zheng, Q. Cooperative deformations of periodically patterned hydrogels. *Science Advances* 2017, 3, No. e1700348.

(164) Bowden, N.; Brittain, S.; Evans, A. G.; Hutchinson, J. W.; Whitesides, G. M. Spontaneous formation of ordered structures in thin films of metals supported on an elastomeric polymer. *Nature* 1998, 393, 146−149.

(165) Kang, M. K.; Huang, R. Swell-induced surface instability of confined hydrogel layers on substrates. *Journal of the Mechanics and Physics of Solids* 2010, 58, 1582−1598.

(166) Bowick, M.; Cacciuto, A.; Thorleifsson, G.; Travesset, A. Universal Negative Poisson Ratio of Self-Avoiding Fixed-Connectivity Membranes. *Physical Review Letters* 2001, 87, No. 148103.

(167) Mazaev, A. V.; Ajeneza, O.; Shitikova, M. V. Auxetics materials: classification, mechanical properties and applications. *IOP Conference Series: Materials Science and Engineering* 2020, 747, No. 012008.

(168) Anderson, J. A.; Lorenz, C. D.; Travesset, A. Micellar crystals in solution from molecular dynamics simulations. *The Journal of Chemical Physics* 2008, 128, No. 184906.

(169) Scotti, A.; Gasser, U.; Herman, E. S.; Pelaez-Fernandez, M.; Han, J.; Menzel, A.; Lyon, L. A.; Fernández-Nieves, A. The role of ions in the self-healing behavior of soft particle suspensions. *Proceedings of the National Academy of Sciences* 2016, 113, 5576−5581.

(170) Hirotsu, S. Static and time-dependent properties of polymer gels around the volume phase transition. *Phase Transitions* 1994, 47, 183−240.

(171) Dimitriyev, M. S.; Chang, Y.-W.; Goldbart, P. M.; Fernández-Nieves, A. Swelling thermodynamics and phase transitions of polymer gels. *Nano Futures* 2019, 3, No. 042001.

(172) Zhou, Y.; Jin, L. Mechanics Underpinning Phase Separation of Hydrogels. *Macromolecules* 2023, 56, 426−439.

(173) Reddy, A.; Buckley, M. B.; Arora, A.; Bates, F. S.; Dorfman, K. D.; Grason, G. M. Stable Frank-Kasper phases of self-assembled, soft matter spheres. *Proceedings of the National Academy of Sciences of the United States of America* 2018, 115, 10233−10238.

(174) Park, S. Y.; Lytton-Jean, A. K. R.; Lee, B.; Weigand, S.; Schatz, G. C.; Mirkin, C. A. DNA-programmable nanoparticle crystallization. *Nature* 2008, 451, 553−556.

(175) Nykypanchuk, D.; Maye, M. M.; van der Lelie, D.; Gang, O. DNA-guided crystallization of colloidal nanoparticles. *Nature* 2008, 451, 549−552.

(176) Seeman, N. C.; Gang, O. Three-dimensional molecular and nanoparticle crystallization by DNA nanotechnology. *MRS Bulletin* 2017, 42, 904−912.

(177) Jones, M. R.; Seeman, N. C.; Mirkin, C. A. Programmable materials and the nature of the DNA bond. *Science* 2015, 347, No. 1260901.

(178) Kahn, J. S.; Gang, O. Designer Nanomaterials through Programmable Assembly. *Angewandte Chemie International Edition* 2022, 61, No. e202105678.

(179) Hong, F.; Zhang, F.; Liu, Y.; Yan, H. DNA Origami: Scaffolds for Creating Higher Order Structures. *Chemical Reviews* 2017, 117, 12584−12640.

(180) Beyeh, N. K.; Nonappa; Liljeström, V.; Mikkilä, J.; Korpi, A.; Bochicchio, D.; Pavan, G. M.; Ikkala, O.; Ras, R. H. A.; Kostiainen, M. A. Crystalline Cyclophane−Protein Cage Frameworks. *ACS Nano* 2018, 12, 8029−8036.

(181) Girard, M.; Millan, J. A.; de la Cruz, M. O. DNA-Driven Assembly: From Polyhedral Nanoparticles to Proteins. *Annual Review of Materials Research* 2017, 47, 33−49.

(182) Kim, K.-H.; Ko, D.-K.; Kim, Y.-T.; Kim, N. H.; Paul, J.; Zhang, S.-Q.; Murray, C. B.; Acharya, R.; DeGrado, W. F.; Kim, Y. H.; Grigoryan, G. Protein-directed self-assembly of a fullerene crystal. *Nature Communications* 2016, 7, No. 11429.

(183) Kostiainen, M. A.; Hiekkataipale, P.; Laiho, A.; Lemieux, V.; Seitsonen, J.; Ruokolainen, J.; Ceci, P. Electrostatic assembly of binary nanoparticle superlattices using protein cages. *Nature Nanotechnology* 2013, 8, 52−56.

(184) Pan, S.; Li, T. I. N. G.; de la Cruz, M. O. Molecular dynamics simulation of DNA-directed assembly of nanoparticle superlattices using patterned templates. *Journal of Polymer Science Part B: Polymer Physics* 2016, 54, 1687−1692.

(185) Preisler, Z.; Saccà, B.; Whitelam, S. Irregular model DNA particles self-assemble into a regular structure. *Soft Matter* 2017, 13, 8894−8902.

(186) Stewart, J. M.; Subramanian, H.; Franco, E. Self-assembly of multi-stranded RNA motifs into lattices and tubular structures. *Nucleic Acids Research* 2017, 45, 5449−5457.

(187) Tian, Y.; Zhang, H. V.; Kiick, K. L.; Saven, J. G.; Pochan, D. J. Fabrication of One- and Two-Dimensional Gold Nanoparticle Arrays on Computationally Designed Self-Assembled Peptide Templates. *Chemistry of Materials* 2018, 30, 8510−8520.

(188) Casey, M. T.; Scarlett, R. T.; Benjamin Rogers, W.; Jenkins, I.; Sinno, T.; Crocker, J. C. Driving diffusionless transformations in colloidal crystals using DNA handshaking. *Nature Communications* 2012, 3, 1209.

(189) Long, A. W.; Zhang, J.; Granick, S.; Ferguson, A. L. Machine learning assembly landscapes from particle tracking data. *Soft Matter* **2015**, *11*, 8141−8153.

(190) Wang, Y.; Wang, Y.; Zheng, X.; Ducrot, E.; Yodh, J. S.; Weck, M.; Pine, D. J. Crystallization of DNA-coated colloids. *Nature communications* **2015**, *6*, 7253.

(191) Liu, W.; Halverson, J.; Tian, Y.; Tkachenko, A. V.; Gang, O. Self-organized architectures from assorted DNA-framed nanoparticles. *Nature Chemistry* **2016**, *8*, 867−873.

(192) Zhang, Y.; He, X.; Zhuo, R.; Sha, R.; Brujic, J.; Seeman, N. C.; Chaikin, P. M. Multivalent, multiflavored droplets by design. *Proc. Natl. Acad. Sci. U.S.A.* **2018**, *115*, 9086−9091, DOI: 10.1073/pnas.1718511115.

(193) Zheng, J.; Constantinou, P. E.; Micheel, C.; Alivisatos, A. P.; Kiehl, R. A.; Seeman, N. C. Two-Dimensional Nanoparticle Arrays Show the Organizational Power of Robust DNA Motifs. *Nano Letters* **2006**, *6*, 1502−1504.

(194) Li, H.; Park, S. H.; Reif, J. H.; LaBean, T. H.; Yan, H. DNA-Templated Self-Assembly of Protein and Nanoparticle Linear Arrays. *Journal of the American Chemical Society* **2004**, *126*, 418−419.

(195) Zhang, J.; Liu, Y.; Ke, Y.; Yan, H. Periodic Square-Like Gold Nanoparticle Arrays Templated by Self-Assembled 2D DNA Nano-grids on a Surface. *Nano Letters* **2006**, *6*, 248−251.

(196) Johnson, J. A.; Dehankar, A.; Winter, J. O.; Castro, C. E. Reciprocal Control of Hierarchical DNA Origami-Nanoparticle Assemblies. *Nano Letters* **2019**, *19*, 8469−8475.

(197) Chen, J.; Seeman, N. C. Synthesis from DNA of a molecule with the connectivity of a cube. *Nature* **1991**, *350*, 631−633.

(198) Hao, Y.; Kristiansen, M.; Sha, R.; Birktoft, J. J.; Hernandez, C.; Mao, C.; Seeman, N. C. A device that operates within a self-assembled 3D DNA crystal. *Nature Chemistry* **2017**, *9*, 824−827.

(199) Seeman, N. C. Nucleic acid junctions and lattices. *Journal of Theoretical Biology* **1982**, *99*, 237−247.

(200) Zheng, J.; Birktoft, J. J.; Chen, Y.; Wang, T.; Sha, R.; Constantinou, P. E.; Ginell, S. L.; Mao, C.; Seeman, N. C. From molecular to macroscopic via the rational design of a self-assembled 3D DNA crystal. *Nature* **2009**, *461*, 74−77.

(201) Wang, X.; Sha, R.; Kristiansen, M.; Hernandez, C.; Hao, Y.; Mao, C.; Canary, J. W.; Seeman, N. C. An Organic Semiconductor Organized into 3D DNA Arrays by "Bottom-up" Rational Design. *Angewandte Chemie International Edition* **2017**, *56*, 6445−6448.

(202) Zhang, F.; Jiang, S.; Wu, S.; Li, Y.; Mao, C.; Liu, Y.; Yan, H. Complex wireframe DNA origami nanostructures with multi-arm junction vertices. *Nature Nanotechnology* **2015**, *10*, 779−784.

(203) Rothemund, P. W. K. Folding DNA to create nanoscale shapes and patterns. *Nature* **2006**, *440*, 297−302.

(204) Iinuma, R.; Ke, Y.; Jungmann, R.; Schlichthaerle, T.; Woehrstein, J. B.; Yin, P. Polyhedra Self-Assembled from DNA Tripods and Characterized with 3D DNA-PAINT. *Science* **2014**, *344*, 65−69.

(205) Jun, H.; Zhang, F.; Shepherd, T.; Ratanalert, S.; Qi, X.; Yan, H.; Bathe, M. Autonomously designed free-form 2D DNA origami. *Science Advances* **2019**, *5*, No. eaav0655.

(206) Jorgenson, T. D.; Mohammed, A. M.; Agrawal, D. K.; Schulman, R. Self-Assembly of Hierarchical DNA Nanotube Architectures with Well-Defined Geometries. *ACS Nano* **2017**, *11*, 1927−1936.

(207) Simmel, F. C.; Schulman, R. Self-organizing materials built with DNA. *MRS Bulletin* **2017**, *42*, 913−919.

(208) He, Y.; Chen, Y.; Liu, H.; Ribbe, A. E.; Mao, C. Self-Assembly of Hexagonal DNA Two-Dimensional (2D) Arrays. *Journal of the American Chemical Society* **2005**, *127*, 12202−12203.

(209) Woo, S.; Rothemund, P. W. K. Self-assembly of two-dimensional DNA origami lattices using cation-controlled surface diffusion. *Nature Communications* **2014**, *5*, 4889.

(210) Huang, C.-M.; Kucinic, A.; Johnson, J. A.; Su, H.-J.; Castro, C. E. Integrated computer-aided engineering and design for DNA assemblies. *Nature Materials* **2021**, *20*, 1264−1271.

(211) Johnson, J. A.; Kolliopoulos, V.; Castro, C. E. Co-self-assembly of multiple DNA origami nanostructures in a single pot. *Chemical Communications* **2021**, *57*, 4795−4798.

(212) Tian, Y.; Lhermitte, J. R.; Bai, L.; Vo, T.; Xin, H. L.; Li, H.; Li, R.; Fukuto, M.; Yager, K. G.; Kahn, J. S.; Xiong, Y.; Minevich, B.; Kumar, S. K.; Gang, O. Ordered three-dimensional nanomaterials using DNA-prescribed and valence-controlled material voxels. *Nature Materials* **2020**, *19*, 789−796.

(213) Liu, W.; Tagawa, M.; Xin, H. L.; Wang, T.; Emamy, H.; Li, H.; Yager, K. G.; Starr, F. W.; Tkachenko, A. V.; Gang, O. Diamond family of nanoparticle superlattices. *Science* **2016**, *351*, 582−586.

(214) Vial, S.; Nykypanchuk, D.; Yager, K. G.; Tkachenko, A. V.; Gang, O. Linear Mesostructures in DNA−Nanorod Self-Assembly. *ACS Nano* **2013**, *7*, 5437−5445.

(215) Vo, T.; Venkatasubramanian, V.; Kumar, S.; Srinivasan, B.; Pal, S.; Zhang, Y.; Gang, O. Stoichiometric control of DNA-grafted colloid self-assembly. *Proceedings of the National Academy of Sciences* **2015**, *112*, 4982−4987.

(216) Knorowski, C.; Travesset, A. Self-assembly and crystallization of hairy (f -star) and DNA-grafted nanocubes. *Journal of the American Chemical Society* **2014**, *136*, 653−659.

(217) Tkachenko, A. V. Morphological Diversity of DNA-Colloidal Self-Assembly. *Physical Review Letters* **2002**, *89*, No. 148303.

(218) Wang, M. X.; Brodin, J. D.; Millan, J. A.; Seo, S. E.; Girard, M.; Olvera De La Cruz, M.; Lee, B.; Mirkin, C. A. Altering DNA-Programmable colloidal crystallization paths by modulating particle repulsion. *Nano Letters* **2017**, *17*, 5126−5132.

(219) Mao, R.; Minevich, B.; McKeen, D.; Chen, Q.; Lu, F.; Gang, O.; Mittal, J. Regulating phase behavior of nanoparticle assemblies through engineering of DNA-mediated isotropic interactions. *Proc. Natl. Acad. Sci.* **2023**, *120*, No. e2302037120, DOI: 10.1073/pnas.2302037120.

(220) Knorowski, C.; Travesset, A. Materials design by DNA programmed self-assembly. *Current Opinion in Solid State and Materials Science* **2011**, *15*, 262−270.

(221) Sknepnek, R.; Vernizzi, G.; de la Cruz, M. Buckling of multicomponent elastic shells with line tension. *Soft Matter* **2012**, *8*, 636−644.

(222) Lin, H.; Lee, S.; Sun, L.; Spellings, M.; Engel, M.; Glotzer, S. C.; Mirkin, C. A. Clathrate colloidal crystals. *Science* **2017**, *355*, 931−935.

(223) O'Brien, M. N.; Jones, M. R.; Lee, B.; Mirkin, C. A. Anisotropic nanoparticle complementarity in DNA-mediated co-crystallization. *Nature Materials* **2015**, *14*, 833−839.

(224) Lu, F.; Vo, T.; Zhang, Y.; Frenkel, A.; Yager, K. G.; Kumar, S.; Gang, O. Unusual packing of soft-shelled nanocubes. *Science Advances* **2019**, *5*, 2399.

(225) Lu, F.; Yager, K. G.; Zhang, Y.; Xin, H.; Gang, O. Superlattices assembled through shape-induced directional binding. *Nature Communications* **2015**, *6*, 6912.

(226) Wang, S.-T.; Minevich, B.; Liu, J.; Zhang, H.; Nykypanchuk, D.; Byrnes, J.; Liu, W.; Bershadsky, L.; Liu, Q.; Wang, T.; Ren, G.; Gang, O. Designed and biologically active protein lattices. *Nature Communications* **2021**, *12*, 3702.

(227) Tian, Y.; Zhang, Y.; Wang, T.; Xin, H. L.; Li, H.; Gang, O. Lattice engineering through nanoparticle−DNA frameworks. *Nature Materials* **2016**, *15*, 654−661.

(228) Zion, M. Y. B.; He, X.; Maass, C. C.; Sha, R.; Seeman, N. C.; Chaikin, P. M. Self-assembled three-dimensional chiral colloidal architecture. *Science* **2017**, *358*, 633−636.

(229) Zhang, T.; Hartl, C.; Frank, K.; Heuer-Jungemann, A.; Fischer, S.; Nickels, P. C.; Nickel, B.; Liedl, T. 3D DNA Origami Crystals. *Advanced Materials* **2018**, *30*, No. 1800273.

(230) Michelson, A.; Minevich, B.; Emamy, H.; Huang, X.; Chu, Y. S.; Yan, H.; Gang, O. Three-dimensional visualization of nanoparticle lattices and multimaterial frameworks. *Science* **2022**, *376*, 203−207.

(231) Zhang, F.; Simmons, C. R.; Gates, J.; Liu, Y.; Yan, H. Self-Assembly of a 3D DNA Crystal Structure with Rationally Designed

Six-Fold Symmetry. *Angewandte Chemie International Edition* **2018**, *57*, 12504−12507.

(232) Lin, Z.; Emamy, H.; Minevich, B.; Xiong, Y.; Xiang, S.; Kumar, S.; Ke, Y.; Gang, O. Engineering Organization of DNA Nano-Chambers through Dimensionally Controlled and Multi-Sequence Encoded Differentiated Bonds. *Journal of the American Chemical Society* **2020**, *142*, 17531−17542.

(233) Jun, H.; Wang, X.; Bricker, W. P.; Bathe, M. Automated sequence design of 2D wireframe DNA origami with honeycomb edges. *Nature Communications* **2019**, *10*, 5419.

(234) Jun, H.; Wang, X.; Parsons, M.; Bricker, W.; John, T.; Li, S.; Jackson, S.; Chiu, W.; Bathe, M. Rapid prototyping of arbitrary 2D and 3D wireframe DNA origami. *Nucleic Acids Research* **2021**, *49*, 10265−10274.

(235) Patra, N.; Tkachenko, A. V. Programmable self-assembly of diamond polymorphs from chromatic patchy particles. *Physical Review E* **2018**, *98*, No. 032611.

(236) Adhikari, S.; Minevich, B.; Redeker, D.; Michelson, A. N.; Emamy, H.; Shen, E.; Gang, O.; Kumar, S. K. Controlling the Self-Assembly of DNA Origami Octahedra via Manipulation of Inter-Vertex Interactions. *Journal of the American Chemical Society* **2023**, *145*, 19578−19587.

(237) Ye, X.; Zhu, C.; Ercius, P.; Raja, S. N.; He, B.; Jones, M. R.; Hauwiller, M. R.; Liu, Y.; Xu, T.; Alivisatos, A. P. Structural diversity in binary superlattices self-assembled from polymer-grafted nanocrystals. *Nature Communications* **2015**, *6*, No. 10052.

(238) Bian, T.; Gardin, A.; Gemen, J.; Houben, L.; Perego, C.; Lee, B.; Elad, N.; Chu, Z.; Pavan, G. M.; Klajn, R. Electrostatic co-assembly of nanoparticles with oppositely charged small molecules into static and dynamic superstructures. *Nature Chemistry* **2021**, *13*, 940−949.

(239) Kim, H. J.; Nayak, B. P.; Zhang, H.; Ocko, B. M.; Travesset, A.; Vaknin, D.; Mallapragada, S. K.; Wang, W. Two-dimensional assembly of gold nanoparticles grafted with charged-end-group polymers. *Journal of Colloid and Interface Science* **2023**, *650*, 1941−1948.

(240) Zhang, H.; Wang, W.; Mallapragada, S.; Travesset, A.; Vaknin, D. Macroscopic and tunable nanoparticle superlattices. *Nanoscale* **2017**, *9*, 164−171.

(241) Zhang, H.; Wang, W.; Akinc, M.; Mallapragada, S.; Travesset, A.; Vaknin, D. Assembling and ordering polymer-grafted nanoparticles in three dimensions. *Nanoscale* **2017**, *9*, 8710−8715.

(242) Zhang, H.; Wang, W.; Mallapragada, S.; Travesset, A.; Vaknin, D. Ion-Specific Interfacial Crystallization of Polymer-Grafted Nanoparticles. *Journal of Physical Chemistry C* **2017**, *121*, 15424−15429.

(243) Yethiraj, A.; van Blaaderen, A. A colloidal model system with an interaction tunable from hard sphere to soft and dipolar. *Nature* **2003**, *421*, 513−517.

(244) Leunissen, M. E.; Christova, C. G.; Hynninen, A.-P.; Royall, C. P.; Campbell, A. I.; Imhof, A.; Dijkstra, M.; van Roij, R.; van Blaaderen, A. Ionic colloidal crystals of oppositely charged particles. *Nature* **2005**, *437*, 235−240.

(245) Alexander, S.; Chaikin, P. M.; Grant, P.; Morales, G. J.; Pincus, P.; Hone, D. Charge renormalization, osmotic pressure, and bulk modulus of colloidal crystals: Theory. *The Journal of Chemical Physics* **1984**, *80*, 5776−5781.

(246) Colla, T. E.; Levin, Y.; Trizac, E. A self-consistent renormalized jellium approach for calculating structural and thermodynamic properties of charge stabilized colloidal suspensions. *The Journal of Chemical Physics* **2009**, *131*, No. 074115.

(247) Castañeda-Priego, R.; Lobaskin, V.; Mixteco-Sánchez, J. C.; Rojas-Ochoa, L. F.; Linse, P. On the calculation of the structure of charge-stabilized colloidal dispersions using density-dependent potentials. *Journal of Physics: Condensed Matter* **2012**, *24*, No. 065102.

(248) Boon, N.; Guerrero-García, G. I.; van Roij, R.; de la Cruz, M. O. Effective charges and virial pressure of concentrated macroion solutions. *Proceedings of the National Academy of Sciences* **2015**, *112*, 9242−9246.

(249) Cats, P.; Evans, R.; Härtel, A.; van Roij, R. Primitive model electrolytes in the near and far field: Decay lengths from DFT and simulations. *The Journal of Chemical Physics* **2021**, *154*, 124504.

(250) Dormidontova, E. E. Role of Competitive PEO Water and Water Water Hydrogen Bonding in Aqueous Solution PEO Behavior. *Macromolecules* **2002**, *35*, 987−1001.

(251) Batista, C. A.; Larson, R. G.; Kotov, N. A. Nonadditivity of nanoparticle interactions. *Science* **2015**, *350*, No. 1242477.

(252) Waltmann, T.; Waltmann, C.; Horst, N.; Travesset, A. Many Body Effects and Icosahedral Order in Superlattice Self-Assembly. *Journal of the American Chemical Society* **2018**, *140*, 8236−8245.

(253) Gao, H.; Bettscheider, S.; Kraus, T.; Müser, M. H. Entropy Can Bundle Nanowires in Good Solvents. *Nano letters* **2019**, *19*, 6993−6999.

(254) Van Lehn, R. C.; Atukorale, P. U.; Carney, R. P.; Yang, Y. S.; Stellacci, F.; Irvine, D. J.; Alexander-Katz, A. Effect of particle diameter and surface composition on the spontaneous fusion of monolayer-protected gold nanoparticles with lipid bilayers. *Nano Letters* **2013**, *13*, 4060−4067.

(255) Chew, A. K.; Van Lehn, R. C. Effect of Core Morphology on the Structural Asymmetry of Alkanethiol Monolayer-Protected Gold Nanoparticles. *The Journal of Physical Chemistry C* **2018**, *122*, 26288−26297.

(256) Dallin, B. C.; Yeon, H.; Ostwalt, A. R.; Abbott, N. L.; Van Lehn, R. C. Molecular Order Affects Interfacial Water Structure and Temperature-Dependent Hydrophobic Interactions between Nonpolar Self-Assembled Monolayers. *Langmuir* **2019**, *35*, 2078−2088.

(257) Dallin, B. C.; Van Lehn, R. C. Spatially Heterogeneous Water Properties at Disordered Surfaces Decrease the Hydrophobicity of Nonpolar Self-Assembled Monolayers. *The Journal of Physical Chemistry Letters* **2019**, *10*, 3991−3997.

(258) Chew, A. K.; Dallin, B. C.; Van Lehn, R. C. The Interplay of Ligand Properties and Core Size Dictates the Hydrophobicity of Monolayer-Protected Gold Nanoparticles. *ACS Nano* **2021**, *15*, 4534−4545.

(259) Petretto, E.; Ong, Q. K.; Olgiati, F.; Mao, T.; Campomanes, P.; Stellacci, F.; Vanni, S. Monovalent ion-mediated charge−charge interactions drive aggregation of surface-functionalized gold nanoparticles. *Nanoscale* **2022**, *14*, 15181−15192.

(260) Guo, P.; Sknepnek, R.; de la Cruz, M. O. Electrostatic-Driven Ridge Formation on Nanoparticles Coated with Charged End-Group Ligands. *The Journal of Physical Chemistry C* **2011**, *115*, 6484−6490.

(261) Kister, T.; Monego, D.; Mulvaney, P.; Widmer-Cooper, A.; Kraus, T. Colloidal Stability of Apolar Nanoparticles: The Role of Particle Size and Ligand Shell Structure. *ACS Nano* **2018**, *12*, 5969−5977.

(262) Monego, D.; Kister, T.; Kirkwood, N.; Mulvaney, P.; Widmer-Cooper, A.; Kraus, T. Colloidal Stability of Apolar Nanoparticles: Role of Ligand Length. *Langmuir* **2018**, *34*, 12982−12989.

(263) Monego, D.; Kister, T.; Kirkwood, N.; Doblas, D.; Mulvaney, P.; Kraus, T.; Widmer-Cooper, A. When Like Destabilizes Like: Inverted Solvent Effects in Apolar Nanoparticle Dispersions. *ACS Nano* **2020**, *14*, 5278−5287.

(264) Hasan, M. R.; Niebuur, B.-J.; Siebrecht, M.; Kuttich, B.; Schweins, R.; Widmer-Cooper, A.; Kraus, T. The Colloidal Stability of Apolar Nanoparticles in Solvent Mixtures. *ACS Nano* **2023**, *17*, 9302−9312.

(265) Xue, Y.; Li, X.; Li, H.; Zhang, W. Quantifying thiol−gold interactions towards the efficient strength control. *Nature Communications* **2014**, *5*, 4348.

(266) Boles, M. A.; Ling, D.; Hyeon, T.; Talapin, D. V. The surface science of nanocrystals. *Nature Materials* **2016**, *15*, 141−153.

(267) Bettscheider, S.; Kuttich, B.; Engel, L. F.; González-García, L.; Kraus, T. Bundling of Nanowires Induced by Unbound Ligand. *The Journal of Physical Chemistry C* **2021**, *125*, 3590−3598.

(268) Abelson, A.; Qian, C.; Salk, T.; Luan, Z.; Fu, K.; Zheng, J.-G.; Wardini, J. L.; Law, M. Collective topo-epitaxy in the self-assembly of a 3D quantum dot superlattice. *Nature Materials* **2020**, *19*, 49−55.

(269) Yang, Y.; Qin, H.; Jiang, M.; Lin, L.; Fu, T.; Dai, X.; Zhang, Z.; Niu, Y.; Cao, H.; Jin, Y.; Zhao, F.; Peng, X. Entropic Ligands for Nanocrystals: From Unexpected Solution Properties to Outstanding Processability. *Nano Letters* **2016**, *16*, 2133–2138.

(270) Hoff, S. E.; Di Silvio, D.; Ziolo, R. F.; Moya, S. E.; Heinz, H. Patterning of Self-Assembled Monolayers of Amphiphilic Multiseg-ment Ligands on Nanoparticles and Design Parameters for Protein Interactions. *ACS Nano* **2022**, *16*, 8766–8783.

(271) Ong, Q.; Luo, Z.; Stellacci, F. Characterization of Ligand Shell for Mixed-Ligand Coated Gold Nanoparticles. *Accounts of Chemical Research* **2017**, *50*, 1911–1919.

(272) Pons-Siepermann, I. C.; Glotzer, S. C. Design of patchy particles using ternary self-assembled monolayers. *Soft Matter* **2012**, *8*, 6226.

(273) Zhao, B.; Zhu, L. Mixed Polymer Brush-Grafted Particles: A New Class of Environmentally Responsive Nanostructured Materials. *Macromolecules* **2009**, *42*, 9369–9383.

(274) Pong, B.-K.; Lee, J.-Y.; Trout, B. L. First Principles Computational Study for Understanding the Interactions between ssDNA and Gold Nanoparticles: Adsorption of Methylamine on Gold Nanoparticulate Surfaces. *Langmuir* **2005**, *21*, 11599–11603.

(275) Bo, A.; Liu, Y.; Kuttich, B.; Kraus, T.; Widmer-Cooper, A.; de Jonge, N. Nanoscale Faceting and Ligand Shell Structure Dominate the Self-Assembly of Nonpolar Nanoparticles into Superlattices. *Advanced Materials* **2022**, *34*, No. 2109093.

(276) Ye, X.; Chen, J.; Engel, M.; Millan, J. A.; Li, W.; Qi, L.; Xing, G.; Collins, J. E.; Kagan, C. R.; Li, J.; Glotzer, S. C.; Murray, C. B. Competition of shape and interaction patchiness for self-assembling nanoplates. *Nature Chemistry* **2013**, *5*, 466–473.

(277) Yuan, Y.; Martinez, A.; Senyuk, B.; Tasinkevych, M.; Smalyukh, I. I. Chiral liquid crystal colloids. *Nature Materials* **2018**, *17*, 71–79.

(278) Zhou, Y.; Senyuk, B.; Zhang, R.; Smalyukh, I. I.; de Pablo, J. J. Degenerate conic anchoring and colloidal elastic dipole-hexadecapole transformations. *Nature Communications* **2019**, *10*, 1000.

(279) Meng, C.; Wu, J.-S.; Smalyukh, I. I. Topological steering of light by nematic vortices and analogy to cosmic strings. *Nature Materials* **2023**, *22*, 64–72.

(280) Liu, Q.; Yuan, Y.; Smalyukh, I. I. Electrically and Optically Tunable Plasmonic Guest–Host Liquid Crystals with Long-Range Ordered Nanoparticles. *Nano Letters* **2014**, *14*, 4071–4077.

(281) Mundoor, H.; Wu, J.-S.; Wensink, H. H.; Smalyukh, I. I. Thermally reconfigurable monoclinic nematic colloidal fluids. *Nature* **2021**, *590*, 268–274.

(282) Liu, Q.; Ackerman, P. J.; Lubensky, T. C.; Smalyukh, I. I. Biaxial ferromagnetic liquid crystal colloids. *Proceedings of the National Academy of Sciences* **2016**, *113*, 10479–10484.

(283) Ghosh, S.; Smalyukh, I. Electrical Switching of Nematic Plasmonic Nanocolloids for Infrared Solar Gain Control. *Advanced Optical Materials* **2022**, *10*, No. 2201513.

(284) Smalyukh, I. I. Review: knots and other new topological effects in liquid crystals and colloids. *Reports on Progress in Physics* **2020**, *83*, No. 106601.

(285) Varilly, P.; Angioletti-Uberti, S.; Mognetti, B. M.; Frenkel, D. A general theory of DNA-mediated and other valence-limited colloidal interactions. *The Journal of Chemical Physics* **2012**, *137*, No. 094108.

(286) Lowensohn, J.; Stevens, L.; Goldstein, D.; Mognetti, B. M. Sliding across a surface: Particles with fixed and mobile ligands. *The Journal of Chemical Physics* **2022**, *156*, No. 164902.

(287) Marbach, S.; Zheng, J. A.; Holmes-Cerfon, M. The Nanocaterpillar's Random Walk: Diffusion With Ligand-Receptor Contacts. *Soft Matter* **2022**, *18*, 3130–3146.

(288) Das, A.; Limmer, D. T. Variational design principles for nonequilibrium colloidal assembly. *The Journal of Chemical Physics* **2021**, *154*, No. 014107.

(289) Rechtsman, M. C.; Stillinger, F. H.; Torquato, S. Optimized Interactions for Targeted Self-Assembly: Application to a Honeycomb Lattice. *Physical Review Letters* **2005**, *95*, No. 228301.

(290) Ma, Y.; Aulicino, J. C.; Ferguson, A. L. Inverse Design of Self-Assembling Diamond Photonic Lattices from Anisotropic Colloidal Clusters. *The Journal of Physical Chemistry B* **2021**, *125*, 2398–2410.

(291) Hens, Z.; De Roo, J. Atomically Precise Nanocrystals. *Journal of the American Chemical Society* **2020**, *142*, 15627–15637.

(292) Schacht, J.; Gaston, N. From the Superatom Model to a Diverse Array of Super-Elements: A Systematic Study of Dopant Influence on the Electronic Structure of Thiolate-Protected Gold Clusters. *ChemPhysChem* **2016**, *17*, 3237–3244.

(293) Aikens, C. M.; Jin, R.; Roy, X.; Tsukuda, T. From atom-precise nanoclusters to superatom materials. *The Journal of Chemical Physics* **2022**, *156*, No. 170401.

(294) Doerk, G. S.; Stein, A.; Bae, S.; Noack, M. M.; Fukuto, M.; Yager, K. G. Autonomous discovery of emergent morphologies in directed self-assembly of block copolymer blends. *Science Advances* **2023**, *9*, No. eadd3687.

(295) Chennakesavalu, S.; Rotskoff, G. M. Probing the theoretical and computational limits of dissipative design. *The Journal of Chemical Physics* **2021**, *155*, No. 194114.

(296) Lieu, U. T.; Yoshinaga, N. Dynamic control of self-assembly of quasicrystalline structures through reinforcement learning. *ArXiv* **2023**, https://arxiv.org/abs/2309.06869.

(297) Choueiri, R. M.; Klinkova, A.; Thérien-Aubin, H.; Rubinstein, M.; Kumacheva, E. Structural Transitions in Nanoparticle Assemblies Governed by Competing Nanoscale Forces. *Journal of the American Chemical Society* **2013**, *135*, 10262–10265.

(298) Liu, F.; Goyal, S.; Forrester, M.; Ma, T.; Miller, K.; Mansoorieh, Y.; Henjum, J.; Zhou, L.; Cochran, E.; Jiang, S. Self-assembly of Janus Dumbbell Nanocrystals and Their Enhanced Surface Plasmon Resonance. *Nano Letters* **2019**, *19*, 1587–1594.

(299) Sashuk, V.; Winkler, K.; Żywociński, A.; Wojciechowski, T.; Górecka, E.; Fiałkowski, M. Nanoparticles in a Capillary Trap: Dynamic Self-Assembly at Fluid Interfaces. *ACS Nano* **2013**, *7*, 8833–8839.

(300) Zheng, F.; Zhang, Y.; Dong, L.; Zhao, D.; Feng, R.; Tao, P.; Shang, W.; Fu, B.; Song, C.; Deng, T. The impact of surface chemistry on the interfacial evaporation-driven self-assembly of thermoplas-monic gold nanoparticles. *Nanoscale* **2021**, *13*, 20521–20530.

(301) Sánchez-Iglesias, A.; Claes, N.; Solís, D. M.; Taboada, J. M.; Bals, S.; Liz-Marzán, L. M.; Grzelczak, M. Reversible Clustering of Gold Nanoparticles under Confinement. *Angewandte Chemie International Edition* **2018**, *57*, 3183–3186.

(302) Liu, D.; Li, C.; Zhou, F.; Zhang, T.; Liu, G.; Cai, W.; Li, Y. Capillary Gradient-Induced Self-Assembly of Periodic Au Spherical Nanoparticle Arrays on an Ultralarge Scale via a Bisolvent System at Air/Water Interface. *Advanced Materials Interfaces* **2017**, *4*, No. 1600976.

(303) Smith, A. M.; Johnston, K. A.; Crawford, S. E.; Marbella, L. E.; Millstone, J. E. Ligand density quantification on colloidal inorganic nanoparticles. *The Analyst* **2017**, *142*, 11–29.

(304) Guzman-Juarez, B.; Abdelaal, A. B.; Reven, L. NMR Characterization of Nanoscale Surface Patterning in Mixed Ligand Nanoparticles. *ACS Nano* **2022**, *16*, 20116–20128.

(305) Wintzheimer, S.; Granath, T.; Oppmann, M.; Kister, T.; Thai, T.; Kraus, T.; Vogel, N.; Mandel, K. Supraparticles: Functionality from Uniform Structural Motifs. *ACS Nano* **2018**, *12*, 5093–5120.

(306) Chu, Z.; Seeger, S. Superamphiphobic surfaces. *Chemical Society Reviews* **2014**, *43*, 2784–2798.

(307) Schulz, M.; Keddie, J. L. A critical and quantitative review of the stratification of particles during the drying of colloidal films. *Soft Matter* **2018**, *14*, 6181–6197.

(308) Liu, W.; Midya, J.; Kappl, M.; Butt, H.-J.; Nikoubashman, A. Segregation in Drying Binary Colloidal Droplets. *ACS Nano* **2019**, *13*, 4972–4979.

(309) Wang, P.-p.; Qiao, Q.; Zhu, Y.; Ouyang, M. Colloidal Binary Supracrystals with Tunable Structural Lattices. *Journal of the American Chemical Society* **2018**, *140*, 9095–9098.

(310) Yang, Y.; Wang, B.; Shen, X.; Yao, L.; Wang, L.; Chen, X.; Xie, S.; Li, T.; Hu, J.; Yang, D.; Dong, A. Scalable Assembly of Crystalline

Binary Nanocrystal Superparticles and Their Enhanced Magnetic and Electrochemical Properties. *Journal of the American Chemical Society* **2018**, *140*, 15038−15047.

(311) Murray, C. B.; Kagan, C. R.; Bawendi, M. G. Synthesis and Characterization of Monodisperse Nanocrystals and Close-Packed Nanocrystal Assemblies. *Annual Review of Materials Science* **2000**, *30*, 545−610.

(312) Dong, A.; Chen, J.; Vora, P. M.; Kikkawa, J. M.; Murray, C. B. Binary nanocrystal superlattice membranes self-assembled at the liquid-air interface. *Nature* **2010**, *466*, 474−477.

(313) Whetten, R. L.; Khoury, J. T.; Alvarez, M. M.; Murthy, S.; Vezmar, I.; Wang, Z. L.; Stephens, P. W.; Cleveland, C. L.; Luedtke, W. D.; Landman, U. Nanocrystal gold molecules. *Advanced Materials* **1996**, *8*, 428−433.

(314) Whetten, R. L.; Shafigullin, M. N.; Khoury, J. T.; Schaaff, T. G.; Vezmar, I.; Alvarez, M. M.; Wilkinson, A. Crystal Structures of Molecular Gold Nanocrystal Arrays. *Accounts of Chemical Research* **1999**, *32*, 397−406.

(315) Hajiw, S.; Pansu, B.; Sadoc, J.-F. Evidence for a C14 Frank-Kasper Phase in One-Size Gold Nanoparticle Superlattices. *ACS Nano* **2015**, *9*, 8116−8121.

(316) Geuchies, J. J.; van Overbeek, C.; Evers, W. H.; Goris, B.; de Backer, A.; Gantapara, A. P.; Rabouw, F. T.; Hilhorst, J.; Peters, J. L.; Konovalov, O.; Petukhov, A. V.; Dijkstra, M.; Siebbeles, L. D. A.; van Aert, S.; Bals, S.; Vanmaekelbergh, D. In situ study of the formation mechanism of two-dimensional superlattices from PbSe nanocrystals. *Nature Materials* **2016**, *15*, 1248−1254.

(317) Shevchenko, E. V.; Talapin, D. V.; Kotov, N. A.; O'Brien, S.; Murray, C. B. Structural diversity in binary nanoparticle superlattices. *Nature* **2006**, *439*, 55−59.

(318) Cherniukh, I.; Rainò, G.; Stöferle, T.; Burian, M.; Travesset, A.; Naumenko, D.; Amenitsch, H.; Erni, R.; Mahrt, R. F.; Bodnarchuk, M. I.; Kovalenko, M. V. Perovskite-type superlattices from lead halide perovskite nanocubes. *Nature* **2021**, *593*, 535−542.

(319) Talapin, D. V.; Shevchenko, E. V.; Bodnarchuk, M. I.; Ye, X.; Chen, J.; Murray, C. B. Quasicrystalline order in self-assembled binary nanoparticle superlattices. *Nature* **2009**, *461*, 964−967.

(320) Ye, X.; Chen, J.; Eric Irrgang, M.; Engel, M.; Dong, A.; Glotzer, S. C.; Murray, C. B. Quasicrystalline nanocrystal superlattice with partial matching rules. *Nature Materials* **2017**, *16*, 214−219.

(321) Elbert, K. C.; Vo, T.; Krook, N. M.; Zygmunt, W.; Park, J.; Yager, K. G.; Composto, R. J.; Glotzer, S. C.; Murray, C. B. Dendrimer Ligand Directed Nanoplate Assembly. *ACS Nano* **2019**, *13*, 14241−14251.

(322) Jarzynski, C. Nonequilibrium equality for free energy differences. *Physical Review Letters* **1997**, *78*, 2690−2693.

(323) Liu, W.; Kappl, M.; Steffen, W.; Butt, H.-J. Controlling supraparticle shape and structure by tuning colloidal interactions. *Journal of Colloid and Interface Science* **2022**, *607*, 1661−1670.

(324) Fan, Z.; Grünwald, M. Orientational Order in Self-Assembled Nanocrystal Superlattices. *Journal of the American Chemical Society* **2019**, *141*, 1980−1988.

(325) Howard, M. P.; Nikoubashman, A.; Panagiotopoulos, A. Z. Stratification Dynamics in Drying Colloidal Mixtures. *Langmuir* **2017**, *33*, 3685−3693.

(326) Kister, T.; Mravlak, M.; Schilling, T.; Kraus, T. Pressure-controlled formation of crystalline, Janus, and core−shell supraparticles. *Nanoscale* **2016**, *8*, 13377−13384.

(327) Osman, A.; Goehring, L.; Patti, A.; Stitt, H.; Shokri, N. Fundamental Investigation of the Drying of Solid Suspensions. *Industrial & Engineering Chemistry Research* **2017**, *56*, 10506−10513.

(328) Howard, M. P.; Nikoubashman, A. Stratification of polymer mixtures in drying droplets: Hydrodynamics and diffusion. *The Journal of Chemical Physics* **2020**, *153*, No. 054901.

(329) Patil, A.; Heil, C. M.; Vanthournout, B.; Bleuel, M.; Singla, S.; Hu, Z.; Gianneschi, N. C.; Shawkey, M. D.; Sinha, S. K.; Jayaraman, A.; Dhinojwala, A. Structural Color Production in Melanin-Based Disordered Colloidal Nanoparticle Assemblies in Spherical Confinement. *Advanced Optical Materials* **2022**, *10*, No. 2102162.

(330) Howard, M. P.; Reinhart, W. F.; Sanyal, T.; Shell, M. S.; Nikoubashman, A.; Panagiotopoulos, A. Z. Evaporation-induced assembly of colloidal crystals. *The Journal of Chemical Physics* **2018**, *149*, No. 094901.

(331) Mampallil, D.; Eral, H. B. A review on suppression and utilization of the coffee-ring effect. *Advances in Colloid and Interface Science* **2018**, *252*, 38−54.

(332) Williams, S. R.; Searles, D. J.; Evans, D. J. Independence of the transient fluctuation theorem to thermostatting details. *Physical Review E* **2004**, *70*, No. 066113.

(333) Yetkin, M.; Wani, Y. M.; Kritika, K.; Howard, M. P.; Kappl, M.; Butt, H.-J.; Nikoubashman, A. Structure Formation in Supra-particles Composed of Spherical and Elongated Particles. *Langmuir* **2024**, *40*, 1096−1108.

(334) Liu, W.; Kappl, M.; Butt, H.-J. Tuning the Porosity of Supraparticles. *ACS Nano* **2019**, *13*, 13949−13956.

(335) Macias, E.; Waltmann, T.; Travesset, A. Assembly of nanocrystal clusters by solvent evaporation: icosahedral order and the breakdown of the Maxwell regime. *Soft Matter* **2020**, *16*, 7350−7358.

(336) Waltmann, T.; Travesset, A. Assembly by solvent evaporation: equilibrium structures and relaxation times. *Nanoscale* **2019**, *11*, 18702−18714.

(337) Howard, M. P.; Nikoubashman, A.; Palmer, J. C. Modeling hydrodynamic interactions in soft materials with multiparticle collision dynamics. *Current Opinion in Chemical Engineering* **2019**, *23*, 34−43.

(338) Rabani, E.; Reichman, D. R.; Geissler, P. L.; Brus, L. E. Drying-mediated self-assembly of nanoparticles. *Nature* **2003**, *426*, 271−274.

(339) Sztrum, C. G.; Hod, O.; Rabani, E. Self-assembly of nanoparticles in three-dimensions: Formation of stalagmites. *Journal of Physical Chemistry B* **2005**, *109*, 6741−6747.

(340) Sztrum, C.; Rabani, E. Out-of-Equilibrium Self-Assembly of Binary Mixtures of Nanoparticles. *Advanced Materials* **2006**, *18*, 565−571.

(341) Kletenik-Edelman, O.; Ploshnik, E.; Salant, A.; Shenhar, R.; Banin, U.; Rabani, E. Drying-mediated hierarchical self-assembly of nanoparticles: A dynamical coarse-grained approach. *Journal of Physical Chemistry C* **2008**, *112*, 4498−4506.

(342) Kletenik-Edelman, O.; Sztrum-Vartash, C. G.; Rabani, E. Coarse-grained lattice models for drying-mediated self-assembly of nanoparticles. *Journal of Materials Chemistry* **2009**, *19*, 2872−2876.

(343) Rudzinski, J. F. Recent Progress towards Chemically-Specific Coarse-Grained Simulation Models with Consistent Dynamical Properties. *Computation* **2019**, *7*, 42.

(344) Geyer, T.; Born, P.; Kraus, T. Switching Between Crystallization and Amorphous Agglomeration of Alkyl Thiol-Coated Gold Nanoparticles. *Physical Review Letters* **2012**, *109*, No. 128302.

(345) Hu, H.; Ji, F.; Xu, Y.; Yu, J.; Liu, Q.; Chen, L.; Chen, Q.; Wen, P.; Lifshitz, Y.; Wang, Y.; Zhang, Q.; Lee, S.-T. Reversible and Precise Self-Assembly of Janus Metal-Organosilica Nanoparticles through a Linker-Free Approach. *ACS Nano* **2016**, *10*, 7323−7330.

(346) Malaspina, D. C.; Viñas, C.; Teixidor, F.; Faraudo, J. Atomistic Simulations of COSAN: Amphiphiles without a Head-and-Tail Design Display "Head and Tail" Surfactant Behavior. *Angewandte Chemie International Edition* **2020**, *59*, 3088−3092.

(347) Hernández-López, L.; Martínez-Esaín, J.; Carné-Sánchez, A.; Grancha, T.; Faraudo, J.; Maspoch, D. Steric Hindrance in Metal Coordination Drives the Separation of Pyridine Regioisomers Using Rhodium(II)-Based Metal−Organic Polyhedra. *Angewandte Chemie International Edition* **2021**, *60*, 11406−11413.

(348) Khobotov-Bakishev, A.; von Baeckmann, C.; Ortín-Rubio, B.; Hernández-López, L.; Cortés-Martínez, A.; Martínez-Esaín, J.; Gándara, F.; Juanhuix, J.; Platero-Prats, A. E.; Faraudo, J.; Carné-Sánchez, A.; Maspoch, D. Multicomponent, Functionalized HKUST-1 Analogues Assembled via Reticulation of Prefabricated Metal−Organic Polyhedral Cavities. *Journal of the American Chemical Society* **2022**, *144*, 15745−15753.

(349) Bian, K.; Choi, J. J.; Kaushik, A.; Clancy, P.; Smilgies, D.-M. M.; Hanrath, T. Shape-Anisotropy Driven Symmetry Transformations in Nanocrystal Superlattice Polymorphs. *ACS Nano* **2011**, *5*, 2815–2823.

(350) Rupich, S. M.; Castro, F. C.; Irvine, W. T. M.; Talapin, D. V. Soft epitaxy of nanocrystal superlattices. *Nature Communications* **2014**, *5*, 5045.

(351) Chen, J.; Fasoli, A.; Cushen, J. D.; Wan, L.; Ruiz, R. Self-Assembly and Directed Assembly of Polymer Grafted Nanocrystals via Solvent Annealing. *Macromolecules* **2017**, *50*, 9636–9646.

(352) Wang, Y.; Chen, J.; Zhu, C.; Zhu, B.; Jeong, S.; Yi, Y.; Liu, Y.; Fiadorwu, J.; He, P.; Ye, X. Kinetically Controlled Self-Assembly of Binary Polymer-Grafted Nanocrystals into Ordered Superstructures via Solvent Vapor Annealing. *Nano Letters* **2021**, *21*, 5053–5059.

(353) Pickering, S. U. CXCVI.—Emulsions. *Journal of the Chemical Society, Transactions* **1907**, *91*, 2001–2021.

(354) Dupont, H.; Maingret, V.; Schmitt, V.; Héroguez, V. New Insights into the Formulation and Polymerization of Pickering Emulsions Stabilized by Natural Organic Particles. *Macromolecules* **2021**, *54*, 4945–4970.

(355) Ponomareva, E.; Volk, K.; Mulvaney, P.; Karg, M. Surface Lattice Resonances in Self-Assembled Gold Nanoparticle Arrays: Impact of Lattice Period, Structural Disorder, and Refractive Index on Resonance Quality. *Langmuir* **2020**, *36*, 13601–13612.

(356) Vogel, N.; Fernández-López, C.; Pérez-Juste, J.; Liz-Marzán, L. M.; Landfester, K.; Weiss, C. K. Ordered Arrays of Gold Nanostructures from Interfacially Assembled Au@PNIPAM Hybrid Nanoparticles. *Langmuir* **2012**, *28*, 8985–8993.

(357) Grillo, F.; Fernandez-Rodriguez, M. A.; Antonopoulou, M.-N.; Gerber, D.; Isa, L. Self-templating assembly of soft microparticles into complex tessellations. *Nature* **2020**, *582*, 219–224.

(358) Style, R. W.; Isa, L.; Dufresne, E. R. Adsorption of soft particles at fluid interfaces. *Soft Matter* **2015**, *11*, 7412–7419.

(359) Guzmán, E.; Abelenda-Núñez, I.; Maestro, A.; Ortega, F.; Santamaria, A.; Rubio, R. G. Particle-laden fluid/fluid interfaces: physico-chemical foundations. *Journal of Physics: Condensed Matter* **2021**, *33*, No. 333001.

(360) Feller, D.; Karg, M. Fluid interface-assisted assembly of soft microgels: recent developments for structures beyond hexagonal packing. *Soft Matter* **2022**, *18*, 6301–6312.

(361) Volk, K.; Fitzgerald, J. P. S.; Retsch, M.; Karg, M. Time-Controlled Colloidal Superstructures: Long-Range Plasmon Resonance Coupling in Particle Monolayers. *Advanced Materials* **2015**, *27*, 7332–7337.

(362) Rey, M.; Fernandez-Rodriguez, M. A.; Steinacher, M.; Scheidegger, L.; Geisel, K.; Richtering, W.; Squires, T. M.; Isa, L. Isostructural solid–solid phase transition in monolayers of soft core–shell particles at fluid interfaces: structure and mechanics. *Soft Matter* **2016**, *12*, 3545–3557.

(363) da Silva, J. C.; Balazs, D. M.; Dunbar, T. A.; Hanrath, T. Fundamental Processes and Practical Considerations of Lead Chalcogenide Mesocrystals Formed via Self-Assembly and Directed Attachment of Nanocrystals at a Fluid Interface. *Chemistry of Materials* **2021**, *33*, 9457–9472.

(364) Balazs, D. M.; Dunbar, T. A.; Smilgies, D.-M.; Hanrath, T. Coupled Dynamics of Colloidal Nanoparticle Spreading and Self-Assembly at a Fluid–Fluid Interface. *Langmuir* **2020**, *36*, 6106–6115.

(365) Vialetto, J.; Camerin, F.; Ramakrishna, S. N.; Zaccarelli, E.; Isa, L. Exploring the 3D Conformation of Hard-Core Soft-Shell Particles Adsorbed at a Fluid Interface. *Advanced Science* **2023**, *10*, No. 2303404.

(366) Mičky, S.; Bodík, M.; Mičetić, M.; Fetzer, F.; Strienz, M.; Held, V.; Jergel, M.; Schnepf, A.; Schreiber, F.; Šiffalovič, P. Multilayer Langmuir Film of Monodisperse Au Nanoclusters: Unusual Growth via Bilayers. *Langmuir* **2022**, *38*, 14850–14856.

(367) Bochenek, S.; Camerin, F.; Zaccarelli, E.; Maestro, A.; Schmidt, M. M.; Richtering, W.; Scotti, A. In-situ study of the impact of temperature and architecture on the interfacial structure of microgels. *Nature Communications* **2022**, *13*, 3744.

(368) Kuk, K.; Abgarjan, V.; Gregel, L.; Zhou, Y.; Fadanelli, V. C.; Buttinoni, I.; Karg, M. Compression of colloidal monolayers at liquid interfaces: in situ vs. ex situ investigation. *Soft Matter* **2023**, *19*, 175–188.

(369) Zhou, Y.; Arya, G. Discovery of two-dimensional binary nanoparticle superlattices using global Monte Carlo optimization. *Nature Communications* **2022**, *13*, 7976.

(370) Muntz, I.; Richards, J. A.; Brown, S.; Schofield, A. B.; Rey, M.; Thijssen, J. H. J. Contactless interfacial rheology: Probing shear at liquid–liquid interfaces without an interfacial geometry via fluorescence microscopy. *Journal of Rheology* **2023**, *67*, 67–80.

(371) Tein, Y. S.; Thompson, B. R.; Majkrzak, C.; Maranville, B.; Renggli, D.; Vermant, J.; Wagner, N. J. Instrument for measurement of interfacial structure–property relationships with decoupled interfacial shear and dilatational flow: " Quadrotrough". *Review of Scientific Instruments* **2022**, *93*, No. 093903.

(372) Giersig, M.; Mulvaney, P. Preparation of ordered colloid monolayers by electrophoretic deposition. *Langmuir* **1993**, *9*, 3408–3413.

(373) Ahmed, S.; Ryan, K. M. Centimetre scale assembly of vertically aligned and close packed semiconductor nanorods from solution. *Chemical Communications* **2009**, 6421–6423.

(374) Zhang, H.; Cadusch, J.; Kinnear, C.; James, T.; Roberts, A.; Mulvaney, P. Direct Assembly of Large Area Nanoparticle Arrays. *ACS Nano* **2018**, *12*, 7529–7537.

(375) Zhang, H.; Liu, Y.; Shahidan, M. F. S.; Kinnear, C.; Maasoumi, F.; Cadusch, J.; Akinoglu, E. M.; James, T. D.; Widmer-Cooper, A.; Roberts, A.; Mulvaney, P. Direct Assembly of Vertically Oriented, Gold Nanorod Arrays. *Advanced Functional Materials* **2021**, *31*, No. 2006753.

(376) Zhang, H.; Liu, Y.; Ashokan, A.; Gao, C.; Dong, Y.; Kinnear, C.; Kirkwood, N.; Zaman, S.; Maasoumi, F.; James, T. D.; Widmer-Cooper, A.; Roberts, A.; Mulvaney, P. A General Method for Direct Assembly of Single Nanocrystals. *Advanced Optical Materials* **2022**, *10*, No. 2200179.

(377) Liu, S.; Hou, Z.; Lin, L.; Li, Z.; Sun, H. 3D Laser Nanoprinting of Functional Materials. *Adv. Funct. Mater.* **2023**, *33*. DOI: 10.1002/adfm.202370233

(378) Pan, J.-A.; Talapin, D. V. 3D-printing nanocrystals with light. *Science* **2022**, *377*, 1046–1047.

(379) Liu, S.-F.; Hou, Z.-W.; Lin, L.; Li, F.; Zhao, Y.; Li, X.-z. 3D Nanoprinting of Semiconductor Quantum Dots by Photo- Excitation-Induced Chemical Bonding. *Science* **2021**, *377*, 1–32.

(380) Li, F.; Liu, S.-F.; Liu, W.; Hou, Z.-W.; Jiang, J.; Fu, Z.; Wang, S.; Si, Y.; Lu, S.; Zhou, H.; Liu, D.; Tian, X.; Qiu, H.; Yang, Y.; Li, Z.; Li, X.; Lin, L.; Sun, H.-B.; Zhang, H.; Li, J. 3D printing of inorganic nanomaterials by photochemically bonding colloidal nanocrystals. *Science* **2023**, *381*, 1468–1474.

(381) Balazs, D. M.; Ibáñez, M. Widening the use of 3D printing. *Science* **2023**, *381*, 1413–1414.

(382) Grzelczak, M.; Liz-Marzán, L. M.; Klajn, R. Stimuli-responsive self-assembly of nanoparticles. *Chemical Society Reviews* **2019**, *48*, 1342–1361.

(383) Pigliacelli, C.; Sánchez-Fernández, R.; García, M. D.; Peinador, C.; Pazos, E. Self-assembled peptide–inorganic nano-particle superstructures: from component design to applications. *Chemical Communications* **2020**, *56*, 8000–8014.

(384) An, X.; Zhu, A.; Luo, H.; Ke, H.; Chen, H.; Zhao, Y. Rational Design of Multi-Stimuli-Responsive Nanoparticles for Precise Cancer Therapy. *ACS Nano* **2016**, *10*, 5947–5958.

(385) Fu, Q.; Li, Z.; Fu, F.; Chen, X.; Song, J.; Yang, H. Stimuli-Responsive Plasmonic Assemblies and Their Biomedical Applications. *Nano Today* **2021**, *36*, No. 101014.

(386) Wu, X.; Hao, C.; Kumar, J.; Kuang, H.; Kotov, N. A.; Liz-Marzán, L. M.; Xu, C. Environmentally responsive plasmonic nanoassemblies for biosensing. *Chemical Society Reviews* **2018**, *47*, 4677–4696.

(387) Li, F.; Lu, J.; Kong, X.; Hyeon, T.; Ling, D. Dynamic Nanoparticle Assemblies for Biomedical Applications. *Adv. Mater.* **2017**, *29*, 1605897. .

(388) Vaghasiya, J. V.; Mayorga-Martinez, C. C.; Matějková, S.; Pumera, M. Pick up and dispose of pollutants from water via temperature-responsive micellar copolymers on magnetite nanorobots. *Nature communications* **2022**, *13*, 1026.

(389) Li, Z.; Yang, F.; Yin, Y. Smart Materials by Nanoscale Magnetic Assembly. *Adv. Funct. Mater.* **2020**, *30*, 1903467.

(390) He, L.; Wang, M.; Ge, J.; Yin, Y. Magnetic Assembly Route to Colloidal Responsive Photonic Nanostructures. *Accounts of Chemical Research* **2012**, *45*, 1431−1440.

(391) Murugan, A.; Zeravcic, Z.; Brenner, M. P.; Leibler, S. Multifarious assembly mixtures: Systems allowing retrieval of diverse stored structures. *Proceedings of the National Academy of Sciences* **2015**, *112*, 54−59.

(392) Keim, N. C.; Paulsen, J. D.; Zeravcic, Z.; Sastry, S.; Nagel, S. R. Memory formation in matter. *Reviews of Modern Physics* **2019**, *91*, No. 035002.

(393) Sartori, P.; Leibler, S. Lessons from equilibrium statistical physics regarding the assembly of protein complexes. *Proceedings of the National Academy of Sciences* **2020**, *117*, 114−120.

(394) Bisker, G.; England, J. L. Nonequilibrium associative retrieval of multiple stored self-assembly targets. *Proceedings of the National Academy of Sciences* **2018**, *115*, E10531−E10538.

(395) Hopfield, J. J. Neural networks and physical systems with emergent collective computational abilities. *Proceedings of the National Academy of Sciences* **1982**, *79*, 2554−2558.

(396) Amit, D. J. *Modeling Brain Function*; Cambridge University Press, 1989.

(397) Zhong, W.; Schwab, D. J.; Murugan, A. Associative Pattern Recognition Through Macro-molecular Self-Assembly. *Journal of Statistical Physics* **2017**, *167*, 806−826.

(398) McMullen, A.; Muñoz Basagoiti, M.; Zeravcic, Z.; Brujic, J. Self-assembly of emulsion droplets through programmable folding. *Nature* **2022**, *610*, 502−506.

(399) Evans, C. G.; O'Brien, J.; Winfree, E.; Murugan, A. Pattern recognition in the nucleation kinetics of non-equilibrium self-assembly. *Nature* **2024**, *625*, 500−507.

(400) Osat, S.; Golestanian, R. Non-reciprocal multifarious self-organization. *Nature Nanotechnology* **2023**, *18*, 79−85.

(401) Soto, R.; Golestanian, R. Self-Assembly of Catalytically Active Colloidal Molecules: Tailoring Activity Through Surface Chemistry. *Physical Review Letters* **2014**, *112*, No. 068301.

(402) Agudo-Canalejo, J.; Golestanian, R. Active Phase Separation in Mixtures of Chemically Interacting Particles. *Physical Review Letters* **2019**, *123*, No. 018101.

(403) Saha, S.; Agudo-Canalejo, J.; Golestanian, R. Scalar Active Mixtures: The Nonreciprocal Cahn-Hilliard Model. *Physical Review X* **2020**, *10*, No. 041009.

(404) You, Z.; Baskaran, A.; Marchetti, M. C. Nonreciprocity as a generic route to traveling states. *Proceedings of the National Academy of Sciences* **2020**, *117*, 19767−19772.

(405) Fruchart, M.; Hanai, R.; Littlewood, P. B.; Vitelli, V. Non-reciprocal phase transitions. *Nature* **2021**, *592*, 363−369.

(406) Winfree, E.; Liu, F.; Wenzler, L. A.; Seeman, N. C. Design and self-assembly of two-dimensional DNA crystals. *Nature* **1998**, *394*, 539−544.

(407) Golestanian, R. *Active Matter and Nonequilibrium Statistical Physics*; Oxford University Press, 2022; pp 230−293.

(408) Royall, C. P.; Charbonneau, P.; Dijkstra, M.; Russo, J.; Smallenburg, F.; Speck, T.; Valeriani, C. Colloidal Hard Spheres: Triumphs, Challenges and Mysteries. *Arxiv* 2023; https://arxiv.org/abs/2305.02452v3.

(409) Pauling, L. The principles determining the structure of complex ionic crystals. *Journal of the American Chemical Society* **1929**, *51*, 1010−1026.

(410) Israelachvili, J. N.; Mitchell, D. J.; Ninham, B. W. Theory of self-assembly of hydrocarbon amphiphiles into micelles and bilayers. *Journal of the Chemical Society, Faraday Transactions 2* **1976**, *72*, 1525.

(411) Damasceno, P. F.; Engel, M.; Glotzer, S. C. Predictive Self-Assembly of Polyhedra into Complex Structures. *Science* **2012**, *337*, 453−457.

(412) Haji-Akbari, A.; Engel, M.; Keys, A. S.; Zheng, X.; Petschek, R. G.; Palffy-Muhoray, P.; Glotzer, S. C. Disordered, quasicrystalline and crystalline phases of densely packed tetrahedra. *Nature* **2009**, *462*, 773−777.

(413) Wang, Y.; Chen, J.; Li, R.; Gotz, A.; Drobek, D.; Przybilla, T.; Hubner, S.; Pelz, P.; Yang, L.; Apeleo Zubiri, B.; Spiecker, E.; Engel, M.; Ye, X. Controlled Self-Assembly of Gold Nanotetrahedra into Quasicrystals and Complex Periodic Supracrystals. *Journal of the American Chemical Society* **2023**, *145*, 17902−17911.

(414) Agarwal, U.; Escobedo, F. A. Mesophase behaviour of polyhedral particles. *Nature Materials* **2011**, *10*, 230−235.

(415) de Graaf, J.; Filion, L.; Marechal, M.; van Roij, R.; Dijkstra, M. Crystal-structure prediction via the Floppy-Box Monte Carlo algorithm: Method and application to hard (non)convex particles. *The Journal of Chemical Physics* **2012**, *137*, No. 214101.

(416) Schultz, B. A.; Damasceno, P. F.; Engel, M.; Glotzer, S. C. Symmetry Considerations for the Targeted Assembly of Entropically Stabilized Colloidal Crystals via Voronoi Particles. *ACS Nano* **2015**, *9*, 2336−2344.

(417) Cersonsky, R. K.; van Anders, G.; Dodd, P. M.; Glotzer, S. C. Relevance of packing to colloidal self-assembly. *Proceedings of the National Academy of Sciences of the United States of America* **2018**, *115*, 1439−1444.

(418) van Anders, G.; Klotsa, D.; Karas, A. S.; Dodd, P. M.; Glotzer, S. C. Digital Alchemy for Materials Design: Colloids and Beyond. *ACS Nano* **2015**, *9*, 9542−9553.

(419) Geng, Y.; van Anders, G.; Glotzer, S. C. Synthesizable nanoparticle eigenshapes for colloidal crystals. *Nanoscale* **2021**, *13*, 13301−13309.

(420) van Anders, G.; Klotsa, D.; Ahmed, N. K.; Engel, M.; Glotzer, S. C. Understanding shape entropy through local dense packing. *Proceedings of the National Academy of Sciences of the United States of America* **2014**, *111*, E4812−E4821.

(421) van Anders, G.; Ahmed, N. K.; Smith, R.; Engel, M.; Glotzer, S. C. Entropically Patchy Particles: Engineering Valence through Shape Entropy. *ACS Nano* **2014**, *8*, 931−940.

(422) Avendano, C.; Escobedo, F. A. Packing, entropic patchiness, and self-assembly of non-convex colloidal particles: A simulation perspective. *Current Opinion in Colloid & Interface Science* **2017**, *30*, 62−69.

(423) Petukhov, A. V.; Tuinier, R.; Vroege, G. J. Entropic patchiness: Effects of colloid shape and depletion. *Current Opinion in Colloid & Interface Science* **2017**, *30*, 54−61.

(424) Teich, E. G.; van Anders, G.; Klotsa, D.; Dshemuchadse, J.; Glotzer, S. C. Clusters of polyhedra in spherical confinement. *Proceedings of the National Academy of Sciences of the United States of America* **2016**, *113*, E669−E678.

(425) Teich, E. G.; van Anders, G.; Glotzer, S. C. Identity crisis in alchemical space drives the entropic colloidal glass transition. *Nature Communications* **2019**, *10*, 64.

(426) Shevchenko, E. V.; Talapin, D. V.; Murray, C. B.; O'Brien, S. Structural Characterization of Self-Assembled Multifunctional Binary Nanoparticle Superlattices. *Journal of the American Chemical Society* **2006**, *128*, 3620−3637.

(427) Boles, M. A.; Talapin, D. V. Many-Body Effects in Nanocrystal Superlattices: Departure from Sphere Packing Explains Stability of Binary Phases. *Journal of the American Chemical Society* **2015**, *137*, 4494−4502.

(428) Landman, U.; Luedtke, W. D. Small is different: energetic, structural, thermal, and mechanical properties of passivated nano-cluster assemblies. *Faraday Discussions* **2004**, *125*, 1−22.

(429) Zha, X.; Travesset, A. The Hard Sphere Diameter of Nanocrystals (Nanoparticles). *Journal of Chemical Physics* **2020**, *152*, No. 094502.

(430) Zha, X.; Travesset, A. Stability and Free Energy of Nanocrystal Chains and Superlattices. *The Journal of Physical Chemistry C* **2018**, *122*, 23153−23164.

(431) Xia, J.; Horst, N.; Guo, H.; Travesset, A. Superlattices of Nanocrystals with Polystyrene Ligands: From the Colloidal to Polymer Limit. *Macromolecules* **2019**, *52*, 8056−8066.

(432) Eldridge, M. D.; Madden, P. A.; Frenkel, D. Entropy-driven formation of a superlattice in a hard-sphere binary mixture. *Nature* **1993**, *365*, 35−37.

(433) Travesset, A. Phase diagram of power law and Lennard-Jones systems: Crystal phases. *The Journal of Chemical Physics* **2014**, *141*, No. 164501.

(434) Zu, M.; Tan, P.; Xu, N. Forming quasicrystals by monodisperse soft core particles. *Nature Communications* **2017**, *8*, 2089.

(435) Jagla, E. A. Phase behavior of a system of particles with core collapse. *Physical Review E* **1998**, *58*, 1478−1486.

(436) Mihalkovič, M.; Henley, C. L. Empirical oscillating potentials for alloys from *ab initio* fits and the prediction of quasicrystal-related structures in the Al-Cu-Sc system. *Physical Review B* **2012**, *85*, No. 092102.

(437) Bommineni, P. K.; Klement, M.; Engel, M. Spontaneous Crystallization in Systems of Binary Hard Sphere Colloids. *Physical Review Letters* **2020**, *124*, No. 218003.

(438) Bommineni, P. K.; Varela-Rosales, N. R.; Klement, M.; Engel, M. Complex Crystals from Size-Disperse Spheres. *Physical Review Letters* **2019**, *122*, No. 128005.

(439) Ren, S.; Sun, Y.; Zhang, F.; Travesset, A.; Wang, C.-Z.; Ho, K.-M. Phase Diagram and Structure Map of Binary Nanoparticle Superlattices from a Lennard-Jones Model. *ACS Nano* **2020**, *14*, 6795−6802.

(440) LaCour, R. A.; Adorf, C. S.; Dshemuchadse, J.; Glotzer, S. C. Influence of Softness on the Stability of Binary Colloidal Crystals. *ACS Nano* **2019**, *13*, 13829−13842.

(441) Travesset, A. Binary nanoparticle superlattices of soft-particle systems. *Proceedings of the National Academy of Sciences of the United States of America* **2015**, *112*, 9563−9567.

(442) Punnathanam, S.; Monson, P. A. Crystal nucleation in binary hard sphere mixtures: A Monte Carlo simulation study. *The Journal of Chemical Physics* **2006**, *125*, No. 024508.

(443) Coli, G. M.; Dijkstra, M. An Artificial Neural Network Reveals the Nucleation Mechanism of a Binary Colloidal AB$_{13}$ Crystal. *ACS Nano* **2021**, *15*, 4335−4346.

(444) Horst, N.; Travesset, A. Prediction of binary nanoparticle superlattices from soft potentials. *Journal of Chemical Physics* **2016**, *144*, No. 014502.

(445) Travesset, A. Topological structure prediction in binary nanoparticle superlattices. *Soft Matter* **2017**, *13*, 147−157.

(446) Zha, X.; Travesset, A. Thermodynamic Equilibrium of Binary Nanocrystal Superlattices. *The Journal of Physical Chemistry C* **2021**, *125*, 18936−18945.

(447) Coropceanu, I.; Boles, M. A.; Talapin, D. V. Systematic Mapping of Binary Nanocrystal Superlattices: The Role of Topology in Phase Selection. *Journal of the American Chemical Society* **2019**, *141*, 5728−5740.

(448) Cherniukh, I.; Rainò, G.; Sekh, T. V.; Zhu, C.; Shynkarenko, Y.; John, R. A.; Kobiyama, E.; Mahrt, R. F.; Stöferle, T.; Erni, R.; Kovalenko, M. V.; Bodnarchuk, M. I. Shape-Directed Co-Assembly of Lead Halide Perovskite Nanocubes with Dielectric Nanodisks into Binary Nanocrystal Superlattices. *ACS Nano* **2021**, *15*, 16488−16500.

(449) Cherniukh, I.; Sekh, T. V.; Raino, G.; Ashton, O. J.; Burian, M.; Travesset, A.; Athanasiou, M.; Manoli, A.; John, R. A.; Svyrydenko, M.; Morad, V.; Shynkarenko, Y.; Montanarella, F.; Naumenko, D.; Amenitsch, H.; Itskos, G.; Mahrt, R. F.; Stoferle, T.; Erni, R.; Kovalenko, M. V.; Bodnarchuk, M. I. Structural Diversity in

(450) Widmer-Cooper, A.; Geissler, P. L. Ligand-Mediated Interactions between Nanoscale Surfaces Depend Sensitively and Nonlinearly on Temperature, Facet Dimensions, and Ligand Coverage. *ACS Nano* **2016**, *10*, 1877−1887.

(451) Doblas, D.; Kister, T.; Cano-Bonilla, M.; González-García, L.; Kraus, T. Colloidal Solubility and Agglomeration of Apolar Nanoparticles in Different Solvents. *Nano Letters* **2019**, *19*, 5246−5252.

(452) Gupta, U.; Escobedo, F. A. Ligand Interactions and Nanoparticle Shapes Guide the Pathways toward Interfacial Self-Assembly. *Langmuir* **2022**, *38*, 1738−1747.

(453) Souza, P. C. T.; Alessandri, R.; Barnoud, J.; Thallmair, S.; Faustino, I.; Grunewald, F.; Patmanidis, I.; Abdizadeh, H.; Bruininks, B. M. H.; Wassenaar, T. A.; Kroon, P. C.; Melcr, J.; Nieto, V.; Corradi, V.; Khan, H. M.; Domanski, J.; Javanainen, M.; Martinez-Seara, H.; Reuter, N.; Best, R. B.; Vattulainen, I.; Monticelli, L.; Periole, X.; Tieleman, D. P.; de Vries, A. H.; Marrink, S. J. Martini 3: a general purpose force field for coarse-grained molecular dynamics. *Nature Methods* **2021**, *18*, 382−388.

(454) Campos-Villalobos, G.; Giunta, G.; Marín-Aguilar, S.; Dijkstra, M. Machine-learning effective many-body potentials for anisotropic particles using orientation-dependent symmetry functions. *The Journal of Chemical Physics* **2022**, *157*, No. 024902.

(455) Chen, Q.; Cho, H.; Manthiram, K.; Yoshida, M.; Ye, X.; Alivisatos, A. P. Interaction Potentials of Anisotropic Nanocrystals from the Trajectory Sampling of Particle Motion using in Situ Liquid Phase Transmission Electron Microscopy. *ACS Central Science* **2015**, *1*, 33−39.

(456) Yao, L.; Ou, Z.; Luo, B.; Xu, C.; Chen, Q. Machine Learning to Reveal Nanoparticle Dynamics from Liquid-Phase TEM Videos. *ACS Central Science* **2020**, *6*, 1421−1430.

(457) Zhong, Y.; Allen, V. R.; Chen, J.; Wang, Y.; Ye, X. Multistep Crystallization of Dynamic Nanoparticle Superlattices in Nonaqueous Solutions. *Journal of the American Chemical Society* **2022**, *144*, 14915−14922.

(458) Zhou, S. Chiral Assemblies of Pinwheel Superlattices on Substrates. *Nature* **2022**, *612*, 259−265.

(459) Li, D.; Chen, Q.; Chun, J.; Fichthorn, K.; De Yoreo, J.; Zheng, H. Nanoparticle Assembly and Oriented Attachment: Correlating Controlling Factors to the Resulting Structures. *Chemical Reviews* **2023**, *123*, 3127−3159.

(460) Unke, O. T.; Chmiela, S.; Sauceda, H. E.; Gastegger, M.; Poltavsky, I.; Schütt, K. T.; Tkatchenko, A.; Müller, K.-R. Machine Learning Force Fields. *Chemical Reviews* **2021**, *121*, 10142−10186.

(461) Kulichenko, M.; Smith, J. S.; Nebgen, B.; Li, Y. W.; Fedik, N.; Boldyrev, A. I.; Lubbers, N.; Barros, K.; Tretiak, S. The Rise of Neural Networks for Materials and Chemical Dynamics. *The Journal of Physical Chemistry Letters* **2021**, *12*, 6227−6243.

(462) Behler, J. Four Generations of High-Dimensional Neural Network Potentials. *Chemical Reviews* **2021**, *121*, 10037−10072.

(463) Fedik, N.; Zubatyuk, R.; Kulichenko, M.; Lubbers, N.; Smith, J. S.; Nebgen, B.; Messerly, R.; Li, Y. W.; Boldyrev, A. I.; Barros, K.; Isayev, O.; Tretiak, S. Extending machine learning beyond interatomic potentials for predicting molecular properties. *Nature Reviews Chemistry* **2022**, *6*, 653−672.

(464) Podryabinkin, E. V.; Shapeev, A. V. Active learning of linearly parametrized interatomic potentials. *Computational Materials Science* **2017**, *140*, 171−180.

(465) Smith, J. S.; Nebgen, B.; Lubbers, N.; Isayev, O.; Roitberg, A. E. Less is more: Sampling chemical space with active learning. *The Journal of Chemical Physics* **2018**, *148*, No. 241733.

(466) Zeni, C.; Rossi, K.; Pavloudis, T.; Kioseoglou, J.; de Gironcoli, S.; Palmer, R. E.; Baletto, F. Data-driven simulation and characterisation of gold nanoparticle melting. *Nature Communications* **2021**, *12*, 6056.

(467) Zubatyuk, R.; Smith, J. S.; Nebgen, B. T.; Tretiak, S.; Isayev, O. Teaching a neural network to attach and detach electrons from molecules. *Nature Communications* **2021**, *12*, 4870.

(468) Bodnarchuk, M. I.; Li, L.; Fok, A.; Nachtergaele, S.; Ismagilov, R. F.; Talapin, D. V. Three-Dimensional Nanocrystal Superlattices Grown in Nanoliter Microfluidic Plugs. *Journal of the American Chemical Society* **2011**, *133*, 8956−8960.

(469) Rogach, A.L.; Talapin, D.V.; Shevchenko, E.V.; Kornowski, A.; Haase, M.; Weller, H. Organization of Matter on Different Size Scales : Monodisperse Nanocrystals and Their Superstructures. *Advanced Functional Materials* **2002**, *12*, 653−664.

(470) Shevchenko, E. V.; Talapin, D. V.; O'Brien, S.; Murray, C. B. Polymorphism in AB13 Nanoparticle Superlattices: An Example of Semiconductor-Metal Metamaterials. *Journal of the American Chemical Society* **2005**, *127*, 8741−8747.

(471) Xue, Z.; Yan, C.; Wang, T. From Atoms to Lives: The Evolution of Nanoparticle Assemblies. *Advanced Functional Materials* **2019**, *29*, No. 1807658.

(472) Galván-Moya, J. E.; Nelissen, K.; Peeters, F. M. Structural ordering of self-assembled clusters with competing interactions: Transition from faceted to spherical clusters. *Langmuir* **2015**, *31*, 917−924.

(473) Merkens, S.; Vakili, M.; Sánchez-Iglesias, A.; Litti, L.; Gao, Y.; Gwozdz, P. V.; Sharpnack, L.; Blick, R. H.; Liz-Marzán, L. M.; Grzelczak, M.; Trebbin, M. Time-Resolved Analysis of the Structural Dynamics of Assembling Gold Nanoparticles. *ACS Nano* **2019**, *13*, 6596−6604.

(474) Galván-Moya, J. E.; Altantzis, T.; Nelissen, K.; Peeters, F. M.; Grzelczak, M.; Liz-Marzán, L. M.; Bals, S.; Van Tendeloo, G. Self-Organization of Highly Symmetric Nanoassemblies: A Matter of Competition. *ACS Nano* **2014**, *8*, 3869−3875.

(475) Woźniak, M.; Derkachov, G.; Kolwas, K.; Archer, J.; Wojciechowski, T.; Jakubczyk, D.; Kolwas, M. Formation of Highly Ordered Spherical Aggregates from Drying Microdroplets of Colloidal Suspension. *Langmuir* **2015**, *31*, 7860−7868.

(476) Boneschanscher, M. P.; Evers, W. H.; Qi, W.; Meeldijk, J. D.; Dijkstra, M.; Vanmaekelbergh, D. Electron Tomography Resolves a Novel Crystal Structure in a Binary Nanocrystal Superlattice. *Nano Letters* **2013**, *13*, 1312−1316.

(477) Xia, J.; Guo, H.; Travesset, A. On the Thermodynamic Stability of Binary Superlattices of Polystyrene-Functionalized Nanocrystals. *Macromolecules* **2020**, *53*, 9929−9942.

(478) Niv, I.; Efrati, E. Geometric frustration and compatibility conditions for two-dimensional director fields. *Soft Matter* **2018**, *14*, 424−431.

(479) Hall, D. M.; Bruss, I. R.; Barone, J. R.; Grason, G. M. Morphology selection via geometric frustration in chiral filament bundles. *Nature Materials* **2016**, *15*, 727−732.

(480) Haddad, A.; Efrati, E.; Aharoni, H.; Sharon, E.; Shtukenberg, A. G.; Kahr, B. Twist renormalization in molecular crystals driven by geometric frustration. *Soft Matter* **2019**, *15*, 116−126.

(481) Li, C.; Shtukenberg, A. G.; Vogt-Maranto, L.; Efrati, E.; Raiteri, P.; Gale, J. D.; Rohl, A. L.; Kahr, B. Why Are Some Crystals Straight? *The Journal of Physical Chemistry C* **2020**, *124*, 15616−15624.

(482) Shtukenberg, A. G.; Drori, R.; Sturm, E. V.; Vidavsky, N.; Haddad, A.; Zheng, J.; Estroff, L. A.; Weissman, H.; Wolf, S. G.; Shimoni, E.; Li, C.; Fellah, N.; Efrati, E.; Kahr, B. Crystals of Benzamide, the First Polymorphous Molecular Compound, Are Helicoidal. *Angewandte Chemie* **2020**, *132*, 14701−14709.

(483) Meiri, S.; Efrati, E. Cumulative geometric frustration and superextensive energy scaling in a nonlinear classical XY-spin model. *Physical Review E* **2022**, *105*, No. 024703.

(484) Hackney, N. W.; Amey, C.; Grason, G. M. Dispersed, Condensed, and Self-Limiting States of Geometrically Frustrated Assembly. *Phys. Rev. X* **2023**, *13*, No. 041010.

(485) Hagan, M. F.; Grason, G. M. Equilibrium mechanisms of self-limiting assembly. *Reviews of Modern Physics* **2021**, *93*, No. 025008.

(486) Kléman, M.; Sadoc, J. A tentative description of the crystallography of amorphous solids. *Journal de Physique Lettres* **1979**, *40*, 569−574.

(487) Frank, F. C.; Kasper, J. S. Complex alloy structures regarded as sphere packings. I. Definitions and basic principles. *Acta Crystallographica* **1958**, *11*, 184−190.

(488) Nelson, D. R. Order, frustration, and defects in liquids and glasses. *Physical Review B* **1983**, *28*, 5515−5535.

(489) Tarjus, G.; Kivelson, S. A.; Nussinov, Z.; Viot, P. The frustration-based approach of supercooled liquids and the glass transition: a review and critical assessment. *Journal of Physics: Condensed Matter* **2005**, *17*, No. R1143.

(490) Turci, F.; Tarjus, G.; Royall, C. P. From Glass Formation to Icosahedral Ordering by Curving Three-Dimensional Space. *Physical Review Letters* **2017**, *118*, No. 215501.

(491) Matsen, M. W. The standard Gaussian model for block copolymer melts. *Journal of Physics: Condensed Matter* **2002**, *14*, R21−R47.

(492) Missoni, L. L.; Tagliazucchi, M. The Phase Behavior of Nanoparticle Superlattices in the Presence of a Solvent. *ACS Nano* **2020**, *14*, 5649−5658.

(493) Missoni, L.; Tagliazucchi, M. Body centered tetragonal nanoparticle superlattices: Why and when they form? *Nanoscale* **2021**, *13*, 14371−14381.

(494) Gunawardana, K. G. S. H.; Song, X. Free Energy Calculations of Crystalline Hard Sphere Complexes Using Density Functional Theory. *The Journal of Physical Chemistry B* **2015**, *119*, 9160−9166.

(495) Sides, S. W.; Kim, B. J.; Kramer, E. J.; Fredrickson, G. H. Hybrid particle-field simulations of polymer nanocomposites. *Physical Review Letters* **2006**, *96*, No. 250601.

(496) Ginzburg, V. V. Modeling the Morphology and Phase Behavior of One-Component Polymer-Grafted Nanoparticle Systems. *Macromolecules* **2017**, *50*, 9445−9455.

(497) Hur, K.; Hennig, R. G.; Escobedo, F. A.; Wiesner, U. Predicting Chiral Nanostructures, Lattices and Superlattices in Complex Multicomponent Nanoparticle Self-Assembly. *Nano Letters* **2012**, *12*, 3218−3223.

(498) Hur, K.; Hennig, R. G.; Escobedo, F. A.; Wiesner, U. Mesoscopic structure prediction of nanoparticle assembly and coassembly: Theoretical foundation. *The Journal of Chemical Physics* **2010**, *133*, No. 194108.

(499) Roth, R.; Evans, R.; Lang, A.; Kahl, G. 2 for hard-sphere mixtures revisited: the White Bear version. *Journal of Physics: Condensed Matter* **2002**, *14*, 12063−12078.

(500) Fan, Z.; Gruenwald, M. Energy vs. Entropy in Superlattices of Ligand-Covered Nanoparticles. *ChemRxiv*, **2019**, doi:10.26434/chemrxiv.9178037.v1.

(501) Weidman, M. C.; Smilgies, D.-M. M.; Tisdale, W. A. Kinetics of the self-assembly of nanocrystal superlattices measured by real-time in situ X-ray scattering. *Nature Materials* **2016**, *15*, 775−781.

(502) Predicting colloidal crystals from shapes via inverse design and machine learning. *Arxiv*, **2018**, arXiv:1801.06219v1.

(503) Long, A. W.; Ferguson, A. L. Rational design of patchy colloids via landscape engineering. *Molecular Systems Design & Engineering* **2018**, *3*, 49−65.

(504) Zhou, P.; Proctor, J. C.; van Anders, G.; Glotzer, S. C. Alchemical molecular dynamics for inverse design. *Molecular Physics* **2019**, *117*, 3968−3980.

(505) Coli, G. M.; Boattini, E.; Filion, L.; Dijkstra, M. Inverse design of soft materials via a deep learning−based evolutionary strategy. *Sci. Adv.* **2022**, *8*. DOI: 10.1126/sciadv.abj6731

(506) Rivera-Rivera, L. Y.; Moore, T. C.; Glotzer, S. C. Inverse design of triblock Janus spheres for self-assembly of complex structures in the crystallization slot via digital alchemy. *Soft Matter* **2023**, *19*, 2726−2736.

(507) Torrie, G.; Valleau, J. Nonphysical sampling distributions in Monte Carlo free-energy estimation: Umbrella sampling. *Journal of Computational Physics* **1977**, *23*, 187−199.

(508) Valsson, O.; Tiwary, P.; Parrinello, M. Enhancing Important Fluctuations: Rare Events and Metadynamics from a Conceptual Viewpoint. *Annual Review of Physical Chemistry* **2016**, *67*, 159−184.

(509) Dellago, C.; Bolhuis, P. G.; Csajka, F. S.; Chandler, D. Transition path sampling and the calculation of rate constants. *The Journal of Chemical Physics* **1998**, *108*, 1964−1977.

(510) van Erp, T. S.; Bolhuis, P. G. Elaborating transition interface sampling methods. *Journal of Computational Physics* **2005**, *205*, 157−181.

(511) Hussain, S.; Haji-Akbari, A. Studying rare events using forward-flux sampling: Recent breakthroughs and future outlook. *The Journal of Chemical Physics* **2020**, *152*, No. 060901.

(512) Auer, S.; Frenkel, D. Prediction of absolute crystal-nucleation rate in hard-sphere colloids. *Nature* **2001**, *409*, 1020−1023.

(513) Filion, L.; Hermes, M.; Ni, R.; Dijkstra, M. Crystal nucleation of hard spheres using molecular dynamics, umbrella sampling, and forward flux sampling: A comparison of simulation techniques. *The Journal of Chemical Physics* **2010**, *133*, 244115.

(514) Gispen, W.; Dijkstra, M. Brute-force nucleation rates of hard spheres compared with rare-event methods and classical nucleation theory. *The Journal of Chemical Physics* **2023**, *159*, 086101.

(515) Gispen, W.; Coli, G. M.; van Damme, R.; Royall, C. P.; Dijkstra, M. Crystal Polymorph Selection Mechanism of Hard Spheres Hidden in the Fluid. *ACS Nano* **2023**, *17*, 8807−8814.

(516) Domingues, T. S.; Hussain, S.; Haji-Akbari, A. Divergence among Local Structure, Dynamics, and Nucleation Outcome in Heterogeneous Nucleation of Close-Packed Crystals. *The Journal of Physical Chemistry Letters* **2024**, *15*, 1279−1287.

(517) Thapar, V.; Escobedo, F. A. Localized Orientational Order Chaperones the Nucleation of Rotator Phases in Hard Polyhedral Particles. *Physical Review Letters* **2014**, *112*, No. 048301.

(518) Lee, S.; Teich, E. G.; Engel, M.; Glotzer, S. C. Entropic colloidal crystallization pathways via fluid−fluid transitions and multidimensional prenucleation motifs. *Proceedings of the National Academy of Sciences* **2019**, *116*, 14843−14851.

(519) Sharma, A. K.; Escobedo, F. A. Effect of particle anisotropy on the thermodynamics and kinetics of ordering transitions in hard faceted particles. *The Journal of Chemical Physics* **2023**, *158*, 044502.

(520) Sosso, G. C.; Chen, J.; Cox, S. J.; Fitzner, M.; Pedevilla, P.; Zen, A.; Michaelides, A. Crystal Nucleation in Liquids: Open Questions and Future Challenges in Molecular Dynamics Simulations. *Chemical Reviews* **2016**, *116*, 7078−7116.

(521) Turnbull, D.; Vonnegut, B. Nucleation Catalysis. *Industrial & Engineering Chemistry* **1952**, *44*, 1292−1298.

(522) Wolde, P. R. t.; Frenkel, D. Enhancement of Protein Crystal Nucleation by Critical Density Fluctuations. *Science* **1997**, *277*, 1975−1978.

(523) Macfarlane, R. J.; Lee, B.; Hill, H. D.; Senesi, A. J.; Seifert, S.; Mirkin, C. A. Assembly and organization processes in DNA-directed colloidal crystallization. *Proceedings of the National Academy of Sciences* **2009**, *106*, 10493−10498.

(524) Ou, Z.; Wang, Z.; Luo, B.; Luijten, E.; Chen, Q. Kinetic pathways of crystallization at the nanoscale. *Nature Materials* **2020**, *19*, 450−455.

(525) Luo, B.; Wang, Z.; Curk, T.; Watson, G.; Liu, C.; Kim, A.; Ou, Z.; Luijten, E.; Chen, Q. Unravelling crystal growth of nanoparticles. *Nature Nanotechnology* **2023**, *18*, 589−595.

(526) O'Brien, M. N.; Lin, H.-X.; Girard, M.; de la Cruz, M. O.; Mirkin, C. A. Programming Colloidal Crystal Habit with Anisotropic Nanoparticle Building Blocks and DNA Bonds. *Journal of the American Chemical Society* **2016**, *138*, 14562−14565.

(527) Dhulipala, S.; Yee, D. W.; Zhou, Z.; Sun, R.; Andrade, J. E.; Macfarlane, R. J.; Portela, C. M. Tunable Mechanical Response of Self-Assembled Nanoparticle Superlattices. *Nano Letters* **2023**, *23*, 5155−5163.

(528) Hammerschmidt, L.; Schacht, J.; Gaston, N. First-principles calculations of the electronic structure and bonding in metal cluster−fullerene materials considered within the superatomic framework. *Physical Chemistry Chemical Physics* **2016**, *18*, 32541−32550.

(529) Lee, J.; Nakouzi, E.; Xiao, D.; Wu, Z.; Song, M.; Ophus, C.; Chun, J.; Li, D. Interplay between Short- and Long-Ranged Forces

Leading to the Formation of Ag Nanoparticle Superlattice. *Small* **2019**, *15*, No. 1901966.

(530) Powers, A. S.; Liao, H.-G.; Raja, S. N.; Bronstein, N. D.; Alivisatos, A. P.; Zheng, H. Tracking Nanoparticle Diffusion and Interaction during Self-Assembly in a Liquid Cell. *Nano Letters* **2017**, *17*, 15−20.

(531) Ou, Z.; Yao, L.; An, H.; Shen, B.; Chen, Q. Imaging how thermal capillary waves and anisotropic interfacial stiffness shape nanoparticle supracrystals. *Nature Communications* **2020**, *11*, 4555.

(532) Wang, L.; Xu, L.; Kuang, H.; Xu, C.; Kotov, N. A. Dynamic Nanoparticle Assemblies. *Accounts of Chemical Research* **2012**, *45*, 1916−1926.

(533) Macfarlane, R. J.; Jones, M. R.; Lee, B.; Auyeung, E.; Mirkin, C. A. Topotactic Interconversion of Nanoparticle Superlattices. *Science* **2013**, *341*, 1222−1225.

(534) Miracle, D. B.; Senkov, O. N. A critical review of high entropy alloys and related concepts. *Acta Materialia* **2017**, *122*, 448−511.

(535) Kagan, C. R.; Lifshitz, E.; Sargent, E. H.; Talapin, D. V. Building devices from colloidal quantum dots. *Science* **2016**, *353*, No. aac5523.

(536) Jansen, M.; Tisdale, W. A.; Wood, V. Nanocrystal phononics. *Nature materials* **2023**, *22*, 161−169.

(537) Begley, M. R.; Gianola, D. S.; Ray, T. R. Bridging functional nanocomposites to robust macroscale devices. *Science (New York, N.Y.)* **2019**, *364*, No. eaav4299.

(538) Efros, A. L.; Rosen, M. The electronic structure of semiconductor nanocrystals. *Annual Review of Materials Science* **2000**, *30*, 475−521.

(539) Neukirch, A. J.; Hyeon-Deuk, K.; Prezhdo, O. V. Time-domain ab initio modeling of excitation dynamics in quantum dots. *Coordination Chemistry Reviews* **2014**, *263-264*, 161−181.

(540) Nozik, A. J.; Beard, M. C.; Luther, J. M.; Law, M.; Ellingson, R. J.; Johnson, J. C. Semiconductor Quantum Dots and Quantum Dot Arrays and Applications of Multiple Exciton Generation to Third-Generation Photovoltaic Solar Cells. *Chemical Reviews* **2010**, *110*, 6873−6890.

(541) Protesescu, L.; Yakunin, S.; Bodnarchuk, M. I.; Krieg, F.; Caputo, R.; Hendon, C. H.; Yang, R. X.; Walsh, A.; Kovalenko, M. V. Nanocrystals of Cesium Lead Halide Perovskites (CsPbX3, X = Cl, Br, and I): Novel Optoelectronic Materials Showing Bright Emission with Wide Color Gamut. *Nano Letters* **2015**, *15*, 3692−3696.

(542) Ben-Shahar, Y.; Stone, D.; Banin, U. Rich Landscape of Colloidal Semiconductor−Metal Hybrid Nanostructures: Synthesis, Synergetic Characteristics, and Emerging Applications. *Chemical Reviews* **2023**, *123*, 3790−3851.

(543) Kilina, S.; Ivanov, S.; Tretiak, S. Effect of Surface Ligands on Optical and Electronic Spectra of Semiconductor Nanoclusters. *Journal of the American Chemical Society* **2009**, *131*, 7717−7726.

(544) Wei, H. H.-Y.; Evans, C. M.; Swartz, B. D.; Neukirch, A. J.; Young, J.; Prezhdo, O. V.; Krauss, T. D. Colloidal Semiconductor Quantum Dots with Tunable Surface Composition. *Nano Letters* **2012**, *12*, 4465−4471.

(545) Baker, H.; Perez, C. M.; Sonnichsen, C.; Strandell, D.; Prezhdo, O. V.; Kambhampati, P. Breaking Phonon Bottlenecks through Efficient Auger Processes in Perovskite Nanocrystals. *ACS Nano* **2023**, *17*, 3913−3920.

(546) Hyeon-Deuk, K.; Prezhdo, O. V. Multiple Exciton Generation and Recombination Dynamics in Small Si and CdSe Quantum Dots: An Ab Initio Time-Domain Study. *ACS Nano* **2012**, *6*, 1239−1250.

(547) Zhu, H.; Yang, Y.; Hyeon-Deuk, K.; Califano, M.; Song, N.; Wang, Y.; Zhang, W.; Prezhdo, O. V.; Lian, T. Auger-Assisted Electron Transfer from Photoexcited Semiconductor Quantum Dots. *Nano Letters* **2014**, *14*, 1263−1269.

(548) Rabani, E.; Baer, R. Distribution of Multiexciton Generation Rates in CdSe and InAs Nanocrystals. *Nano Letters* **2008**, *8*, 4488−4492.

(549) Wang, L.-W.; Zunger, A. Pseudopotential calculations of nanoscale CdSe quantum dots. *Physical Review B* **1996**, *53*, 9579−9582.

(550) Gao, Y.; Neuhauser, D.; Baer, R.; Rabani, E. Sublinear scaling for time-dependent stochastic density functional theory. *The Journal of Chemical Physics* **2015**, *142*, No. 034106.

(551) Jacob, C. R.; Neugebauer, J. Subsystem density-functional theory. *Wiley Interdisciplinary Reviews: Computational Molecular Science* **2014**, *4*, 325−362.

(552) Jiang, X.; Zheng, Q.; Lan, Z.; Saidi, W. A.; Ren, X.; Zhao, J. Real-time GW-BSE investigations on spin-valley exciton dynamics in monolayer transition metal dichalcogenide. *Sci. Adv.* **2021**, *7*. DOI: 10.1126/sciadv.abf3759

(553) Rabani, E.; Baer, R.; Neuhauser, D. Time-dependent stochastic Bethe-Salpeter approach. *Physical Review B* **2015**, *91*, No. 235302.

(554) Giansante, C.; Infante, I. Surface Traps in Colloidal Quantum Dots: A Combined Experimental and Theoretical Perspective. *The Journal of Physical Chemistry Letters* **2017**, *8*, 5209−5215.

(555) Voznyy, O. Mobile Surface Traps in CdSe Nanocrystals with Carboxylic Acid Ligands. *The Journal of Physical Chemistry C* **2011**, *115*, 15927−15932.

(556) Kim, Y.-H.; Zhai, Y.; Gaulding, E. A.; Habisreutinger, S. N.; Moot, T.; Rosales, B. A.; Lu, H.; Hazarika, A.; Brunecky, R.; Wheeler, L. M.; Berry, J. J.; Beard, M. C.; Luther, J. M. Strategies to Achieve High Circularly Polarized Luminescence from Colloidal Organic−Inorganic Hybrid Perovskite Nanocrystals. *ACS Nano* **2020**, *14*, 8816−8825.

(557) Liu, P.; Chen, W.; Okazaki, Y.; Battie, Y.; Brocard, L.; Decossas, M.; Pouget, E.; Müller-Buschbaum, P.; Kauffmann, B.; Pathan, S.; Sagawa, T.; Oda, R. Optically Active Perovskite CsPbBr$_3$ Nanocrystals Helically Arranged on Inorganic Silica Nanohelices. *Nano Letters* **2020**, *20*, 8453−8460.

(558) Puri, M.; Ferry, V. E. Circular Dichroism of CdSe Nanocrystals Bound by Chiral Carboxylic Acids. *ACS Nano* **2017**, *11*, 12240−12246.

(559) Elliott, S. D.; Moloney, M. P.; Gun'ko, Y. K. Chiral shells and achiral cores in CdS quantum dots. *Nano Letters* **2008**, *8*, 2452−2457.

(560) Fujisawa, J.-i.; Kaneko, N.; Eda, T.; Hanaya, M. Visible-light circular dichroism of colourless chiral organic compounds enabled by interfacial charge-transfer transitions. *Chemical Communications* **2018**, *54*, 8490−8493.

(561) Purcell, T. A. R.; Seideman, T. Modeling the Chiral Imprinting Response of Oriented Dipole Moments on Metal Nanostructures. *ACS Photonics* **2018**, *5*, 4801−4809.

(562) Forde, A.; Ghosh, D.; Kilin, D.; Evans, A. C.; Tretiak, S.; Neukirch, A. J. Induced Chirality in Halide Perovskite Clusters through Surface Chemistry. *The Journal of Physical Chemistry Letters* **2022**, *13*, 686−693.

(563) Voznyy, O.; Zhitomirsky, D.; Stadler, P.; Ning, Z.; Hoogland, S.; Sargent, E. H. A Charge-Orbital Balance Picture of Doping in Colloidal Quantum Dot Solids. *ACS Nano* **2012**, *6*, 8448−8455.

(564) McGuire, J. A.; Joo, J.; Pietryga, J. M.; Schaller, R. D.; Klimov, V. I. New Aspects of Carrier Multiplication in Semiconductor Nanocrystals. *Accounts of Chemical Research* **2008**, *41*, 1810−1819.

(565) Jaeger, H. M.; Hyeon-Deuk, K.; Prezhdo, O. V. Exciton Multiplication from First Principles. *Accounts of Chemical Research* **2013**, *46*, 1280−1289.

(566) Smith, M. B.; Michl, J. Recent Advances in Singlet Fission. *Annual Review of Physical Chemistry* **2013**, *64*, 361−386.

(567) Galland, C.; Ghosh, Y.; Steinbrück, A.; Sykora, M.; Hollingsworth, J. A.; Klimov, V. I.; Htoon, H. Two types of luminescence blinking revealed by spectroelectrochemistry of single quantum dots. *Nature* **2011**, *479*, 203−207.

(568) Huang, M.-Y.; Li, X.-B.; Gao, Y.-J.; Li, J.; Wu, H.-L.; Zhang, L.-P.; Tung, C.-H.; Wu, L.-Z. Surface stoichiometry manipulation enhances solar hydrogen evolution of CdSe quantum dots. *Journal of Materials Chemistry A* **2018**, *6*, 6015−6021.

(569) Newton, M. D.; Sutin, N. Electron Transfer Reactions in Condensed Phases. *Annual Review of Physical Chemistry* **1984**, *35*, 437−480.

(570) Ranasingha, O.; Wang, H.; Zobač, V.; Jelínek, P.; Panapitiya, G.; Neukirch, A. J.; Prezhdo, O. V.; Lewis, J. P. Slow Relaxation of Surface Plasmon Excitations in Au$_5$S: The Key to Efficient Plasmonic Heating in Au/TiO$_2$. *The Journal of Physical Chemistry Letters* **2016**, *7*, 1563−1569.

(571) Chu, W.; Saidi, W. A.; Prezhdo, O. V. Long-Lived Hot Electron in a Metallic Particle for Plasmonics and Catalysis: Ab Initio Nonadiabatic Molecular Dynamics with Machine Learning. *ACS Nano* **2020**, *14*, 10608−10615.

(572) Long, R.; Prezhdo, O. V. Instantaneous Generation of Charge-Separated State on TiO$_2$ Surface Sensitized with Plasmonic Nanoparticles. *Journal of the American Chemical Society* **2014**, *136*, 4343−4354.

(573) Xu, C.; Yong, H. W.; He, J.; Long, R.; Cadore, A. R.; Paradisanos, I.; Ott, A. K.; Soavi, G.; Tongay, S.; Cerullo, G.; Ferrari, A. C.; Prezhdo, O. V.; Loh, Z.-H. Weak Distance Dependence of Hot-Electron-Transfer Rates at the Interface between Monolayer MoS$_2$ and Gold. *ACS Nano* **2021**, *15*, 819−828.

(574) Tomko, J. A.; Runnerstrom, E. L.; Wang, Y.-S.; Chu, W.; Nolen, J. R.; Olson, D. H.; Kelley, K. P.; Cleri, A.; Nordlander, J.; Caldwell, J. D.; Prezhdo, O. V.; Maria, J.-P.; Hopkins, P. E. Long-lived modulation of plasmonic absorption by ballistic thermal injection. *Nature Nanotechnology* **2021**, *16*, 47−51.

(575) Schirato, A.; Maiuri, M.; Cerullo, G.; Valle, G. D. Ultrafast hot electron dynamics in plasmonic nanostructures: experiments, modelling, design. *Nanophotonics* **2023**, *12*, 1−28.

(576) Li, W.; Xue, T.; Mora-Perez, C.; Prezhdo, O. V. Ab initio quantum dynamics of plasmonic charge carriers. *Trends in Chemistry* **2023**, *5*, 634−645.

(577) Guo, Y.; Xu, Z.; Curto, A. G.; Zeng, Y.-J.; Van Thourhout, D. Plasmonic semiconductors: materials, tunability and applications. *Progress in Materials Science* **2023**, *138*, No. 101158.

(578) Lee, S. W. Hot electron-driven chemical reactions: A review. *Applied Surface Science Advances* **2023**, *16*, No. 100428.

(579) Guo, Z.; Habenicht, B. F.; Liang, W.-Z.; Prezhdo, O. V. Ab initio study of phonon-induced dephasing of plasmon excitations in silver quantum dots. *Physical Review B* **2010**, *81*, No. 125415.

(580) Neukirch, A. J.; Guo, Z.; Prezhdo, O. V. Time-Domain Ab Initio Study of Phonon-Induced Relaxation of Plasmon Excitations in a Silver Quantum Dot. *The Journal of Physical Chemistry C* **2012**, *116*, 15034−15040.

(581) Wu, X.; van der Heide, T.; Wen, S.; Frauenheim, T.; Tretiak, S.; Yam, C.; Zhang, Y. Molecular dynamics study of plasmon-mediated chemical transformations. *Chemical Science* **2023**, *14*, 4714−4723.

(582) Wu, K.; Chen, J.; McBride, J. R.; Lian, T. Efficient hot-electron transfer by a plasmon-induced interfacial charge-transfer transition. *Science* **2015**, *349*, 632−635.

(583) Zhang, Z.; Liu, L.; Fang, W.-H.; Long, R.; Tokina, M. V.; Prezhdo, O. V. Plasmon-Mediated Electron Injection from Au Nanorods into MoS2: Traditional versus Photoexcitation Mechanism. *Chem* **2018**, *4*, 1112−1127.

(584) Ossia, Y.; Levi, A.; Panfil, Y. E.; Koley, S.; Scharf, E.; Chefetz, N.; Remennik, S.; Vakahi, A.; Banin, U. Electric-field-induced colour switching in colloidal quantum dot molecules at room temperature. *Nature Materials* **2023**, *22*, 1210−1217.

(585) Koley, S.; Cui, J.; Panfil, Y. E.; Ossia, Y.; Levi, A.; Scharf, E.; Verbitsky, L.; Banin, U. Photon correlations in colloidal quantum dot molecules controlled by the neck barrier. *Matter* **2022**, *5*, 3997−4014.

(586) Park, Y. S.; Bae, W. K.; Pietryga, J. M.; Klimov, V. I. Auger recombination of biexcitons and negative and positive trions in individual quantum dots. *ACS Nano* **2014**, *8*, 7288−7296.

(587) Reiss, P.; Protière, M.; Li, L. Core/shell semiconductor nanocrystals. *Small* **2009**, *5*, 154−168.

(588) Brus, L. E. A simple model for the ionization potential, electron affinity, and aqueous redox potentials of small semiconductor crystallites. *The Journal of Chemical Physics* **1983**, *79*, 5566−5571.

(589) Wang, L.-W.; Zunger, A. Pseudopotential calculations of nanoscale CdSe quantum dots. *Phys. Rev. B* **1996**, *53*, 9579−9582.

(590) Rabani, E.; Hetenyi, B.; Berne, B. J.; Brus, L. E. Electronic properties of CdSe nanocrystals in the absence and presence of a dielectric medium. *J. Chem. Phys.* **1999**, *110*, 5355−5369.

(591) Franceschetti, A.; Zunger, A. Pseudopotential calculations of electron and hole addition spectra of InAs, InP, and Si quantum dots. *Phys. Rev. B* **2000**, *62*, 2614−2623.

(592) Jasrasaria, D.; Weinberg, D.; Philbin, J. P.; Rabani, E. Simulations of nonradiative processes in semiconductor nanocrystals. *J. Chem. Phys.* **2022**, *157*, No. 020901.

(593) Hou, B.; Thoss, M.; Banin, U.; Rabani, E. Incoherent Nonadiabatic to Coherent Adiabatic Transition of Electron Transfer in Colloidal Quantum Dot Molecules. *Nature Communications* **2023**, *14*, 3073.

(594) Paik, T.; Diroll, B. T.; Kagan, C. R.; Murray, C. B. Binary and Ternary Superlattices Self-Assembled from Colloidal Nanodisks and Nanorods. *Journal of the American Chemical Society* **2015**, *137*, 6662−6669.

(595) Nagaoka, Y.; Schneider, J.; Zhu, H.; Chen, O. Quasicrystalline materials from non-atom building blocks. *Matter* **2023**, *6*, 30−58.

(596) Mueller, N. S.; Okamura, Y.; Vieira, B. G. M.; Juergensen, S.; Lange, H.; Barros, E. B.; Schulz, F.; Reich, S. Deep strong light−matter coupling in plasmonic nanoparticle crystals. *Nature* **2020**, *583*, 780−784.

(597) Chen, J.; Dong, A.; Cai, J.; Ye, X.; Kang, Y.; Kikkawa, J. M.; Murray, C. B. Collective Dipolar Interactions in Self-Assembled Magnetic Binary Nanocrystal Superlattice Membranes. *Nano Letters* **2010**, *10*, 5103−5108.

(598) Guyot-Sionnest, P. Electrical Transport in Colloidal Quantum Dot Films. *The Journal of Physical Chemistry Letters* **2012**, *3*, 1169−1175.

(599) Liu, Y.; Gibbs, M.; Puthussery, J.; Gaik, S.; Ihly, R.; Hillhouse, H. W.; Law, M. Dependence of Carrier Mobility on Nanocrystal Size and Ligand Length in PbSe Nanocrystal Solids. *Nano Letters* **2010**, *10*, 1960−1969.

(600) Yu, Y.; Yu, D.; Sadigh, B.; Orme, C. A. Space- and time-resolved small angle X-ray scattering to probe assembly of silver nanocrystal superlattices. *Nature Communications* **2018**, *9*, 4211.

(601) Lan, X.; Chen, M.; Hudson, M. H.; Kamysbayev, V.; Wang, Y.; Guyot-Sionnest, P.; Talapin, D. V. Quantum dot solids showing state-resolved band-like transport. *Nature Materials* **2020**, *19*, 323−329.

(602) Mamode, M. Electrical resistance between pairs of vertices of a conducting cube and continuum limit for a cubic resistor network. *Journal of Physics Communications* **2017**, *1*, No. 035002.

(603) Shabaev, A.; Efros, A. L.; Efros, A. L. Dark and Photo-Conductivity in Ordered Array of Nanocrystals. *Nano Letters* **2013**, *13*, 5454−5461.

(604) Beloborodov, I. S.; Lopatin, A. V.; Vinokur, V. M.; Efetov, K. B. Granular electronic systems. *Reviews of Modern Physics* **2007**, *79*, 469−518.

(605) Lee, J.-S.; Kovalenko, M. V.; Huang, J.; Chung, D. S.; Talapin, D. V. Band-like transport, high electron mobility and high photoconductivity in all-inorganic nanocrystal arrays. *Nature Nanotechnology* **2011**, *6*, 348−352.

(606) García, G. I. G.; de la Cruz, M. O. Polarization Effects of Dielectric Nanoparticles in Aqueous Charge-Asymmetric Electrolytes. *The Journal of Physical Chemistry B* **2014**, *118*, 8854−8862.

(607) Kreibig, U.; Vollmer, M. *Optical Properties of Metal Clusters*; Springer: Berlin Heidelberg, 1995; Vol. *25*.

(608) Sönnichsen, C.; Franzl, T.; Wilk, T.; von Plessen, G.; Feldmann, J.; Wilson, O.; Mulvaney, P. Drastic Reduction of Plasmon Damping in Gold Nanorods. *Physical Review Letters* **2002**, *88*, No. 077402.

(609) Zou, S.; Janel, N.; Schatz, G. C. Silver nanoparticle array structures that produce remarkably narrow plasmon lineshapes. *The Journal of Chemical Physics* **2004**, *120*, 10871−10875.

(610) Gupta, V.; Probst, P. T.; Goßler, F. R.; Steiner, A. M.; Schubert, J.; Brasse, Y.; König, T. A. F.; Fery, A. Mechanotunable Surface Lattice Resonances in the Visible Optical Range by Soft Lithography Templates and Directed Self-Assembly. *ACS Applied Materials and Interfaces* **2019**, *11*, 28189−28196.

(611) Scarabelli, L.; Vila-Liarte, D.; Mihi, A.; Liz-Marzán, L. M. Templated Colloidal Self-Assembly for Lattice Plasmon Engineering. *Accounts of Materials Research* **2021**, *2*, 816−827.

(612) Goerlitzer, E. S. A.; Mohammadi, R.; Nechayev, S.; Volk, K.; Rey, M.; Banzer, P.; Karg, M.; Vogel, N. Chiral Surface Lattice Resonances. *Advanced Materials* **2020**, *32*, No. 2001330.

(613) Manoccio, M.; Tasco, V.; Todisco, F.; Passaseo, A.; Cuscuna, M.; Tarantini, I.; Gigli, G.; Esposito, M. Surface Lattice Resonances in 3D Chiral Metacrystals for Plasmonic Sensing. *Advanced Science* **2023**, *10*, No. 2206930.

(614) Goerlitzer, E. S. A.; Zapata-Herrera, M.; Ponomareva, E.; Feller, D.; Garcia-Etxarri, A.; Karg, M.; Aizpurua, J.; Vogel, N. Molecular-Induced Chirality Transfer to Plasmonic Lattice Modes. *ACS Photonics* **2023**, *10*, 1821−1831.

(615) Owen, J.; Brus, L. Chemical Synthesis and Luminescence Applications of Colloidal Semiconductor Quantum Dots. *Journal of the American Chemical Society* **2017**, *139*, 10939−10943.

(616) Nguyen, H. A.; Dixon, G.; Dou, F. Y.; Gallagher, S.; Gibbs, S.; Ladd, D. M.; Marino, E.; Ondry, J. C.; Shanahan, J. P.; Vasileiadou, E. S.; Barlow, S.; Gamelin, D. R.; Ginger, D. S.; Jonas, D. M.; Kanatzidis, M. G.; Marder, S. R.; Morton, D.; Murray, C. B.; Owen, J. S.; Talapin, D. V.; Toney, M. F.; Cossairt, B. M. Design Rules for Obtaining Narrow Luminescence from Semiconductors Made in Solution. *Chemical Reviews* **2023**, *123*, 7890−7952.

(617) Gibbs, H. M. *Coherence in Spectroscopy and Modern Physics*; Springer US: Boston, MA, 1978; pp 121−129.

(618) Gross, M.; Haroche, S. Superradiance: an essay on the theory of collective spontaneous emission. *Phys. Rep.* **1982**, *93*, 301−396.

(619) Cong, K.; Zhang, Q.; Wang, Y.; Noe, G. T.; Belyanin, A.; Kono, J. Dicke superradiance in solids [Invited]. *Journal of the Optical Society of America B* **2016**, *33*, C80.

(620) Hou, L.; Tamarat, P.; Lounis, B. Revealing the Exciton Fine Structure in Lead Halide Perovskite Nanocrystals. *Nanomaterials* **2021**, *11*, 1058.

(621) Sercel, P. C.; Lyons, J. L.; Wickramaratne, D.; Vaxenburg, R.; Bernstein, N.; Efros, A. L. Exciton Fine Structure in Perovskite Nanocrystals. *Nano Letters* **2019**, *19*, 4068−4077.

(622) Toso, S.; Baranov, D.; Altamura, D.; Scattarella, F.; Dahl, J.; Wang, X.; Marras, S.; Alivisatos, A. P.; Singer, A.; Giannini, C.; Manna, L. Multilayer Diffraction Reveals That Colloidal Superlattices Approach the Structural Perfection of Single Crystals. *ACS Nano* **2021**, *15*, 6243−6256.

(623) Krieg, F.; Sercel, P. C.; Burian, M.; Andrusiv, H.; Bodnarchuk, M. I.; Stöferle, T.; Mahrt, R. F.; Naumenko, D.; Amenitsch, H.; Rainò, G.; Kovalenko, M. V. Monodisperse Long-Chain Sulfobetaine-Capped CsPbBr₃ Nanocrystals and Their Superfluorescent Assemblies. *ACS Central Science* **2021**, *7*, 135−144.

(624) Boehme, S. C.; Bodnarchuk, M. I.; Burian, M.; Bertolotti, F.; Cherniukh, I.; Bernasconi, C.; Zhu, C.; Erni, R.; Amenitsch, H.; Naumenko, D.; Andrusiv, H.; Semkiv, N.; John, R. A.; Baldwin, A.; Galkowski, K.; Masciocchi, N.; Stranks, S. D.; Raino, G.; Guagliardi, A.; Kovalenko, M. V. Strongly Confined CsPbBr3 Quantum Dots as Quantum Emitters and Building Blocks for Rhombic Superlattices. *ACS Nano* **2023**, *17*, 2089−2100.

(625) Baranov, D.; Fieramosca, A.; Yang, R. X.; Polimeno, L.; Lerario, G.; Toso, S.; Giansante, C.; Giorgi, M. D.; Tan, L. Z.; Sanvitto, D.; Manna, L. Aging of Self-Assembled Lead Halide Perovskite Nanocrystal Superlattices: Effects on Photoluminescence and Energy Transfer. *ACS Nano* **2021**, *15*, 650−664.

(626) Rainò, G.; Utzat, H.; Bawendi, M.; Kovalenko, M. Superradiant emission from self-assembled light emitters: From molecules to quantum dots. *MRS Bulletin* **2020**, *45*, 841−848.

(627) Liu, Z.; Qin, X.; Chen, Q.; Jiang, T.; Chen, Q.; Liu, X. Metal−Halide Perovskite Nanocrystal Superlattice: Self-Assembly and Optical Fingerprints. *Advanced Materials* **2023**, *35*, No. 2209279.

(628) Findik, G.; Biliroglu, M.; Seyitliyev, D.; Mendes, J.; Barrette, A.; Ardekani, H.; Lei, L.; Dong, Q.; So, F.; Gundogdu, K. High-

temperature superfluorescence in methyl ammonium lead iodide. *Nature Photonics* **2021**, *15*, 676−680.

(629) Biliroglu, M.; Findik, G.; Mendes, J.; Seyitliyev, D.; Lei, L.; Dong, Q.; Mehta, Y.; Temnov, V. V.; So, F.; Gundogdu, K. Room-temperature superfluorescence in hybrid perovskites and its origins. *Nature Photonics* **2022**, *16*, 324−329.

(630) Dral, P. O.; Barbatti, M. Molecular excited states through a machine learning lens. *Nature Reviews Chemistry* **2021**, *5*, 388−405.

(631) Westermayr, J.; Marquetand, P. Machine Learning for Electronically Excited States of Molecules. *Chemical Reviews* **2021**, *121*, 9873−9926.

(632) Gallegos, L. C.; Luchini, G.; St. John, P. C.; Kim, S.; Paton, R. S. Importance of Engineered and Learned Molecular Representations in Predicting Organic Reactivity, Selectivity, and Chemical Properties. *Accounts of Chemical Research* **2021**, *54*, 827−836.

(633) Toyao, T.; Maeno, Z.; Takakusagi, S.; Kamachi, T.; Takigawa, I.; Shimizu, K.-i. Machine Learning for Catalysis Informatics: Recent Applications and Prospects. *ACS Catalysis* **2020**, *10*, 2260−2297.

(634) Yang, X.; Wang, Y.; Byrne, R.; Schneider, G.; Yang, S. Concepts of Artificial Intelligence for Computer-Assisted Drug Discovery. *Chemical Reviews* **2019**, *119*, 10520−10594.

(635) Guo, H.; Wang, Q.; Stuke, A.; Urban, A.; Artrith, N. Accelerated Atomistic Modeling of Solid-State Battery Materials With Machine Learning. *Frontiers in Energy Research* **2021**, *9*, No. 695902.

(636) Habib, A.; Lubbers, N.; Tretiak, S.; Nebgen, B. Machine Learning Models Capture Plasmon Dynamics in Ag Nanoparticles. *The Journal of Physical Chemistry A* **2023**, *127*, 3768−3778.

(637) Roncaglia, C.; Ferrando, R. Machine Learning Assisted Clustering of Nanoparticle Structures. *Journal of Chemical Information and Modeling* **2023**, *63*, 459−473.

(638) Brown, K. A.; Brittman, S.; Maccaferri, N.; Jariwala, D.; Celano, U. Machine Learning in Nanoscience: Big Data at Small Scales. *Nano Letters* **2020**, *20*, 2−10.

(639) Mekki-Berrada, F.; Ren, Z.; Huang, T.; Wong, W. K.; Zheng, F.; Xie, J.; Tian, I. P. S.; Jayavelu, S.; Mahfoud, Z.; Bash, D.; Hippalgaonkar, K.; Khan, S.; Buonassisi, T.; Li, Q.; Wang, X. Two-step machine learning enables optimized nanoparticle synthesis. *npj Computational Materials* **2021**, *7*, 55.

(640) Reynolds, N. P.; Adamcik, J.; Berryman, J. T.; Handschin, S.; Zanjani, A. A. H.; Li, W.; Liu, K.; Zhang, A.; Mezzenga, R. Competition between crystal and fibril formation in molecular mutations of amyloidogenic peptides. *Nature Communications* **2017**, *8*, 1338.

(641) Fernández-Higuero, J. A.; Muga, A.; Vilar, J. M. Extraction and Refolding Determinants of Chaperone-Driven Aggregated Protein Reactivation. *Journal of Molecular Biology* **2020**, *432*, 3239−3250.

(642) Chuang, E.; Hori, A. M.; Hesketh, C. D.; Shorter, J. Amyloid assembly and disassembly. *Journal of Cell Science* **2018**, *131*, No. jcs189928.

(643) Franco, A.; Gracia, P.; Colom, A.; Camino, J. D.; Fernandez-Higuero, J. A.; Orozco, N.; Dulebo, A.; Saiz, L.; Cremades, N.; Vilar, J. M.G.; Prado, A.; Muga, A. All-or-none amyloid disassembly via chaperone-triggered fibril unzipping favors clearance of α-synuclein toxic species. *Proceedings of the National Academy of Sciences* **2021**, *118*, No. e2105548118.

(644) Vilar, J. M. G.; Rubi, J. M.; Saiz, L. Chaperone-driven entropic separation of amyloid nanofilament bundles. *bioRxiv*, 2023; https://www.biorxiv.org/content/early/2023/05/24/2023.05.24.542046.

(645) Bates, K. A.; Verdile, G.; Li, Q.-X.; Ames, D.; Hudson, P.; Masters, C. L.; Martins, R. N. Clearance mechanisms of Alzheimer's amyloid-β peptide: implications for therapeutic design and diagnostic tests. *Molecular Psychiatry* **2009**, *14*, 469−486.

(646) Zasloff, M. Antimicrobial peptides of multicellular organisms. *Nature* **2002**, *415*, 389−395.

(647) Yeaman, M. R.; Yount, N. Y. Mechanisms of Antimicrobial Peptide Action and Resistance. *Pharmacological Reviews* **2003**, *55*, 27−55.

(648) Schmidt, N. W.; Jin, F.; Lande, R.; Curk, T.; Xian, W.; Lee, C.; Frasca, L.; Frenkel, D.; Dobnikar, J.; Gilliet, M.; Wong, G. C. L.

Liquid-crystalline ordering of antimicrobial peptide−DNA complexes controls TLR9 activation. *Nature Materials* **2015**, *14*, 696−700.

(649) Lee, E. Y.; Zhang, C.; Di Domizio, J.; Jin, F.; Connell, W.; Hung, M.; Malkoff, N.; Veksler, V.; Gilliet, M.; Ren, P.; Wong, G. C. L. Helical antimicrobial peptides assemble into protofibril scaffolds that present ordered dsDNA to TLR9. *Nature Communications* **2019**, *10*, 1012.

(650) Tursi, S. A.; Lee, E. Y.; Medeiros, N. J.; Lee, M. H.; Nicastro, L. K.; Buttaro, B.; Gallucci, S.; Wilson, R. P.; Wong, G. C. L.; Tukel, C. Çagla Tükel Bacterial amyloid curli acts as a carrier for DNA to elicit an autoimmune response via TLR2 and TLR9. *PLOS Pathogens* **2017**, *13*, No. e1006315.

(651) Lee, E. Y.; Takahashi, T.; Curk, T.; Dobnikar, J.; Gallo, R. L.; Wong, G. C. L. Crystallinity of Double-Stranded RNA-Antimicrobial Peptide Complexes Modulates Toll-Like Receptor 3-Mediated Inflammation. *ACS Nano* **2017**, *11*, 12145−12155.

(652) Kagan, B. Antimicrobial Amyloids? *Biophysical Journal* **2011**, *100*, 1597−1598.

(653) Kumar, D. K. V.; Choi, S. H.; Washicosky, K. J.; Eimer, W. A.; Tucker, S.; Ghofrani, J.; Lefkowitz, A.; McColl, G.; Goldstein, L. E.; Tanzi, R. E.; Moir, R. D. Amyloid-β peptide protects against microbial infection in mouse and worm models of Alzheimer's disease. *Science Translational Medicine* **2016**, *8*, 340ra72−340ra72.

(654) Martinez-Veracoechea, F. J.; Frenkel, D. Designing super selectivity in multivalent nano-particle binding. *Proc. Natl. Acad. Sci. U.S.A.* **2011**, *108*, 10963−10968.

(655) Chen, X.; Yang, X.; de Anda, J.; Huang, J.; Li, D.; Xu, H.; Shields, K. S.; Džunková, M.; Hansen, J.; Patel, I. J.; Yee, E. U.; Golenbock, D. T.; Grant, M. A.; Wong, G. C.; Kelly, C. P. Clostridioides difficile Toxin A Remodels Membranes and Mediates DNA Entry Into Cells to Activate Toll-Like Receptor 9 Signaling. *Gastroenterology* **2020**, *159*, 2181−2192.

(656) Zhang, Y. Viral afterlife: SARS-CoV-2 as a reservoir of immunomimetic peptides that re-assemble into pro-inflammatory supramolecular complexes. *Proc. Natl. Acad. Sci. U.S.A.* **2024**, *121*, No. e2300644120. DOI: 10.1073/pnas.2300644120.

(657) Montanarella, F.; Kovalenko, M. V. Three Millennia of Nanocrystals. *ACS Nano* **2022**, *16*, 5085−5102.

(658) Osat, S.; Metson, J.; Kardar, M.; Golestanian, R. Escaping kinetic traps using non-reciprocal interactions, 2023, https://arxiv.org/abs/2309.00562.